

A distributed optimization approach to complete vehicle energy management

Citation for published version (APA):

Romijn, T. C. J. (2017). *A distributed optimization approach to complete vehicle energy management*. [Phd Thesis 1 (Research TU/e / Graduation TU/e), Electrical Engineering]. Technische Universiteit Eindhoven.

Document status and date:

Published: 05/10/2017

Document Version:

Publisher's PDF, also known as Version of Record (includes final page, issue and volume numbers)

Please check the document version of this publication:

- A submitted manuscript is the version of the article upon submission and before peer-review. There can be important differences between the submitted version and the official published version of record. People interested in the research are advised to contact the author for the final version of the publication, or visit the DOI to the publisher's website.
- The final author version and the galley proof are versions of the publication after peer review.
- The final published version features the final layout of the paper including the volume, issue and page numbers.

[Link to publication](#)

General rights

Copyright and moral rights for the publications made accessible in the public portal are retained by the authors and/or other copyright owners and it is a condition of accessing publications that users recognise and abide by the legal requirements associated with these rights.

- Users may download and print one copy of any publication from the public portal for the purpose of private study or research.
- You may not further distribute the material or use it for any profit-making activity or commercial gain
- You may freely distribute the URL identifying the publication in the public portal.

If the publication is distributed under the terms of Article 25fa of the Dutch Copyright Act, indicated by the "Taverne" license above, please follow below link for the End User Agreement:

www.tue.nl/taverne

Take down policy

If you believe that this document breaches copyright please contact us at:

openaccess@tue.nl

providing details and we will investigate your claim.

A Distributed Optimization Approach to Complete Vehicle Energy Management

PROEFSCHRIFT

ter verkrijging van de graad van doctor aan de Technische Universiteit Eindhoven, op gezag van de rector magnificus prof.dr.ir. F.P.T. Baaijens, voor een commissie aangewezen door het College voor Promoties, in het openbaar te verdedigen op donderdag 5 oktober 2017 om 16.00 uur

door

Thomas Constantijn Jonathan Romijn

geboren te Kockengen

Dit proefschrift is goedgekeurd door de promotoren en de samenstelling van de promotiecommissie is als volgt:

voorzitter: prof.dr.ir. A.B. Smolders
1^e promotor: prof.dr. S. Weiland
copromotoren: dr.ir. M.C.F. Donkers
dr.ir. J.T.B.A. Kessels
leden: prof.dr. B. Egardt (Chalmers Techniska Högskola)
prof.dr. L. Grüne (Universität Bayreuth)
prof.dr.ir J.M.A. Scherpen (Rijksuniversiteit Groningen)
prof.dr.ir. M. Steinbuch

Het onderzoek of ontwerp dat in dit proefschrift wordt beschreven is uitgevoerd in overeenstemming met de TU/e Gedragscode Wetenschapsbeoefening.



This project has received funding from the European Union's Seventh Framework Program for research, technological developments and demonstration under the grant CONVENIENT (312314)

A Distributed Optimization Approach to Complete Vehicle Energy Management
by T.C.J. Romijn. – Eindhoven : Technische Universiteit Eindhoven, 2017
Proefschrift.

A catalogue record is available from the Eindhoven University of Technology Library.
ISBN: 978-90-386-4324-3

Copyright © 2017 by T.C.J. Romijn.

This thesis was prepared with the L^AT_EX documentation system.
Cover Design: Luke Lathouwers and Constantijn Romijn
Printed by: Gildeprint - Enschede

Summary

A Distributed Optimization Approach to Complete Vehicle Energy Management

Fuel economy and emission legislation play a dominant role in the development process of modern commercial heavy-duty vehicles. To satisfy future requirements on fuel consumption and exhaust gas emissions, new technologies are introduced in these vehicles. Clear examples are energy efficient (electrified) auxiliaries, hybrid electric powertrains and waste-heat recovery from the exhaust gas. To facilitate integration of all these subsystems, a flexible and scalable energy management system is needed. In this thesis, a holistic system approach is taken that considers all energy sources, sinks and buffers present in the vehicle. This approach is referred to as complete vehicle energy management (CVEM).

Solution methods for solving the energy management problem of a hybrid electric vehicle, that consider the power split between the internal combustion engine and the electric machine, are very well covered in today's available literature. However, expanding these solution methods with integrated control of all energy sources, sinks and buffers, i.e., CVEM, is neither straightforward and nor does it lead to a flexible and scalable approach for designing a holistic energy management system. In this thesis, a distributed optimization approach is proposed for CVEM, with focus on the optimal control of all the auxiliary systems in the truck.

Both an offline as well as an online solution method are developed. For the offline solution method, it is assumed that all disturbances (such as the driving cycle) are known. Even though the optimal solution can be computed, the control

strategy cannot be implemented in the vehicle (online). The solution, however, gives a valuable benchmark to verify the performance of other (online) solution methods. The offline solution method, proposed in this thesis, uses a two-step decomposition. First, dual decomposition is used to split the large-scale optimal control problem of the energy management problem into smaller optimal control problems per subsystem. For the second part of the approach, the optimal control problem for every subsystem is solved with three different methods. The first two methods rely on splitting the control horizon into several smaller horizons. The first method uses the alternating direction method of multipliers and divides the horizon a priori, while the second method divides the horizon iteratively by solving unconstrained optimization problems analytically. The third method, based on dynamic programming, is used to solve the optimal control problem related to subsystems with on/off control. The approach is demonstrated on a CVEM problem of a hybrid truck with a refrigerated semi-trailer, an air supply system, an alternator, a DCDC converter, a low-voltage battery and a climate control system. Offline simulation results show that the fuel consumption can be reduced up to 1.42 % by optimizing the power flow to the auxiliaries with the CVEM strategy. This requires, however, that the auxiliaries are continuous controlled or that the number of switches is unbounded. More interestingly, the computation time is reduced by a factor of 64 up to 1825, compared with solving a centralized convex optimization problem.

For the online solution method proposed in this thesis, the disturbances are not assumed to be known, but are predicted. The CVEM problem is solved with a distributed economic model predictive control approach that uses a receding control horizon in combination with a dual decomposition. The energy management problem is decomposed with the dual decomposition approach that result in smaller energy management problems that can be efficiently solved with an embedded quadratic programming solver. The receding horizon control problem is formulated with variable sample time intervals, allowing for large prediction horizons with only a limited number of decision variables and constraints in the optimization problem. Furthermore, a novel on/off control concept for control of the refrigerated semi-trailer, the air supply system and the climate control system is introduced. Simulation results show that a close to optimal fuel reduction can be achieved. The fuel reduction for the on/off controlled subsystems strongly

depends on the number of switches allowed. By allowing up to 15 times more switches, a fuel reduction of 1.3 % can be achieved.

Finally, the online solution method is validated on a high-fidelity vehicle model. The propulsion power needed for driving and the engine speed are predicted by assuming that the vehicle follows a reference speed set by the cruise control or the downhill speed control, which is valid for high-way driving. This allows the vehicle speed to be predicted over a trajectory with a road slope predicted by an e-horizon sensor, e.g., ADASIS, leading to a prediction of the propulsion power and engine speed. The prediction algorithm is validated with measured ADASIS information on a public road around Eindhoven, which demonstrates that accurate prediction of the propulsion power and engine speed is feasible if the vehicle follows the most probable path. Simulations with the high-fidelity vehicle model show that a fuel reduction of 0.98 % can be obtained. The control strategy is implemented on a dSpace Autobox and shows that the maximum computation time is only 3.2 ms per iteration. This demonstrates that real-time implementation is feasible.

The optimal control concepts in this thesis are presented in the context of smart control of the auxiliaries, such as the refrigerate semi-trailer. The fuel reduction potential for these auxiliaries can be limited compared to, e.g., the fuel reduction potential of a hybrid system. Still, the main contribution of this thesis is not the fuel reduction for these auxiliaries, but the step that is taken towards a flexible and scalable framework that can handle the growing complexity of energy management systems that take into account more than just the power split between an internal combustion engine and electric machine. This will ultimately lead to close to optimal fuel consumption for the complete vehicle.

Table of Contents

Summary	v
Table of Contents	ix
1 Introduction	1
1.1 Motivation	1
1.2 Complete Vehicle Energy Management	5
1.3 Research Question and Objectives	7
1.4 Literature Review on Vehicle Energy Management	9
1.5 Distributed Optimization Approach	12
1.6 Thesis Outline	13
1.7 Publications	14
2 Convex Modeling of a Heavy-Duty Vehicle	17
2.1 Introduction	18
2.2 Objective and Topology	19
2.3 Subsystem Modeling	21
2.4 Conclusions and Discussion	39
3 Distributed Optimization for Offline Energy Management	41
3.1 Introduction	42
3.2 Distributed Optimization of Power Nets	43
3.3 Evaluating the Dual Functions	50
3.4 Application to the CVEM problem	62
3.5 Simulation Results	66
3.6 Conclusions and Discussion	80

4	Distributed Economic MPC for Online Energy Management	83
4.1	Introduction	84
4.2	Distributed Economic Model Predictive Control	86
4.3	Prediction of Disturbance Signals	95
4.4	Simulation Results	96
4.5	Conclusions and Discussion	103
5	Validation on a High-Fidelity Vehicle Model	107
5.1	Introduction	108
5.2	High-fidelity Simulation Model	109
5.3	Prediction of Disturbance Signals with ADASIS	113
5.4	Simulation Results	118
5.5	Conclusions and Discussion	129
6	Conclusions	131
6.1	Conclusions	132
6.2	Recommendations for Future Research	135
6.3	Implications	137
A	State Trajectories	139
A.1	Optimal state trajectories with continuous control	139
A.2	State trajectories for the low-fidelity vehicle model	139
A.3	State trajectories for the high-fidelity vehicle model	140
	Bibliography	145
	Acknowledgements	159
	Curriculum Vitae	161

1

Introduction

1.1 Motivation

Despite a growing number of climate change mitigation policies, the worldwide annual greenhouse gas emissions grew on average by 1.0 gigatonne carbon dioxide (CO₂) per year from 2000 to 2010 compared to 0.4 gigatonne CO₂ per year from 1970 to 2000. Without additional efforts to reduce the greenhouse gas emissions, this emission growth is expected to persist [46]. The combustion of fossil fuels (coal, natural gas and oil) for energy and transportation is a large contributor to the emission of CO₂. According to the latest report of the intergovernmental panel on climate change (IPCC [46]), the worldwide road transportation is responsible for 10.2 % of the global CO₂ emissions (see Figure 1.1 [46]). This corresponds to 4.9 gigatonne CO₂ per year. As CO₂ emissions are one to one related to the combustion of fuel, improving the road transport fuel efficiency contributes to the climate change mitigation. It is also well known that the supply of fossil fuels is not endless. Smart solutions for reducing the fuel consumption therefore contribute to the road map towards a smart and sustainable society.

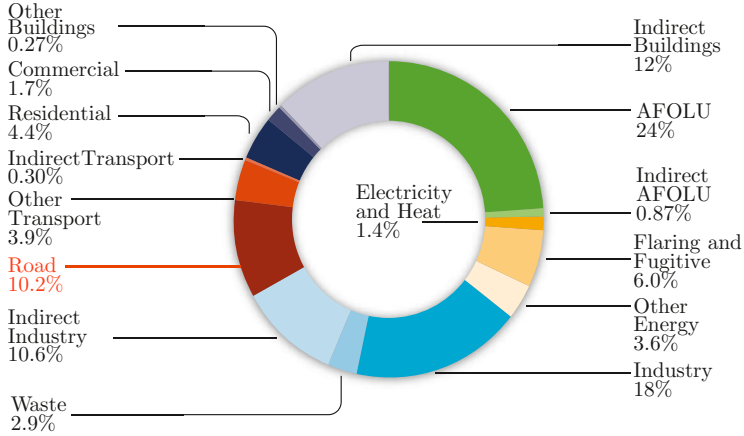


Figure 1.1: Allocation of total greenhouse gas emissions per sector in 2010 (AFOLU: Agriculture, Forestry and Other Land Use) [46].

For these reasons, an ongoing trend is visible to improve the fuel economy of road transportation vehicles, partly enforced by legislation.

Legislation is not the only drive for road transport manufacturers to improve fuel economy. European freight transport over roads is characterized by high fuel prices, high weights and large volumes and involves relatively long distances [64]. Fuel efficiency is therefore one of the most important competitive factors in developing and selling trucks and buses. Fuel cost is estimated to be 30 % of the total operational costs of a 40 tonne tractor semi-trailer combination in Europe (see Figure 1.2 [64]). Fuel efficiency is therefore the third purchasing criteria, behind reliability (1) and service quality (2), for West European customers and the second purchasing criteria for East European customers [85].

Fuel efficiency of a heavy-duty vehicle can be analyzed by considering the dissipation of the fuel energy. This analysis has been carried out in [43] for a tractor semi-trailer combination and shown in Figure 1.3. A lot of energy is dissipated in the exhaust (29%), mainly in the form of thermal energy that disappears by convection. Waste heat recovery systems [125] can recover some of this energy that can be re-used, e.g., by the supply of power to the auxiliaries. Another major energy dissipation factor (20 %) is cooling in the form of heat that dissipates by conduction through the engine structure, the cooling radiator and oil cooler. Studies have shown that the electrification of the cooling pump and smart cooling

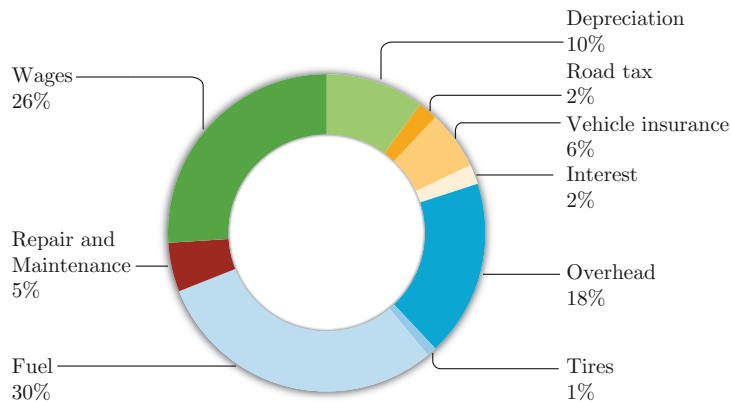


Figure 1.2: Operational cost of a 40 tonne tractor semi-trailer combination in Europe [64].

strategies can reduce the energy losses in the cooling system (see, e.g. [20]). Air drag accounts for 18 % of the energy losses and can be reduced by improving the aerodynamics of the vehicle (see, e.g., [75]). Another 3 % is lost to energy consuming auxiliaries, e.g., an air supply system. The electrification of these auxiliaries is a current trend to improve the energy efficiency (see, e.g. [41, 97]). Finally, 31 % of the energy is lost through the brakes, the rolling resistance of the tyres, the transmission and the engine as a result of friction. Recent developments that reduce energy losses in these domains are engine downsizing [35], low friction bearings [127] and regenerative braking.

Regenerative braking is possible by hybridization of the drive train. This technology is extensively studied to reduce the energy losses in heavy-duty vehicles (see, e.g. [91, 119]). The drive train with the primary power source, i.e., the internal combustion engine, is extended with a secondary power source, typically an electric motor/generator in combination with a secondary energy buffer, typically a high-voltage battery system. Both power sources can be utilized to provide propulsion power to the vehicle. Some of the kinetic energy in the vehicle can be recovered by the secondary power source when braking the vehicle (regenerative braking) and can be stored in the secondary energy buffer. The stored energy can, at a later moment, be utilized to provide propulsion power to the vehicle, thereby increasing the overall vehicle efficiency.

Hybrid drive trains require an energy management strategy to find the most

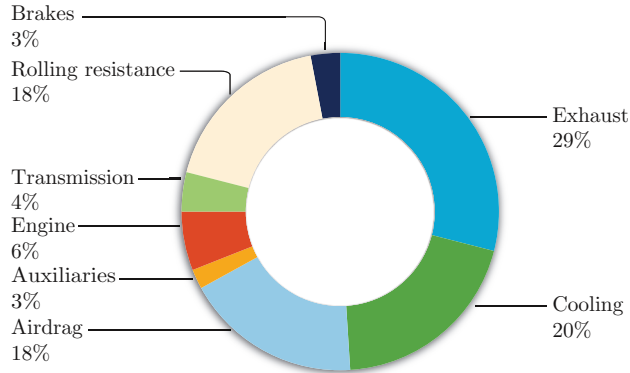


Figure 1.3: Breakdown of the global average energy consumption for a tractor semi-trailer combination [43].

efficient power split between both power sources. Energy management strategies have also been developed to optimize the efficiency of individual systems, e.g., exhaust heat recovery systems and electrified auxiliaries. Optimization of all these subsystems individually will not automatically guarantee global fuel efficiency at vehicle level. Therefore, control of all these subsystems needs to be coordinated into one complete vehicle energy management (CVEM) strategy [52]. Besides global fuel efficiency, the CVEM strategy should satisfy the following major requirements:

- Scalable:** Modern vehicles are characterized by the broad range of power train configurations augmented by a long list of auxiliaries. Customers expect to choose their own vehicle configuration, specialized for their specific application area. This requires that the energy management strategy should not be limited by the number of subsystems in the vehicle and complexity should not increase rapidly with the number of subsystems.
- Flexible (Plug & Play):** As customers can choose from almost an infinite number of configurations, the development of an energy management strategy for each of these configurations is very time consuming, inefficient and extremely expensive. The CVEM strategy must therefore satisfy a certain degree of flexibility, that allows the same strategy to be used for many different vehicle configurations. In the ultimate case, a plug & play design philosophy is foreseen to integrate new subsystems in the vehicle.

This means that auxiliaries can be added or removed without changing (or having knowledge of) the rest of the system and optimal fuel efficiency is still guaranteed. This would also allow easy integration of hardware from different suppliers.

- **Include on/off auxiliaries:** Often, the electrification of the auxiliaries allows for continuous control, e.g., any power setpoint between an upper and lower limit can be send to the auxiliary. Today’s heavy-duty vehicles, however, are still equipped with auxiliaries that can only receive a setpoint that turns the auxiliary on or off. Straightforward integration of auxiliaries with on/off control is therefore essential.

To develop a scalable and flexible CVEM strategy, suitable for on/off control, that guarantees global fuel efficiency at vehicle level is challenging. Therefore, a novel approach is needed, which will be the main contribution of this thesis: a distributed optimization approach for Complete Vehicle Energy Management (CVEM).

1.2 Complete Vehicle Energy Management

Hybrid drive trains require an energy management strategy because multiple (controllable) energy storage buffers are present in the vehicle. This means that fuel energy can be converted to mechanical energy with the internal combustion engine and chemical energy in the battery system can be converted to mechanical energy through the electric motor as well. Via the gearbox and the wheels, the mechanical energy is converted to kinetic energy in the vehicle mass. The energy buffers in the vehicle are constrained by the maximum and minimum battery capacity, the maximum and minimum fuel capacity and the maximum and minimum velocity of the vehicle. An energy management strategy is essential to manage these energy flows, while satisfying the maximum and minimum amount of energy in each of the energy buffers.

Energy can be stored in many different ways. Specifically, since any vehicle combines physical properties from the mechanical, the thermal, the electrical, the pneumatic and the chemical energy domain. An overview of these domains and examples of energy storage systems in those domains are given in Figure 1.4.

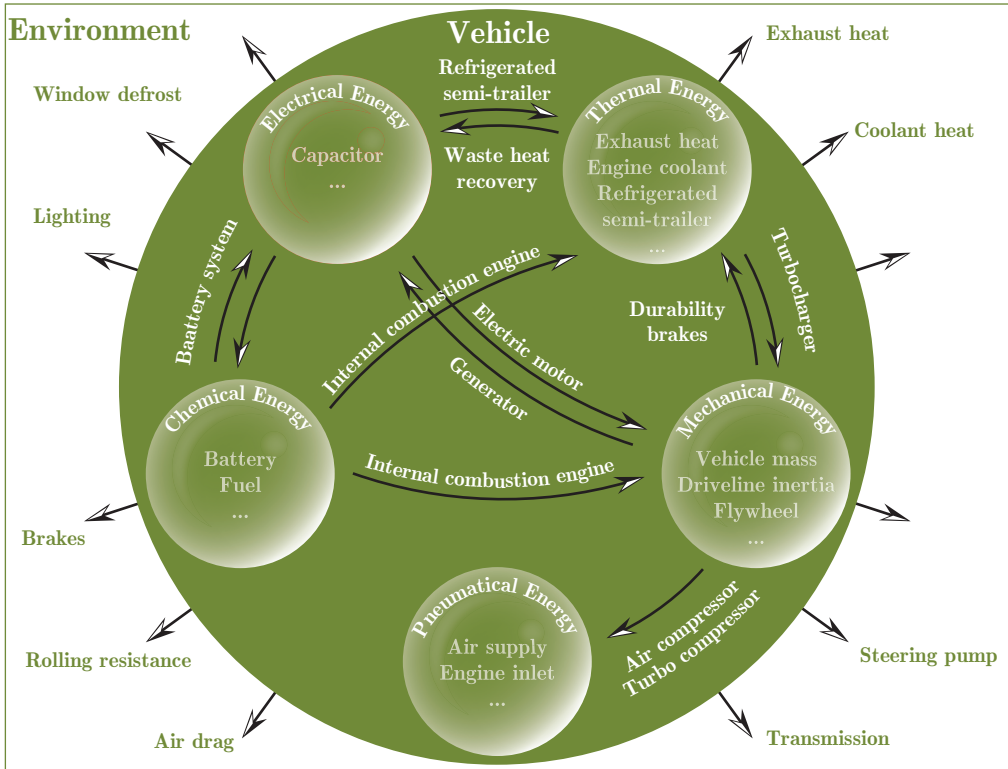


Figure 1.4: Energy storage and energy flows in heavy-duty vehicles.

Energy can be converted from one domain to another via the converters, however, some energy will be dissipated in the conversion process. The internal combustion engine, for example, converts the fuel energy into mechanical energy with an efficiency given by

$$\text{efficiency} = \frac{\text{Mechanical energy}}{\text{Fuel energy}} 100\% = \left(1 - \frac{\text{Energy losses}}{\text{Fuel energy}}\right) 100\%. \quad (1.1)$$

The energy losses in the internal combustion engine are dissipated through, e.g., exhaust heat and coolant heat. Some of the heat can be converted to electrical energy, if the vehicle is equipped with a waste heat recovery system. The electrical energy can be converted and stored as chemical energy via the battery system. Every energy conversion leads to energy dissipation. A proper energy management strategy recognizes this and chooses the most efficient energy path for each of these energy flows.

It should also be noted that the internal combustion engine allows fuel energy to be converted into mechanical energy. However, mechanical energy cannot be converted to fuel energy. Similarly, the refrigerated semi-trailer allows electrical energy to be converted to thermal energy, but today's refrigerated semi-trailers do not have a converter that converts the thermal energy to any other energy domain. This is a significant disadvantage for energy management. After all, energy that is converted can never be used for any other application. Still, fluctuations between the maximum and minimum temperature are allowed, so that the amount of energy flowing to the refrigerated semi-trailer can be scheduled over time. This observation yields an opportunity for energy management, where energy of different subsystems can be scheduled over time to balance energy production with energy demand while maximizing efficiency. The development of an energy management strategy that can optimize multiple energy flows, while taking dynamics and constraints of each subsystem into account, while at the same time meeting a certain degree of flexibility and scalability, is not trivial. Therefore, this research on CVEM is initiated and incorporated as part of the European project CONVENIENT¹. We will elaborate more on the objectives in this research in the next section.

1.3 Research Question and Objectives

Research in the field of CVEM has not received substantial attention yet. Therefore, the research question posed in this thesis is formulated as follows:

What is the fuel reduction potential of a CVEM strategy that takes into account all energy flows and energy buffers in the vehicle?

To answer this question, a novel control concept has to be developed that is scalable, flexible and suitable for on/off control as well as real-time implementable and robust with respect to model uncertainty. To do so, we can divide the research question into two major objectives:

¹The CONVENIENT project aims to develop a novel long-distance heavy-truck prototype featuring a suite of technologies enabling a 30% fuel saving. To demonstrate the feasibility of the fuel reduction measures, e.g., internal combustion engine downsizing, aerodynamic drag minimization and CVEM, a prototype heavy-duty vehicle has been developed. This prototype has a hybrid drive train with an internal combustion engine and an electric machine attached to a high-voltage battery system and all auxiliaries are electrified.

1. **Objective 1: The development of a flexible and scalable *optimal* control concept for CVEM with on/off controlled auxiliaries**

A proper energy management strategy (EMS) manages the energy flows in the vehicle in real-time with limited knowledge on the disturbances acting on the components in the vehicle. A real-time EMS, however, typically does not guarantee the global optimal solution. Without knowledge of the global optimal solution, the performance of the real-time EMS cannot be guaranteed. Therefore, optimal control concepts that guarantee the global optimal solution have always been used in energy management to define a benchmark. These optimal control concepts require that all disturbances, e.g., the reference speed and road slope, are known prior to the optimization for each time instant, which precludes these optimal control concepts to be implemented in real-time.

The requirements (flexibility, scalability and integration of on/off auxiliaries) introduced in the first section, are not met by the optimal control concepts used so far in energy management. A novel optimal control concept needs to be developed, with as goal to maximize the energy efficiency of the vehicle, generally expressed as minimizing the total fuel consumption.

2. **Objective 2: The development of a flexible and scalable *real-time* energy management strategy for CVEM with on/off controlled auxiliaries**

The optimal control concept developed under Objective 1 can never be implemented in real-time as disturbances are never known exactly a priori. Moreover, the behavior of the mathematical models that are used to optimize the energy flows are never equivalent to the behavior of the real vehicle. The second objective in this research is therefore to develop a real-time EMS for CVEM. The fuel reduction should be close to the optimal fuel reduction obtained with the optimal control concept. As with the optimal control concept, flexibility, scalability and control of on/off auxiliaries are a major requirement. Contrary to the optimal control concept, the real-time EMS cannot rely on exact knowledge of the disturbances, e.g., the reference speed and road slope, but taking into account prediction of these disturbances is essential. The latter requirement follows from the current trends in automotive technology that allow for prediction of future events

and communication between vehicles, so that it is necessary to develop a real-time EMS that is ready for this technology.

These objectives will be evaluated along the research lines that can be found in today's literature in the next section.

1.4 Literature Review on Vehicle Energy Management

Research on the 'classical' energy management problem, i.e., the power-split problem between a primary power source, e.g., the internal combustion engine, and a secondary power source, e.g., the electric machine, has received numerous attention over the last decades. This is visible from the numerous books that have appeared on this topic, see, e.g., [74, 44, 40, 30, 73, 130, 22]. The control concepts that are used for energy management can roughly be classified into three domains 1) Optimal control 2) real-time EMS based on heuristic strategies and artificial intelligence and 3) real-time EMS derived from an optimal control concept.

In the first domain, three optimal control concepts for solving the energy management problem received most attention in literature: dynamic programming (DP) [5, 2, 3, 58, 67, 114], Pontryagin's minimum principle (PMP) [38, 110, 18, 23, 106] and convex optimization [9, 115, 112, 78, 31]. For these optimal control concepts, all the disturbances, e.g., the reference velocity and road slope, are assumed to be known for each time instant. These optimal control concepts can therefore not be used in real-time. Still, they are frequently used to provide a valuable benchmark for a real-time EMS.

The second domain covers the very first strategies that were used to arrive at a real-time EMS. Various heuristic strategies have been developed over the past decades by using rule-based strategies [17, 42, 47, 122], neural networks [62, 123] or fuzzy logic [4, 105]. These EMS strategies have been favoured as they are often easy to implement. Optimality, however, is not guaranteed and, moreover, the fuel reduction is strongly correlated to the parameters, e.g., the rules, of the strategy. Often these strategies are tuned based on results from optimal control or through experimental validation, but as a result, robustness of these strategies cannot be guaranteed and flexibility is lacking.

To overcome these calibration issues and to obtain a certain degree of optimality, a complete line of research has been dedicated to real-time strategies derived

from the optimal control concepts. Indeed, for all of the optimal control concepts in the first domain, there exist a real-time equivalent strategy. For dynamic programming, the real-time equivalent strategy is obtained by solving a stochastic dynamic programming problem [60, 66, 77, 49], which results in a stochastic optimal operation policy that can be evaluated in real-time.

A well known real-time equivalent strategy for PMP is the equivalent consumption minimization strategy (ECMS) [107, 88, 89]. Applying PMP to the energy management problem results in a cost function with a co-state related to the energy in the battery. The physical interpretation to the co-state related to the battery energy is that it translates the battery power into a fuel equivalent contribution to the cost function, which explains the terminology ECMS. Whereas for PMP, the co-state can be calculated under certain conditions, e.g., when the complete drive cycle is known, for ECMS, the co-state is estimated and updated over time. Estimating and updating the co-state is difficult and many different methods can be found in literature [16, 39, 50, 51, 56, 59, 69, 79, 13] and an extensive comparison of adaptive ECMS can be found in [86].

Finally, the real-time equivalent strategy for convex optimization is (nonlinear) model predictive control [36]. This requires solving the (nonlinear) optimal control problem at each time instant over a finite-time horizon and only implementing the decisions at the current time instant. Often, the optimal control problem is linearized and the disturbances over the horizon are predicted, which can be assumed deterministic as in [3, 53, 84, 8, 104, 116] or stochastic as in [25, 129]. Interesting applications of nonlinear model predictive control for energy management can be found in [7, 57].

Extensions to the above mentioned ‘classical’ energy management problem with additional decision variables can be found in literature as well and can be seen as first steps towards CVEM. Interesting extensions to the energy management problem with engine exhaust emission management are given in [24, 54, 125]. As battery degradation is a major concern in hybrid electric vehicles, the energy management problem is extended with battery state-of-health in [26, 94, 93, 108] and extended with thermal management of the battery in [87, 92, 72]. Although, each of these extensions is interesting, all of the papers use solutions methods from ‘classical’ energy management to solve the optimal control problem.

The CVEM concept is first introduced in [52] where a holistic approach is fore-

seen, taking into account all power flows and energy sources in the vehicle. Here, it is recognized that existing energy management strategies based on the methods discussed above will face severe limitations in handling the complexity of CVEM and alternative approaches are needed. Indeed, scalability of the optimal control methods (first domain) is poor as DP suffers from the curse of dimensionality and solving the two-point boundary value problem resulting from PMP is difficult, particularly when state constraints are present, see, e.g., [72] in the context of thermal dynamics. Finally, a convex approximation of the energy management problem can lead to a globally optimal solution, but still requires a large-scale optimization problem to be solved.

Flexibility is the main concern for the real-time methods in the second and third domain. Adding or removing components to these frameworks can be a cumbersome task. Moreover, changing the energy management problem by adding or removing components requires calibration of the entire energy management strategy.

For this reason, distributed solutions for energy management start to appear. These solutions are characterized by the fact that all subsystems share a limited amount of information and decisions are taken autonomously at subsystem level. In [12, 14, 11, 81], a real-time game-theoretic approach to CVEM is presented for which prediction information is not utilized. In [82, 83], scalability is obtained by using the Alternating Direction Method of Multipliers (ADMM) while ideas based on ECMS are used to calculate the equivalent costs at a supervisory level. This still requires a calibration effort at supervisory level. Moreover, these distributed solutions all lead to real-time energy management strategies for which the global optimal solution is not guaranteed.

In this thesis, we will extend the research on distributed solutions. In particular we will develop an optimal control concept to find the global optimal solution to the CVEM problem. Moreover, we will develop a real-time energy management strategy that fully exploits prediction information and does not require calibration at supervisory level. We will do so along the lines of a distributed optimization approach explained in the next section.

1.5 Distributed Optimization Approach

It has been outlined in the previous section that in today's literature, dynamic programming, Pontryagin's minimum principle and convex optimization are most often used to find the global optimal solution to the energy management problem. From these three optimal control concepts, convex optimization is the only concept for which distributed solutions already exist. These solutions are part of the field of distributed optimization. In particular, the dual decomposition method is popular and has already been used since the early 1960s [21] to solve large-scale convex optimization problems. Since then, this method has been applied to problems with large-scale dynamical systems, e.g., the optimal routing of data in wireless data networks [128] or optimal scheduling of appliances in smart electricity grids [37]. The dual decomposition allows a large-scale optimization problem to be decomposed into smaller optimization problems that are only coupled through so-called dual variables. This problem can be solved, by iteratively solving the smaller optimization problems followed by the update of the dual variables by a master algorithm. This has an interesting economic interpretation. The dual variables can be interpreted as prices for resources. Each smaller optimization problem tries to minimize its own cost, while the master algorithm adjusts the prices in order to bring the demand in consistency with the supply. This interpretation matches exactly the price-based philosophy envisioned in [52] as a viable strategy for CVEM. Indeed, in this thesis, the application of the dual decomposition to the convex approximation of the CVEM problem leads to smaller optimization problems related to each subsystem in the vehicle. It will be shown in this thesis how each of these smaller optimization problems can be solved efficiently with a Lagrangian method, with another method from distributed optimization called Alternating Direction Method of Multipliers or with dynamic programming to optimally control auxiliaries with on/off decisions.

Similarly, as the dual decomposition can be used to find the global optimal solution to a large-scale convex optimization problem, the dual decomposition can also be used to arrive at a distributed solution for the real-time equivalent strategy, i.e., distributed model predictive control [70, 96]. Indeed, the dual decomposition has been used, e.g., in [63, 6] to develop real-time strategies for control in smart energy grids. In this thesis, the real-time energy management

strategy is similarly obtained by defining the CVEM problem over a shorter receding horizon to which we apply the dual decomposition. This again leads to smaller optimization problems related to each subsystem in the vehicle that can be solved efficiently with embedded quadratic programming solvers. Moreover, the optimization problem associated with on/off auxiliaries is solved with a mixed integer quadratic programming approach in this thesis.

In the next section, we will explain the different steps in the distributed optimization approach along the outline of this thesis.

1.6 Thesis Outline

The outline of this thesis is schematically given in Figure 1.5. The distributed optimization approach requires a model of the heavy-duty vehicle that approximates the behavior of the heavy-duty vehicle while at the same time is sufficiently simple to be used for optimization and control. A convex (low-fidelity) vehicle model of the heavy-duty vehicle is for this purpose developed and will be presented in Chapter 2.

This vehicle model is used in Chapter 3 to find the optimal complete vehicle energy management strategy for the case where all disturbances, e.g., the velocity and road slope, are known a priori. This chapter, which is based on [101, 102, 99], provides key results on the fuel reduction that can be expected by smart control of multiple subsystems in a unified CVEM strategy. These results provide a benchmark for the real-time CVEM strategy developed in Chapter 4.

In Chapter 4, which is based on [103, 100], the disturbances are not known a priori, but are predicted over a horizon. The distributed optimal control problem is solved at each time instant and only the decisions at the first time instant are implemented, as with distributed model predictive control. The real-time strategy is evaluated on the low-fidelity vehicle model and compared with the benchmark results of Chapter 3.

In Chapter 5, which is based on [100], the real-time CVEM strategy is implemented in a complex high-fidelity vehicle model to analyze its performance in a realistic simulation environment. Finally, Chapter 6 presents the major conclusions, recommendations and implications that follow from this research on distributed optimization for CVEM.

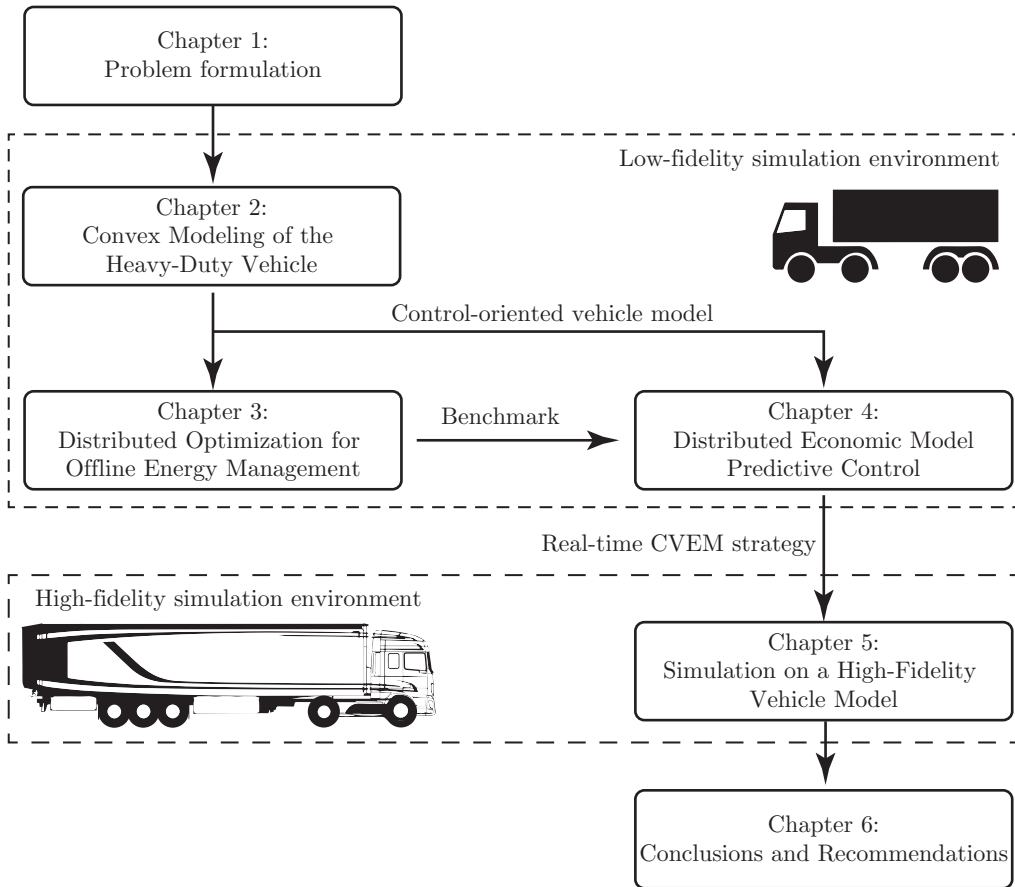


Figure 1.5: Thesis outline.

1.7 Publications

The research described in this thesis, also led to the following publications.

- T.C.J. Romijn, M.C.F. Donkers, J.T.B.A. Kessels, and S. Weiland. A dual decomposition approach to complete energy management for a heavy-duty vehicle. *In Proceedings 53rd Annual Conference on Decision and Control, 2014.*
- T.C.J. Romijn, M.C.F. Donkers, J.T.B.A. Kessels, and S. Weiland. Complete vehicle energy management with large horizon optimization. *In Proceedings 54rd Annual Conference on Decision and Control, 2015.*

-
- T.C.J. Romijn, M.C.F. Donkers, J.T.B.A. Kessels, and S. Weiland. Receding horizon control for distributed energy management of a hybrid truck with auxiliaries. *In Proceedings IFAC Workshop on Engine and Powertrain Control, Simulation and Modeling, 2015.*
 - Z. Khalik, T.C.J. Romijn, M.C.F. Donkers, and S. weiland. Effects of battery charge acceptance and battery aging in complete vehicle energy management. *In Proceedings IFAC World Congress, 2017.*
 - T.C.J. Romijn, M.C.F. Donkers, J.T.B.A. Kessels, and S. Weiland. A distributed optimization approach for complete vehicle energy management. *Submitted to IEEE Transactions on Control Systems Technology.*
 - T.C.J. Romijn, M.C.F. Donkers, J.T.B.A. Kessels, and S. Weiland. Real-time distributed model predictive control for complete vehicle energy management. *MDPI Energies: Special issue on Energy Management Control*

2

Convex Modeling of a Heavy-Duty Vehicle

Abstract - *In this chapter, a low-fidelity control-oriented model of a heavy-duty vehicle, suitable for a model-based energy management approach, is presented. The vehicle model is entirely defined in the input and output power of each subsystem, which allows the topology of the vehicle to be fully described by the power balances on the mechanical, high-voltage and low-voltage network. The input-output power behavior of all subsystems is approximated with a strictly convex quadratic equality constraint. The dynamics of particular subsystems in the vehicle, i.e., the energy in the high-voltage battery, the low-voltage battery, the refrigerated semi-trailer, the air-supply system and climate control system are described by a linear differential equation. The behavior of each subsystem is compared with simulation data from the high-fidelity vehicle model to quantify the approximation error.*

2.1 Introduction

Many design processes are nowadays model-based to reduce design time and costs. This means that a model, in this case a vehicle model, is used to design, optimize and analyse different aspects of the vehicle, such as, the impact of the vehicle configuration on the fuel consumption. The models used for design, optimization and analysis are generally not the same. Two different models will be used in this research. A high-fidelity vehicle model of the heavy-duty vehicle, developed by the Institute für Kraftfahrzeugen Aachen (see [28, 76]), that is used to analyse the fuel reduction of the Complete Vehicle Energy Management (CVEM) strategy without the need for testing on the real vehicle. These analyses will be presented in Chapter 5 together with a detailed explanation of the high-fidelity vehicle model. This model can accurately simulate the behavior of the heavy-duty vehicle, but is not suitable for optimal control due to its large complexity.

Therefore, a second, low-fidelity vehicle model will be presented in this chapter, that is suitable for optimization. This model is a simplified model of the heavy-duty vehicle for which we use only (strictly) convex functions and is essential to take a distributed optimization approach to CVEM. The approximated behavior of each subsystem in the vehicle is compared with measured data from experiments or simulation data from the high-fidelity vehicle model to demonstrate that the usage of only (strictly) convex functions is not overly restrictive. The model will be introduced in a continuous-time framework. In Chapter 3 and Chapter 4 we will derive a discrete-time model specifically for each chapter from the continuous-time model. The sampling times in the discrete-time approach are taken relatively large, e.g., 1 second or larger, as faster time dynamics do not have a significant influence on fuel consumption. This is commonly referred to as a quasi-static modeling approach (see, e.g., [40]) and will explain some of the assumptions that are made in this chapter.

The remaining sections of this chapter are organized as follows. A power-based vehicle topology describing the interconnection of all subsystems in the heavy-duty vehicle is discussed in the second section. In Section 3, the models of each of the subsystems will be presented and finally, Section 4 provides conclusions and a discussion on the models presented in this chapter.

2.2 Objective and Topology

The objective in energy management is to minimize the cumulative fuel consumption, i.e.,

$$\min_{\dot{m}_f} \int_0^{t_f} \dot{m}_f(t) dt \quad (2.1)$$

for $t_f \in \mathbb{R}_+$ where \dot{m}_f is the fuel consumption rate and needs to be solved subject to all the constraints acting on the vehicle and the subsystems in the vehicle. These constraints and subsystem models will be developed below. The fuel consumption of the engine typically depends on the engine output power and engine speed, i.e., $\dot{m}_f(t) = \dot{m}_f(y_{\text{ice}}(t), \omega_{\text{ice}}(t))$, where the engine output power at time $t \in \mathbb{R}_+$ is defined as

$$y_{\text{ice}}(t) = T_{\text{ice}}(t)\omega_{\text{ice}}(t), \quad (2.2)$$

where $T_{\text{ice}}(t)$ is the engine torque at time t and $\omega_{\text{ice}}(t)$ is the engine speed at time $t \in \mathbb{R}_+$. We can also define the engine input power by

$$u_{\text{ice}}(t) = H_0 \dot{m}_f(t), \quad (2.3)$$

where H_0 is the constant lower heating value of the fuel in kJ/kg . The definition of the engine input power allows (2.1) to be rewritten in a more general expression of minimizing the energy consumption, i.e.,

$$\min_{u_{\text{ice}}} \int_0^{t_f} u_{\text{ice}}(t) dt. \quad (2.4)$$

which has the same optimal solution as (2.1) because H_0 is a constant value. In (2.4), the engine input power is a function of the engine output power and engine speed, i.e., $u_{\text{ice}}(t) = u_{\text{ice}}(y_{\text{ice}}(t), \omega_{\text{ice}}(t))$ for which an approximation is given in Section 2.3.1. Indeed, each of the subsystems in the heavy-duty vehicle can be expressed in terms of their input and output power, as is done in [29] for a hybrid electric vehicle.

The subsystems considered throughout this thesis are shown in Figure 2.1. The topology under consideration includes an internal combustion engine (ICE),

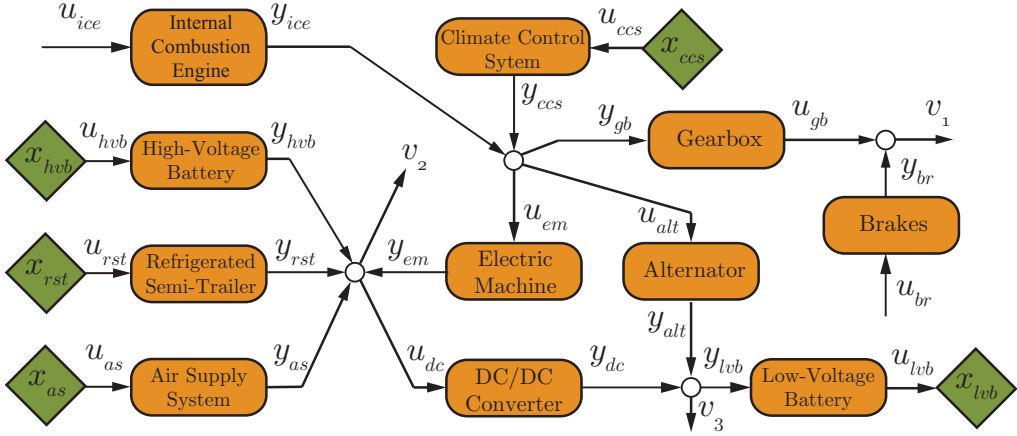


Figure 2.1: Topology of a hybrid truck with high-voltage and low-voltage auxiliaries and where the arrows indicate the direction of a positive power flow.

an electric machine, an alternator, a high- and low-voltage battery, a refrigerated semi-trailer, an air supply system, a DC/DC converter, a climate control system (CCS), a gearbox and mechanical friction brakes. In this figure, u_m is the (scalar) input power and y_m is the (scalar) output power for $m \in \mathcal{M} = \{\text{ice}, \text{em}, \text{hvb}, \text{rst}, \text{as}, \text{ccs}, \text{dc}, \text{lvb}, \text{alt}, \text{br}\}$. Furthermore, x_m is the state for subsystem $m \in \mathcal{M}_{\text{dyn}} = \{\text{hvb}, \text{rst}, \text{as}, \text{ccs}, \text{lvb}\} \subseteq \mathcal{M}$ that represent the energy in the energy storage devices, which is only present for the subsystems $m \in \mathcal{M}_{\text{dyn}}$, i.e., the high-voltage battery, the low-voltage battery, the refrigerated semi-trailer, the air supply system and the climate control system. We will assume that the power losses in the gearbox are negligible, i.e., $u_{\text{gb}}(t) = y_{\text{gb}}(t)$, so that the two nodes connected via the gearbox can be lumped together and the remaining three nodes in the topology where power is aggregated can be described by

$$v_1(t) - y_{\text{br}}(t) - y_{\text{ice}}(t) + u_{\text{em}}(t) + u_{\text{alt}}(t) - y_{\text{ccs}}(t) = 0, \quad (2.5a)$$

$$v_2(t) - y_{\text{em}}(t) - y_{\text{hvb}}(t) - y_{\text{rst}}(t) - y_{\text{as}}(t) + u_{\text{dc}}(t) = 0, \quad (2.5b)$$

$$v_3(t) - y_{\text{alt}}(t) - y_{\text{lvb}}(t) - y_{\text{dc}}(t) = 0, \quad (2.5c)$$

where (2.5a) gives the aggregation of mechanical power at the mechanical side of the topology, (2.5b) gives the aggregation of high-voltage power at the high-voltage side of the topology and (2.5c) gives the aggregation of low-voltage power

at the low-voltage side of the topology. In (2.5), $v_1(t)$, $v_2(t)$ and $v_3(t)$ are the disturbances acting on each node, which are the power required to follow a specified velocity profile, the power required for unmodeled high-voltage loads and the power for unmodeled low-voltage loads, respectively. These disturbances can either be assumed to be known as in Chapter 3 or predicted as in Chapter 4.

To complete the vehicle model for the topology given in Figure 2.1, a model is required for each of the subsystems that describes the input power u_m , the output power y_m for $m \in \mathcal{M}$ and the state x_m for $m \in \{\text{hvb, lvb, rst, as, ccs}\}$.

2.3 Subsystem Modeling

In this section, the models will be given for each of the subsystems in the heavy-duty vehicle. For all these subsystems, the relation between the input and output power is approximated with a quadratic equality constraint, i.e.,

$$\frac{1}{2}q_m(t)u_m(t)^2 + f_m(t)u_m(t) + e_m(t) + y_m(t) = 0, \quad (2.6a)$$

for all $m \in \mathcal{M}$ with (time-dependent) efficiency coefficients $q_m(t) \in \mathbb{R}_+$, $f_m(t) \in \mathbb{R}$ and $e_m(t) \in \mathbb{R}$. The input power is constrained to

$$\underline{u}_m(t) \leq u_m(t) \leq \bar{u}_m(t), \quad (2.6b)$$

for all $m \in \mathcal{M}$. Furthermore, we model the energy in the dynamic subsystems with a linear differential equation, i.e.,

$$\frac{d}{dt}x_m(t) = \tilde{A}_m x_m(t) + \tilde{B}_{m,w} w_m(t) + \tilde{B}_{m,u} u_m(t), \quad (2.6c)$$

for all $m \in \mathcal{M}_{\text{dyn}} = \{\text{hvb, lvb, rst, as, ccs}\}$ and with specific matrices \tilde{A}_m , $\tilde{B}_{m,w}$, $\tilde{B}_{m,u}$ and disturbance $w_m(t)$ and where the energy stored inside the subsystem is constrained to

$$\underline{x}_m \leq x_m(t) \leq \bar{x}_m. \quad (2.6d)$$

for all $m \in \mathcal{M}_{\text{dyn}}$. Modeling each of the subsystems with (2.6) will lead in Chapter 3 and Chapter 4 to an energy management problem that can be solved by solving multiple linearly constrained quadratic programs, for which many

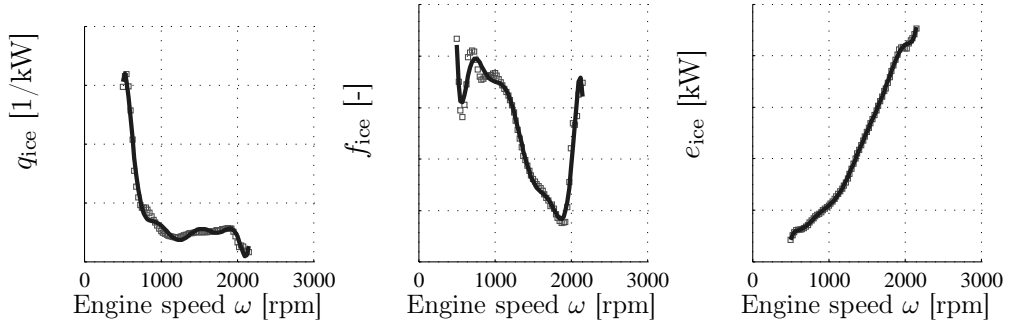


Figure 2.2: Polynomial approximation of the efficiency coefficients of the internal combustion engine.

(embedded) solvers exists. We will show below that each of the subsystems in the heavy-duty vehicle can be accurately modeled as in (2.6).

2.3.1 Internal Combustion Engine

The internal combustion engine (ICE) of the vehicle considered in this thesis is an 11 litre Euro VI engine. In this work, only the fuel consumption of the ICE is considered, but extensions to take into account the emissions and thermal management are interesting and have been done in, e.g., [19, 80]. The energy management problem will be solved with a quasi-static approach with relatively large sample time intervals, i.e., 1 second or larger, so that fast dynamics of the ICE can be neglected (see, e.g., [40]).

By neglecting the fast dynamics of the ICE, the fuel consumption can be given by a static map, which is obtained by measuring the fuel consumption at a grid of steady-state operating points, i.e., at a grid of engine torques T_{ice} and engine speeds ω_{ice} . With the engine output and input power given by (2.2) and (2.3), respectively, the input-output power behaviour can be described by (2.6a) for $m = ice$, where the efficiency coefficients typically depend on engine speed, i.e.,

$$q_{ice}(t) = q_{ice}(\omega_{ice}), \quad f_{ice}(t) = f_{ice}(\omega_{ice}), \quad e_{ice}(t) = e_{ice}(\omega_{ice}). \quad (2.7)$$

These functions can be estimated directly by solving a least-squares problem that minimizes the difference between the input-output power behaviour as in (2.6a) with the measured input-output power behavior. Depending on the type of func-

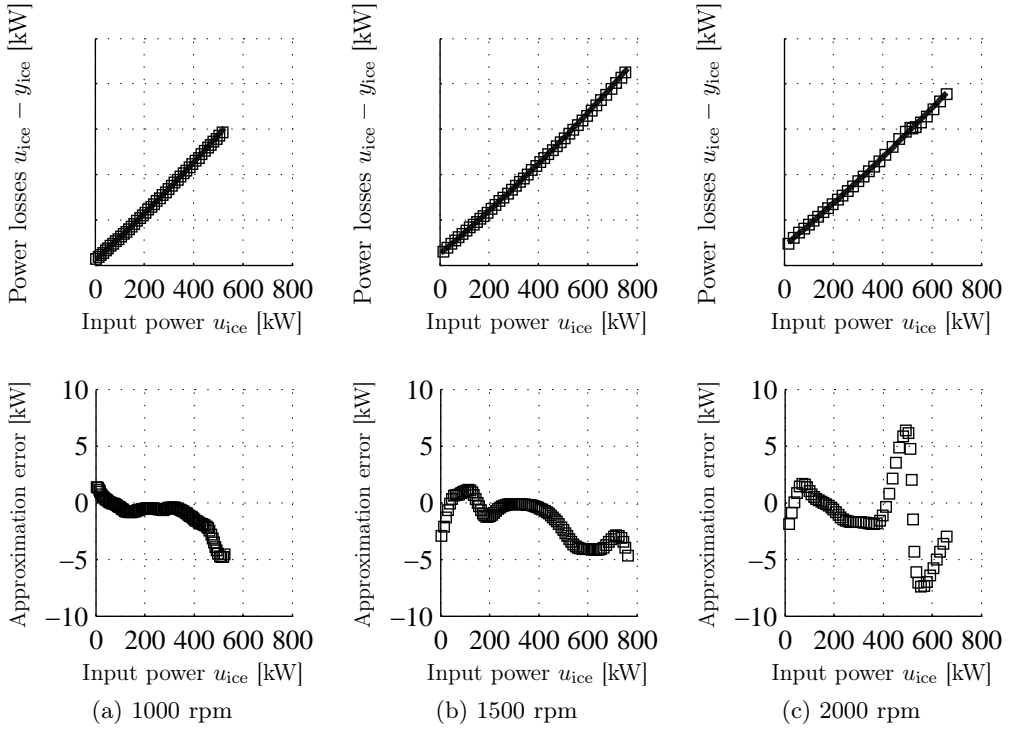


Figure 2.3: Approximation of the power losses in the internal combustion engine and the approximation error.

tions, this can be hard as the functions as well as the output power depends on the engine speed. A more simple, yet indirect, approach is taken, which amounts to finding the coefficients \tilde{q}_{ice} , \tilde{f}_{ice} , and \tilde{e}_{ice} through a quadratic approximation of the measured input-output behavior as in (2.6a) for a grid of steady-state engine operating speeds. The second step is to solve a least-squares problem that minimizes the difference between the functions $q_{ice}(\omega_{ice})$, $f_{ice}(\omega_{ice})$ and $e_{ice}(\omega_{ice})$ and the gridded coefficients \tilde{q}_{ice} , \tilde{f}_{ice} , and \tilde{e}_{ice} . With this method, the type of functions is not restricted and can even be linear interpolation. Still, a polynomial expressions is preferred as these functions can be evaluated computationally efficient on an embedded platform. The polynomial approximation as well as the coefficients \tilde{q}_{ice} , \tilde{f}_{ice} , and \tilde{e}_{ice} are shown in Figure 2.2.

Note that the quadratic equality constraint on the input-output power implies power losses, i.e., $u_{ice} - y_{ice} > 0$, that are quadratic in the input power. The measured power losses are compared with the modeled power losses in Figure 2.3

for three different engine speeds. The approximation error on the input-output behaviour is within 1 % of the maximum engine input power at 1000 and 1500 rpm and within 1.4 % at 2000 rpm. Note that the power losses as function of the engine input power can also be approximated well with a (more simple) linear function. However, this mapping is not strictly convex, which is not favorable for the dual decomposition approach as will be explained the next chapter.

Finally, the input power is constrained to (2.6a) for $m = \text{ice}$, where the minimum input power $\underline{u}_{\text{ice}}(t) = \underline{u}_{\text{ice}}(\omega_{\text{ice}})$ and maximum input power $\bar{u}_{\text{ice}}(t) = \bar{u}_{\text{ice}}(\omega_{\text{ice}})$ typically depend on engine speed.

2.3.2 Electric Machine

The electric machine subsystem of the vehicle considered in this thesis is the combination of the integrated starter generator (ISG) from ZF and an inverter that allows the alternating current ISG to be connected to the high-voltage direct current board net of the vehicle. The electric machine can be operated in two modes, i.e., the motor mode and the generator mode. In the motor mode, energy is flowing from the electrical side to the mechanical side creating a positive mechanical torque to provide for part of the requested vehicle propulsion torque. In the generator mode, energy is flowing from the mechanical side to the electrical side resulting in a negative torque on the mechanical side that can be used to decelerate the vehicle, i.e., regenerative braking.

Similar as with the internal combustion engine, the fast dynamics are neglected such that the component characteristics are given by a map with power losses at steady-state operating conditions, i.e., at a grid of electric machine torques T_{em} and speeds ω_{em} . The input power of the electric machine is defined as

$$u_{\text{em}}(t) = T_{\text{em}}(t)\omega_{\text{em}}(t) \quad (2.8)$$

and the output power is defined as

$$y_{\text{em}}(t) = U_{\text{HV}}(t)I_{\text{em}}(t) \quad (2.9)$$

where $U_{\text{HV}}(t)$ is the voltage of the high-voltage board net and $I_{\text{em}}(t)$ is the current flowing through the electric machine. The electric machine input-output power behaviour can be described by (2.6a) for $m = \text{em}$, where the efficiency coefficients

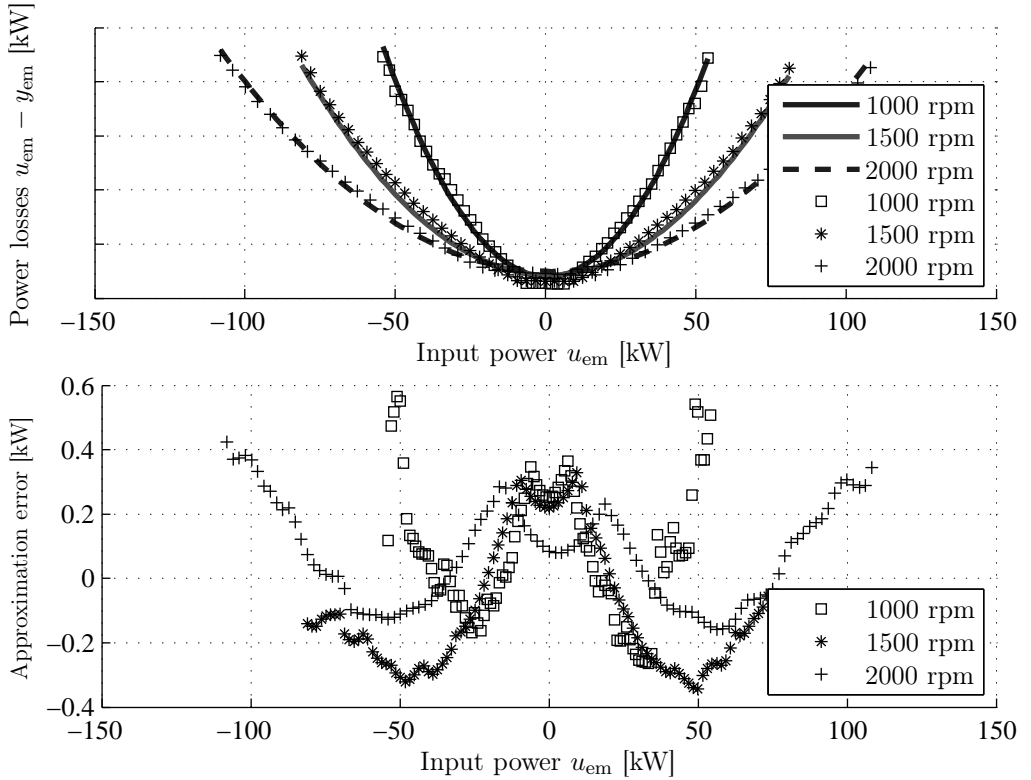


Figure 2.4: Approximation of the power losses in the electric machine and the approximation error.

typically depend on the electric machine speed, i.e.,

$$q_{em}(t) = q_{em}(\omega_{em}), \quad f_{em}(t) = f_{em}(\omega_{em}), \quad e_{em}(t) = e_{em}(\omega_{em}). \quad (2.10)$$

These functions are estimated with the same indirect approach as used for the internal combustion engine, i.e., the coefficients \tilde{q}_{em} , \tilde{f}_{em} , and \tilde{e}_{em} are estimated through a quadratic approximation of the measured input-output behavior as in (2.6a) for a grid of steady-state electric machine operating speeds. The second step is to solve a least-squares problem that minimizes the difference between the functions $q_{em}(\omega_{em})$, $f_{em}(\omega_{em})$ and $e_{em}(\omega_{em})$ and the gridded coefficients \tilde{q}_{em} , \tilde{f}_{em} , and \tilde{e}_{em} . Again, a polynomial expression is preferred as these functions can be evaluated computationally efficient on an embedded platform. The measured power losses, i.e., $u_{em} - y_{em} > 0$, are compared with the modeled power losses in

Figure 2.4 for three different electric machine speeds. The approximation error on the input-output behavior of the electric machine is within 0.6 % of the maximum electric machine input power.

Finally, the electric machine input power is constrained to (2.6b) for $m = \text{em}$ where the minimum input power $\underline{u}_{\text{em}}(t) = \underline{u}_{\text{em}}(\omega_{\text{em}})$ and maximum input power $\overline{u}_{\text{em}}(t) = \overline{u}_{\text{em}}(\omega_{\text{em}})$ depend on the electric machine speed.

2.3.3 Alternator

The alternator is similar to the electric machine. A major difference is that the alternator is only used in generator mode to supply power to the low-voltage board net in the vehicle. The input power is similarly defined as

$$u_{\text{alt}}(t) = T_{\text{alt}}(t)\omega_{\text{alt}}(t) \quad (2.11)$$

where $T_{\text{alt}}(t)$ is the alternator torque and $\omega_{\text{alt}}(t)$ is the alternator speed. The output power is defined as

$$y_{\text{alt}}(t) = U_{\text{LV}}(t)I_{\text{alt}}(t) \quad (2.12)$$

where $U_{\text{LV}}(t)$ is the voltage of the low-voltage board net and $I_{\text{alt}}(t)$ is the current flowing through the alternator. The input-output behavior can be described by (2.6a) for $m = \text{alt}$ where the efficiency coefficients typically depend on the alternator speed, i.e.,

$$q_{\text{alt}}(t) = q_{\text{alt}}(\omega_{\text{alt}}), \quad f_{\text{alt}}(t) = f_{\text{alt}}(\omega_{\text{alt}}), \quad e_{\text{alt}}(t) = e_{\text{alt}}(\omega_{\text{alt}}). \quad (2.13)$$

A measured efficiency map is not available for the alternator. Still, the high-fidelity vehicle model that will be presented in Chapter 5 includes a model of the alternator. The simulated power losses over a drive cycle are used here to obtain the functions $q_{\text{alt}}(\omega_{\text{alt}})$, $f_{\text{alt}}(\omega_{\text{alt}})$ and $e_{\text{alt}}(\omega_{\text{alt}})$. These functions are estimated with the same indirect approach as used for the internal combustion engine, i.e., the coefficients \tilde{q}_{alt} , \tilde{f}_{alt} , and \tilde{e}_{alt} are estimated through a quadratic approximation of the measured input-output behavior as in (2.6a) for a grid of steady-state alternator operating speeds. The second step is to solve a least-squares problem that minimizes the difference between the functions $q_{\text{alt}}(\omega_{\text{alt}})$, $f_{\text{alt}}(\omega_{\text{alt}})$ and

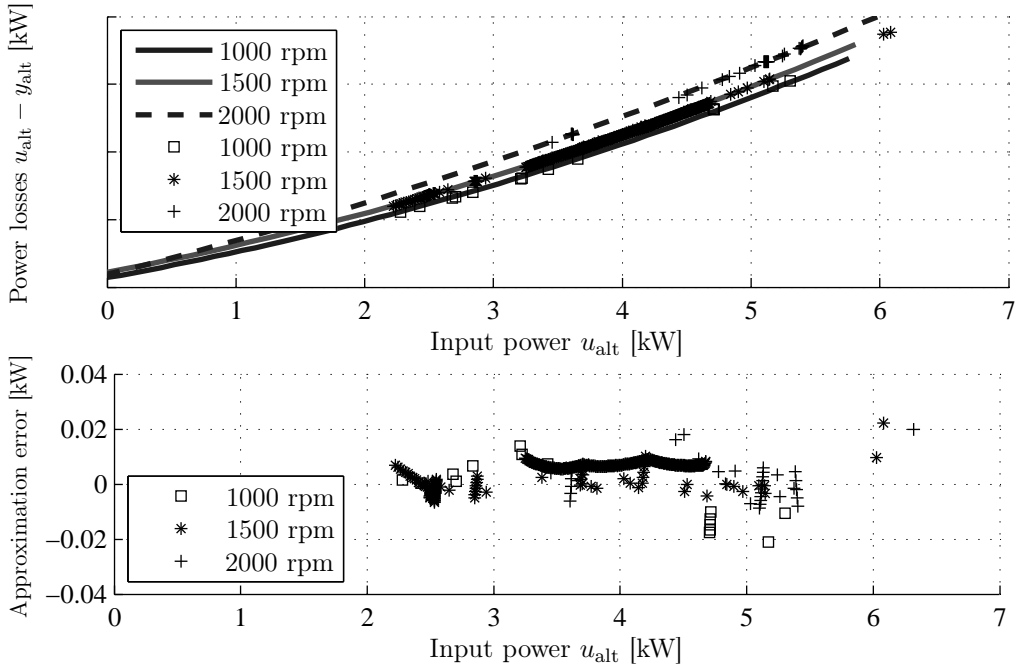


Figure 2.5: Approximation of the power losses in the alternator and the approximation error.

$e_{\text{alt}}(\omega_{\text{alt}})$ and the gridded coefficients \tilde{q}_{alt} , \tilde{f}_{alt} , and \tilde{e}_{alt} . Again, a polynomial expression is preferred as these functions can be evaluated computationally efficient on an embedded platform. The measurements are compared with the modeled power losses in Figure 2.5 for three different alternator speeds. The approximation error on the input-output behavior of the alternator is within 0.3 % of the maximum alternator input power.

Finally, the alternator input power is constrained to (2.6b) for $m = \text{alt}$, where the minimum input power $\underline{u}_{\text{alt}}(t) = \underline{u}_{\text{alt}}(\omega_{\text{alt}})$ and maximum input power $\overline{u}_{\text{alt}}(t) = \overline{u}_{\text{alt}}(\omega_{\text{alt}})$ depend on the alternator speed.

2.3.4 DCDC Converter

The heavy-duty vehicle is also equipped with a DCDC converter, which allows energy from the high-voltage domain to be converted to energy for the low-voltage

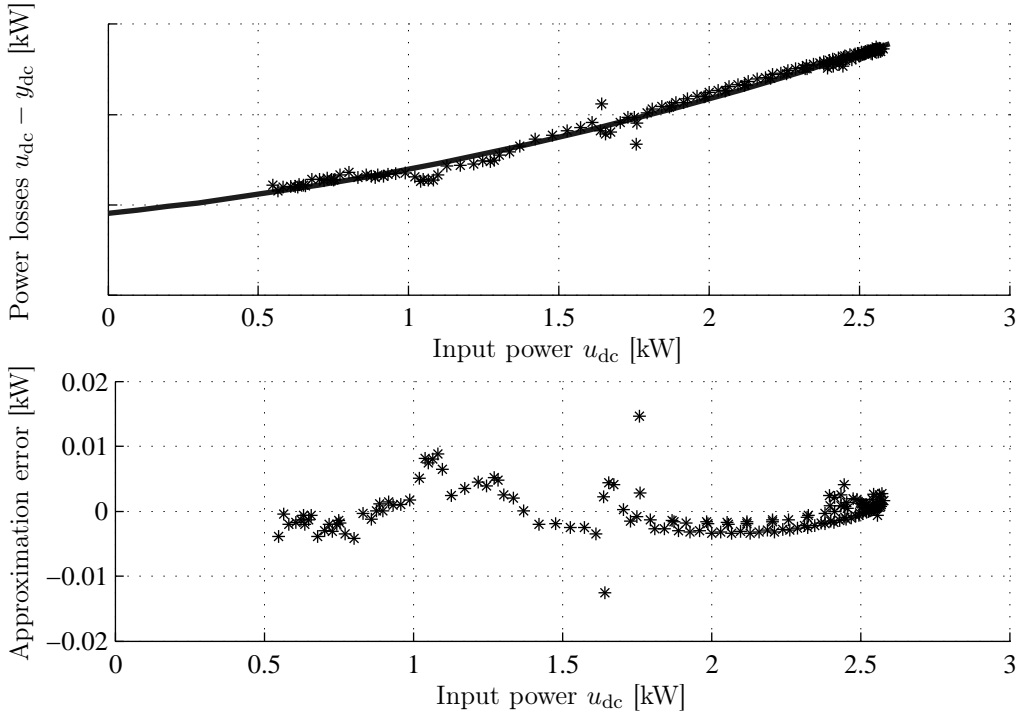


Figure 2.6: Approximation of the power losses in the DCDC converter and the approximation error.

domain. The input and output power of the DCDC converter are defined by

$$u_{dc}(t) = I_{dc,high}(t)U_{HV}(t), \quad (2.14a)$$

$$y_{dc}(t) = I_{dc,low}(t)U_{LV}(t), \quad (2.14b)$$

respectively, where $I_{dc,high}(t)$ is the DCDC current at the high-voltage side, $I_{dc,low}(t)$ is the DCDC current at the low-voltage side, $U_{HV}(t)$ is the voltage at the high-voltage board net and $U_{LV}(t)$ is the voltage at the low-voltage board net. The input-output power behavior can be described by (2.6a) for $m = dc$, with constant efficiency coefficients $q_{dc}(t) = q_{dc}$, $f_{dc}(t) = f_{dc}$ and $e_{dc}(t) = e_{dc}$. A measured efficiency map is not available for the DCDC converter as well. Still, the high-fidelity vehicle model includes the DCDC converter and the simulated power losses are used to fit the efficiency coefficients q_{dc} , f_{dc} and e_{dc} . In particular, these coefficients are obtained by solving a least-squares problem, minimizing the difference between the input-output behavior as in (2.6a) and the measured

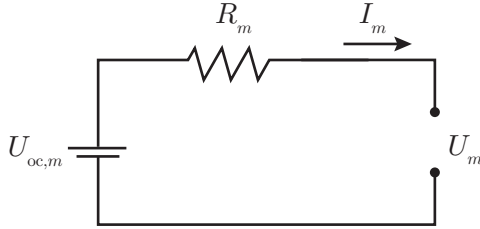


Figure 2.7: Battery equivalent circuit model.

input-output behavior. The measurements are compared with the modeled power losses in Figure 2.6. The approximation error on the input-output behavior of the DCDC converter is within 0.6 % of the maximum input power.

Finally, the DCDC converter input power is constrained to (2.6b) for $m = \text{dc}$, where the minimum input power $\underline{u}_{\text{dc}}(t) = \underline{u}_{\text{dc}}$ and the maximum input power $\bar{u}_{\text{dc}}(t) = \bar{u}_{\text{dc}}$ are constant.

2.3.5 High- and Low-Voltage Battery System

The vehicle includes a 660 Volt high-power lithium iron phosphate battery (high-voltage battery) connected to the high-voltage network and a 24 Volt lead-acid battery (low-voltage battery) connected to the low-voltage network. Both batteries in the vehicle are modeled using an equivalent circuit model as shown in Figure 2.7. This model contains a voltage source with a constant open circuit voltage $U_{\text{oc},m}$ in series with a resistance R_m and is frequently used for energy management applications (see, e.g., [22, 40]). The Kirchhoff's voltage law for this battery model is given by

$$U_m(t) - U_{\text{oc},m} + I_m(t)R_m = 0, \quad (2.15)$$

for $m \in \{\text{hvb}, \text{lvb}\}$. By defining the battery output power as $y_m(t) = U_m(t)I_m(t)$ and the battery input power as $u_m(t) = U_{\text{oc},m}I_m(t)$, (2.15) can be rewritten as (2.6a) with $q_m = \frac{R_m}{U_{\text{oc},m}^2}$, $f_m = -1$ and $e_m = 0$ for $m \in \{\text{hvb}, \text{lvb}\}$. The input power of the high-voltage and low-voltage battery is constrained to (2.6b) for $m \in \{\text{hvb}, \text{lvb}\}$ where the minimum power $\underline{u}_m(t) = \underline{u}_m$ and maximum power $\bar{u}_m(t) = \bar{u}_m$ for $m \in \{\text{hvb}, \text{lvb}\}$ are constant. The battery charge dynamics can

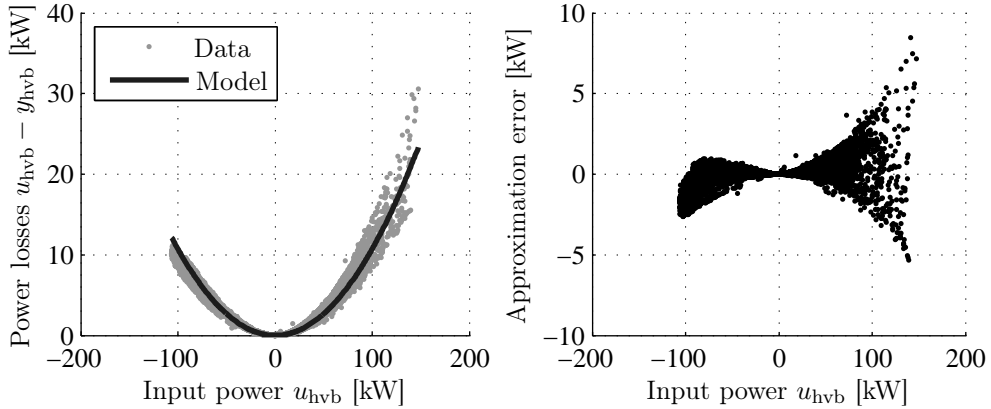


Figure 2.8: Approximation of the power losses in the high-voltage battery and the approximation error.

approximately be related to the current $I_m(t)$ (see, e.g., [40]) with

$$\frac{d}{dt}Q_m(t) = -I_m(t), \quad (2.16)$$

for $m \in \{\text{hvb}, \text{lvb}\}$ where $Q_m(t)$ is the battery charge and negative current is defined as charging the battery. The energy in the battery is given by

$$x_m(t) = Q_m(t)U_{oc,m}, \quad (2.17)$$

so that (2.16) can be rewritten as (2.6c) for $m \in \{\text{hvb}, \text{lvb}\}$ with $\tilde{A}_m = 0$, $\tilde{B}_{m,w} = 0$, $w_m(t) = 0$ and $\tilde{B}_{m,u} = -1$. This equation is obtained by taking the derivative of $x_m(t)$ with respect to time and assuming that the open-circuit voltage is time independent. Furthermore, the energy in the battery is constrained to (2.6d) for $m \in \{\text{hvb}, \text{lvb}\}$.

The power losses in the high-voltage battery, i.e., $u_{hvb} - y_{hvb} > 0$, and low-voltage battery, i.e., $u_{lvb} - y_{lvb}$, according to the equivalent circuit model are shown in Figure 2.8 and Figure 2.9, respectively. The power losses are compared with simulation data from the high-fidelity simulation models of the high-voltage and low-voltage battery (see Chapter 5). It can be observed that the equivalent circuit model as in Figure 2.7 does not fully capture the input-output behavior of the high-fidelity simulation models. The approximation error is mainly caused by the complex dynamic behaviour of the high-fidelity battery simulation models.

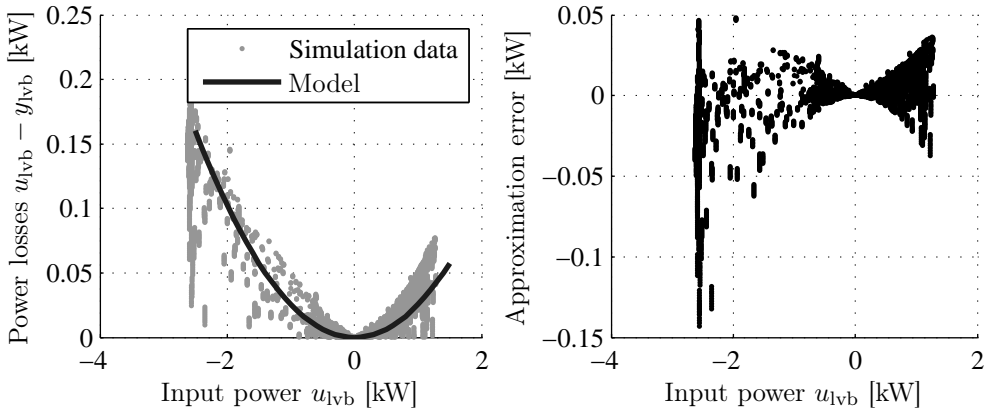


Figure 2.9: Approximation of the power losses in the low-voltage battery and the approximation error.

The equivalent circuit model can be extended with additional capacitors and resistors as in [55], to better capture these dynamics, but each capacitor adds a state to the model, which is less attractive for optimal control.

2.3.6 Refrigerated Semi-Trailer

Modeling a refrigerated semi-trailer (RST) and its cargo load is complicated. To fully describe the dynamics, many influential factors need to be taken into account, e.g., heat transfer between the outside air and the container, heat transfer from container to the inside air and heat transfer between the food and the refrigerated air [48], which typically lead to higher order models. For optimal control, these higher-order models are computationally not attractive. Therefore, the thermal dynamics of the air inside the refrigerated semi-trailer (see Figure 2.10) is modeled with a first-order differential equation, i.e.,

$$C_{rst} \frac{d}{dt} T_{rst}(t) = u_{rst}(t) + \eta_1 (\eta_2 T_{amb} - T_{rst}(t)), \quad (2.18)$$

where C_{rst} is the thermal capacity of the air in the RST, T_{rst} is the air temperature in the RST, $u_{rst}(t)$ is the thermal power flowing into the RST where negative powers indicate cooling, η_1 is a heat transfer coefficient between the ambient temperature T_{amb} and the RST temperature and $0 \leq \eta_2 \leq 1$ is an insulation coefficient. By only modeling the air temperature in the RST, it is assumed that

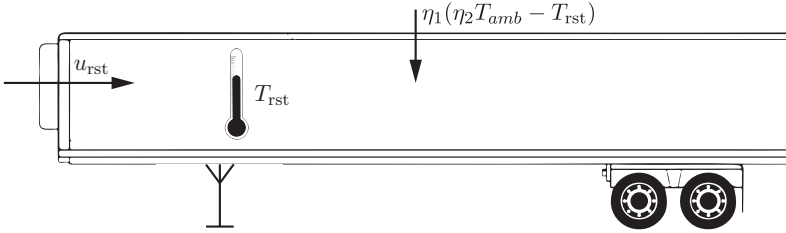


Figure 2.10: Thermal dynamics of the air inside the refrigerated semi-trailer.

the temperature of the cargo load remains within acceptable bounds as long as the air temperature remains within acceptable bounds. We can represent the RST model in terms of stored energy by defining the thermal energy relative to the ambient temperature, i.e., $x_{\text{rst}}(t) = C_{\text{rst}}(\eta_2 T_{\text{amb}} - T_{\text{rst}}(t))$ so that the thermal energy is described by (2.6c) for $m \in \{\text{rst}\}$ with $\tilde{A}_{\text{rst}} = -\frac{\eta_1}{C_{\text{rst}}}$, $\tilde{B}_{\text{rst},w} = 0$, $w_{\text{rst}}(t) = 0$ and $\tilde{B}_{\text{rst},u} = -1$. The thermal energy in the refrigerated semi-trailer is constrained to (2.6d) for $m = \text{rst}$.

A refrigerated semi-trailer is typically a switched system that can only be turned on or off, i.e., the thermal power $u_{\text{rst}}(t)$ is constrained to

$$u_{\text{rst}}(t) \in \{\underline{u}_{\text{rst}}(t), \bar{u}_{\text{rst}}(t)\}. \quad (2.19)$$

The thermal power is not continuous with this constraint and this set is not a convex set, which is not attractive for optimal control. Therefore, a model with continuous input-output behaviour is derived, which will be used to simplify the optimal control problem in some parts in this thesis. The continuous input-output behavior is described by (2.6a) for $m = \text{rst}$ with constant efficiency coefficients $q_{\text{rst}}(t) = q_{\text{rst}}$, $f_{\text{rst}}(t) = f_{\text{rst}}$ and $e_{\text{rst}}(t) = e_{\text{rst}}$. The input power constrained to (2.6b) for $m = \text{rst}$, where the minimum input power $\underline{u}_{\text{rst}}(t) = \underline{u}_{\text{rst}}$ and the maximum input power $\bar{u}_{\text{rst}}(t) = \bar{u}_{\text{rst}}$ are constant.

The high-fidelity vehicle model of the vehicle also includes a model of the refrigerated semi-trailer (see [121] for more details on this model). The input and output power for this high-fidelity vehicle model are given by

$$u_{\text{rst}}(t) = \{-4.2, \quad 0\} \text{ kW}, \quad (2.20a)$$

$$y_{\text{rst}}(t) = \{-11.6, \quad -1.6\} \text{ kW}. \quad (2.20b)$$

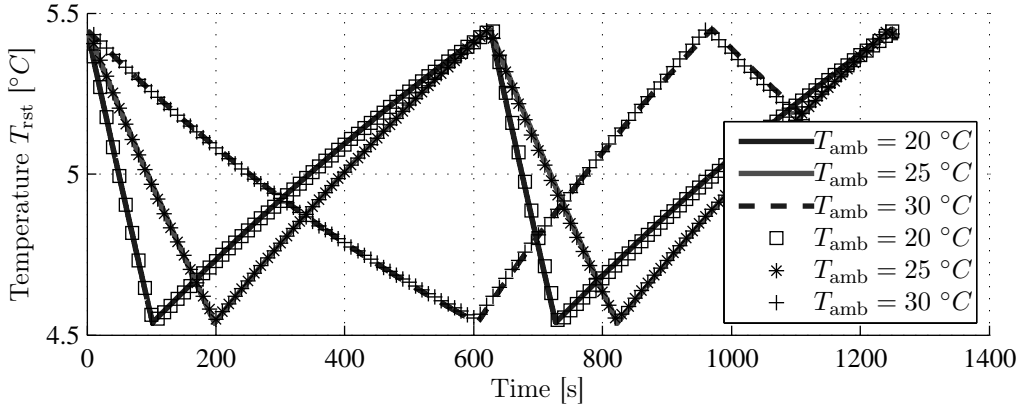


Figure 2.11: Temperature inside the refrigerated semi-trailer for different ambient temperatures compared to simulation data from the high-fidelity vehicle model.

As only two data points are available for the switched system, the coefficients q_{rst} , f_{rst} and e_{rst} are not uniquely defined. Therefore, $q_{rst} = 0.03$ is chosen in (2.6a) for which the input-output power behavior is close to linear and f_{rst} and e_{rst} are calculated such that (2.20) is satisfied. Note that q_{rst} is required to be slightly positive for strict convexity, which is necessary for the distributed optimization approach.

The air temperature of the refrigerated semi-trailer is shown in Figure 2.11 for three different ambient temperatures and a default hysteresis controller where the cooling is turned on when the temperature hits the upper bound and turned off when the temperature hits the lower bound. Also the air temperature from the high-fidelity vehicle model is shown, which demonstrates that the first-order differential equation (2.18) approximates the high-fidelity vehicle model well. Here, the parameters C_{rst} , η_1 and η_2 depend on the ambient temperature to arrive at a simplified model that is close to the behavior of the high-fidelity model.

2.3.7 Air Supply System

The air supply system in the vehicle is schematically shown in Figure 2.12. In this system, air is compressed by a compressor that is driven by an electric motor. The compressed air flows through a desiccant cartridge, which removes the water from the air. As water builds up in the cartridge, compressed air is used at regular intervals to dry the cartridge, which is referred to as regeneration. The dried

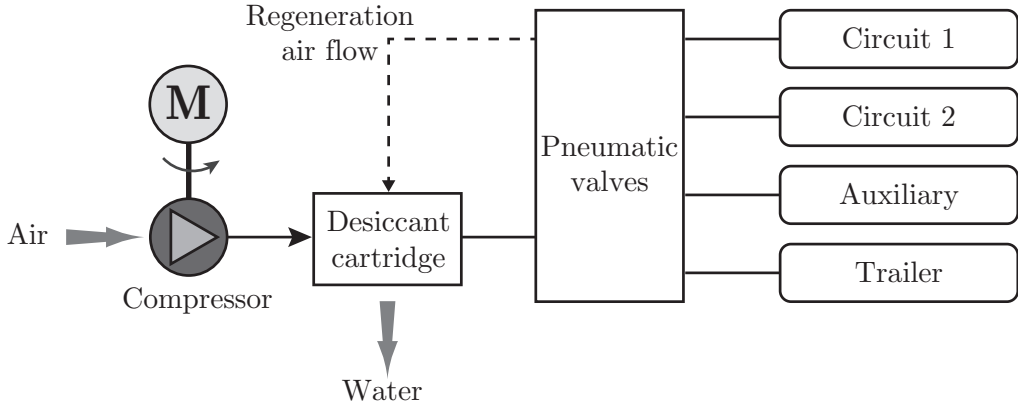


Figure 2.12: Schematic overview of the air supply system.

air is directed through a system of valves to the right air circuit in the vehicle where each circuit has at least one air vessel to store compressed air. Any vehicle configuration has at least Circuit 1 and Circuit 2, because a separate circuit is necessary for the front and rear brakes for safety reasons. Often, auxiliary circuits are installed on the vehicle depending on the application and additional air circuits might be present on the trailer as well.

To reduce the amount of states in the air supply system, the air vessels of Circuit 1 and Circuit 2 are lumped into one vessel with a lumped volume V and air pressure p_{as} . The other air vessels are not considered as they are only sometimes present and often not allowed to store air under very high pressure. The dynamics of the air pressure in the lumped system are assumed to satisfy a mass energy balance (see, e.g. [81]) given by

$$V \frac{d}{dt} p_{\text{as}}(t) = R(T_{\text{in}} \dot{m}_{\text{in}}(t) - T_{\text{out}} \dot{m}_{\text{out}}(t)), \quad (2.21)$$

where R is the specific gas constant for air, V is the lumped volume of the air tanks, $\dot{m}_{\text{in}}(t)$ is the mass flow into the air vessels with air temperature T_{in} and $\dot{m}_{\text{out}}(t)$ is the mass flow out of the air vessels with air temperature T_{out} .

We can represent the air supply model in terms of stored energy by defining the pneumatic energy relative to the ambient pressure, i.e.,

$$x_{\text{as}}(t) = \frac{(p_{\text{as}}(t) - p_{\text{amb}})V}{\gamma - 1}, \quad (2.22)$$

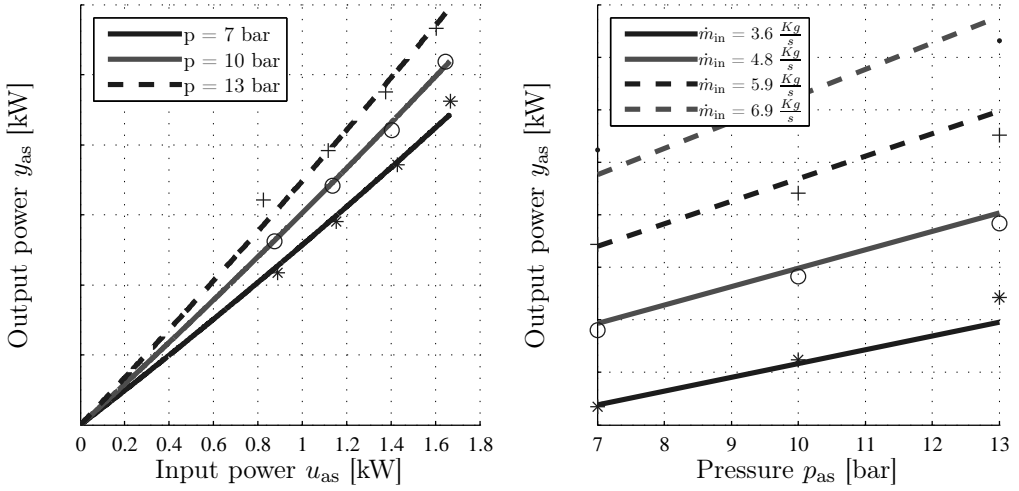


Figure 2.13: Air supply input-output power behaviour.

where p_{amb} is the ambient pressure and $\gamma = c_p/c_v$ is the ratio of specific heats (approximately 1.4 for air). Furthermore, we define the pneumatic input power by

$$u_{\text{as}}(t) = \frac{RT_{\text{in}}\dot{m}_{\text{in}}(t)}{\gamma-1}, \quad (2.23)$$

and the pneumatic power released to the environment as

$$w_{\text{as}}(t) = \frac{RT_{\text{out}}\dot{m}_{\text{out}}(t)}{\gamma-1}, \quad (2.24)$$

so that the dynamics (2.21) can be represented by (2.6c) for $m \in \{\text{as}\}$ with $\tilde{A}_{\text{as}} = 0$, $\tilde{B}_{\text{as},w} = -1$ and $\tilde{B}_{\text{as},u} = 1$. The pneumatic energy in the air supply system is constrained to (2.6d) for $m = \text{as}$.

The input-output behavior is described by (2.6a) for $m = \text{as}$ with efficiency coefficients $q_{\text{as}}(t) = q_{\text{as}}$, $f_{\text{as}}(t) = f_{\text{as}}(p_{\text{as}}(t))$ that depend on the air pressure $p_{\text{as}}(t)$ and $e_{\text{as}}(t) = e_{\text{rst}}$. These coefficients are obtained by solving a least-squares problem that minimizes the difference between the input-output power behavior as in (2.6a) and the measured input-output behavior. The quadratic input-output power behaviour is shown in Figure 2.13 together with measurement data of the compressor. The input power is constrained to (2.6b) for $m = \text{as}$ where the minimum input power $\underline{u}_{\text{as}}(t) = \underline{u}_{\text{as}}(p_{\text{as}}(t))$ and the maximum input power

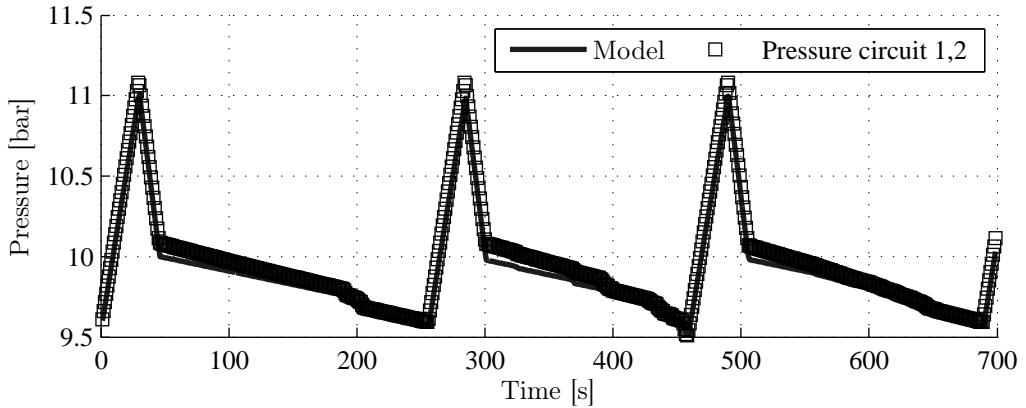


Figure 2.14: Air pressure in the air supply system compared with simulation data from the high-fidelity vehicle model.

$\bar{u}_{\text{as}}(t) = \bar{u}_{\text{as}}(p_{\text{as}}(t))$ depend on the air pressure as well.

Although, the electric motor potentially allows the air compressor to be continuously controlled, in practice the air compressor is still only switched on or off, i.e., $u_{\text{as}}(t) \in \{\underline{u}_{\text{as}}, \bar{u}_{\text{as}}\}$. The air pressure from the simplified air supply system model is compared with the air pressure in Circuit 1 and Circuit 2 of the high-fidelity vehicle model of the air supply system (see Chapter 5) in Figure 2.14.

2.3.8 Climate Control System

A schematic drawing of the climate control system in the vehicle is shown in Figure 2.15. In this system, the compressor is attached via a clutch to the engine and can only be switched on or off. The compressor pumps refrigerant vapor under high pressure to the condenser where heat is drawn from the refrigerant, which leads to condensation of the refrigerant. An expansion valve is then present to regulate the amount of refrigerant flowing to the evaporator. In the evaporator, the refrigerant absorbs heat from the air flow. The cooled (and possibly dehumidified) air flow is directed through a heat exchanger with warm air from the internal combustion to have the air with the right air temperature send to the cabin. The heated refrigerant vapor coming from the evaporator is then fed back to the compressors again. A simplified version of the model developed in [118] will be used to model the behaviour of the climate control system. As in [118],

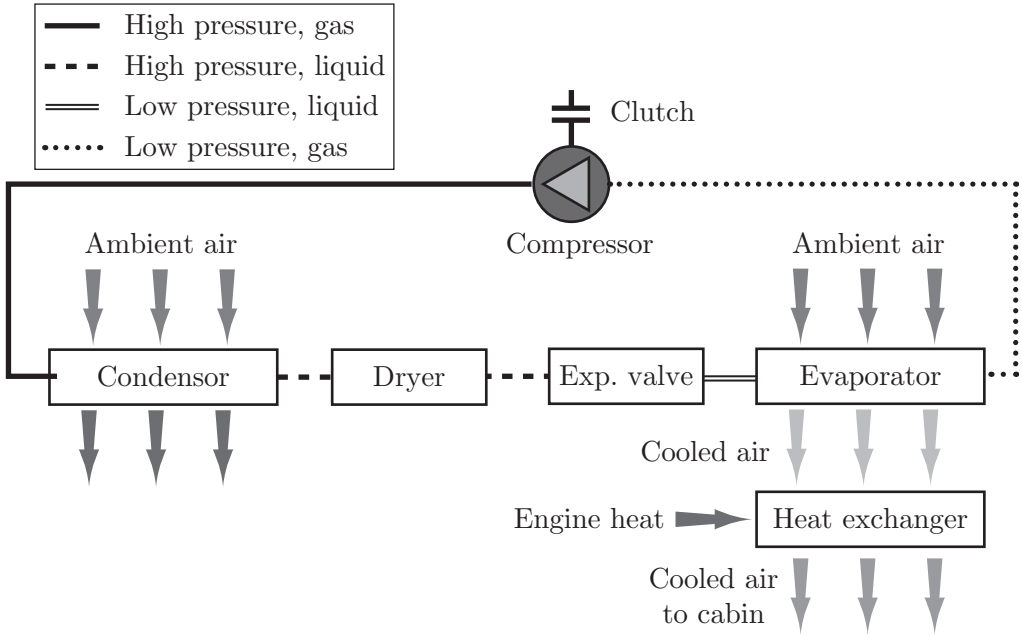


Figure 2.15: Schematic overview of a climate control system in a heavy-duty vehicle.

only the evaporator is modeled, which is assumed to satisfy a coupled thermal energy balance given by

$$C_r \frac{d}{dt} T_r(t) = h_i(T_w(t) - T_r(t)) + u_{ccs}(t), \quad (2.25a)$$

$$C_w \frac{d}{dt} T_w(t) = Q_1(T_{amb}, \Phi_{amb}) + h_o(T_{amb} - T_w(t)) + h_i(T_r(t) - T_w(t)), \quad (2.25b)$$

where C_r and C_w are the heat capacities of the refrigerant and the walls of the evaporator, respectively, $T_r(t)$ and $T_w(t)$ are the temperatures of the refrigerant and walls of the evaporator, respectively, $u_{ccs}(t)$ is the effective cooling power from the compressor, T_{amb} is the ambient temperature, h_i and h_o are the heat transfer coefficients between the inner and outer walls of the evaporator, respectively, and Q_1 is the heat generated when the inlet air is condensed (latent heat). For the simplified model, the latent heat is assumed to only depend on the ambient air temperature T_{amb} and humidity Φ_{amb} . Similar to the battery, we can represent the CCS model in terms of stored energy by defining the thermal energy in the

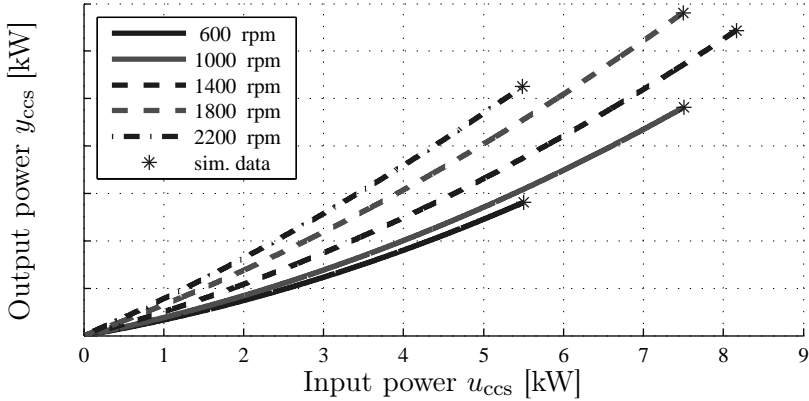


Figure 2.16: Input-output power behaviour of the climate control system for different engine speeds.

wall and refrigerant relative to the ambient temperature, i.e.,

$$x_{\text{ccs}}(t) = [C_r (T_{\text{amb}} - T_r(t)) \quad C_w (T_{\text{amb}} - T_w(t))]^T, \quad (2.26)$$

which allows (2.25) to be rewritten as (2.6c) for $m = \text{ccs}$ with

$$\tilde{A}_{\text{ccs}} = \begin{bmatrix} -\frac{h_i}{C_r} & \frac{h_i}{C_w} \\ \frac{h_i}{C_r} & -\frac{(h_i + h_o)}{C_w} \end{bmatrix}, \quad \tilde{B}_{\text{ccs},w} = \begin{bmatrix} 0 \\ -1 \end{bmatrix}, \quad \tilde{B}_{\text{ccs},u} = \begin{bmatrix} -1 \\ 0 \end{bmatrix}, \quad (2.27)$$

and $w_{\text{ccs}}(t) = Q_1$. The thermal energy in the wall and refrigerant is constrained to (2.6d) for $m = \text{ccs}$.

A climate control system is typically a switched system that can only be turned on or off, i.e., the input power $u_{\text{ccs}}(t)$ is constrained to $u_{\text{ccs}}(t) \in \{\underline{u}_{\text{ccs}}(t), \bar{u}_{\text{ccs}}(t)\}$. The input power is not continuous with this constraint and this set is not a convex set, which is not attractive for optimal control. Therefore, a model with continuous input-output behaviour is derived, which will be used to simplify the optimal control problem in some parts in this thesis. The continuous input-output behavior is described by (2.6a) for $m = \text{ccs}$ with efficiency coefficients $q_{\text{ccs}}(t) = q_{\text{ccs}}$, $f_{\text{ccs}}(t) = f_{\text{ccs}}(\omega_{\text{ice}})$ that depend on the engine speed ω_{ice} and $e_{\text{ccs}}(t) = e_{\text{ccs}}$. The input power constrained to (2.6b) for $m = \text{ccs}$ where the minimum input power $\underline{u}_{\text{ccs}}(t) = \underline{u}_{\text{ccs}}(\omega_{\text{ice}})$ and the maximum input power $\bar{u}_{\text{ccs}}(t) = \bar{u}_{\text{ccs}}(\omega_{\text{ice}})$ depend on the engine speed ω_{ice} as well.

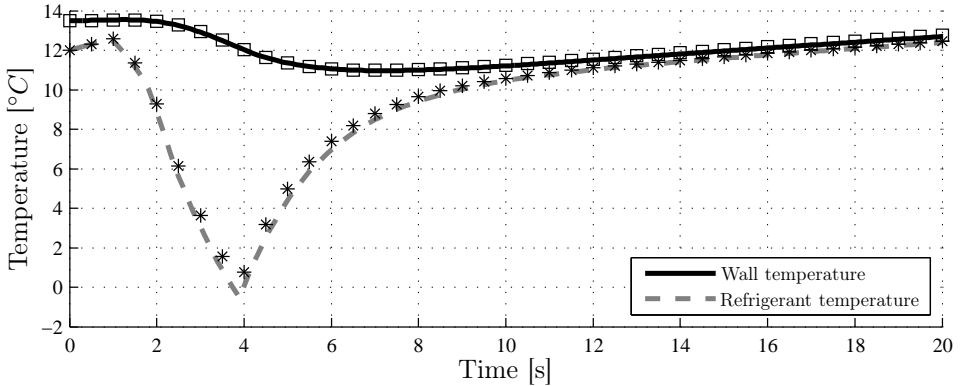


Figure 2.17: Wall and refrigerant temperature of the climate control system compared with simulation data of the high-fidelity vehicle model.

As with the refrigerated semi-trailer, only two data points are available for the switched system for a given engine speed ω_{ice} so that the coefficients q_{ccs} , f_{ccs} and e_{ccs} are not uniquely defined. Therefore $q_{ccs} = 0.03$ is chosen in (2.6a) for which the input-output power behavior is close to linear. The function $f_{ccs}(\omega_{ice})$ is described as a polynomial function of the engine speed ω_{ice} and is obtained together with e_{ccs} by solving a least-squares problem that minimizes the difference between the input-output behavior as in (2.6a) and the compressor data. Note that q_{ccs} is required to be slightly positive for strict convexity, which is necessary for the distributed optimization approach. The quadratic approximation of the input-output behavior, as well as the data points from the compressor are shown in Figure 2.16.

Furthermore, the evaporator wall temperature and refrigerant temperature of the simplified model (2.25) are compared with the evaporator wall temperature and refrigerant temperature of the high-fidelity vehicle model in Figure 2.17.

2.4 Conclusions and Discussion

The low-fidelity vehicle model of the heavy-duty hybrid vehicle, suitable for a model-based energy management approach, has been introduced and analyzed in this chapter. Defining the subsystems in terms of their input and output power allowed the topology of the vehicle to be fully described by the power balances on the mechanical, high-voltage and low-voltage network. Furthermore,

the input-output power behavior of all subsystems can be approximated well with a (strictly) convex quadratic equality constraint. Constrained states have been introduced for the high-voltage battery, the low-voltage battery, the refrigerated semi-trailer, the air-supply system and climate control system, that represent the energy in the subsystems. The dynamics for these states have been described by a linear differential equation that approximates well the simulation data from the high-fidelity vehicle model. The low-fidelity vehicle model of the heavy-duty vehicle presented in this chapter will be used to find the optimal CVEM strategy via a distributed optimization approach in the next chapter.

3

Distributed Optimization for Offline Energy Management

Abstract - In this chapter, a distributed optimization approach is presented to solve the complete vehicle energy management problem introduced in the previous chapter. The first part of the approach is a dual decomposition, which allows the underlying optimal control problem to be solved for every subsystem separately. For the second part of the approach, the optimal control problem for every subsystem is solved with three different methods. The first two methods rely on splitting the control horizon into several smaller horizons. The first method uses the Alternating Direction Method of Multipliers and divides the horizon a priori, while the second method divides the horizon iteratively by solving unconstrained optimization problems analytically. The third method, based on dynamic programming, is used to solve the optimal control problem related to subsystems with on/off control. The approach is demonstrated by solving the complete vehicle energy management problem for a pan European driving cycle. Simulation results show that the fuel consumption can be reduced up to 1.42 % by including smart auxiliaries in the energy management problem. This requires, however, that the auxiliaries are continuous controlled or that the number of switches is unbounded. More interestingly, the computation time is reduced by a factor of 64 up to 1825, compared with solving a centralized convex optimization problem.

3.1 Introduction

To efficiently manage all energy flows in the complete vehicle energy management (CVEM) problem, an energy management strategy is needed that is scalable, flexible and suitable for on/off control. Many different solution strategies for solving the energy management problem have been proposed over the past decades. The proposed solution strategies can be divided into so-called *online* and *offline* solution strategies [22, 40].

Online solution strategies are real-time implementable and rely on feedback and/or predictions and therefore cannot guarantee the global optimal solution. To verify the performance of the online solution strategies and to analyze different configurations, so-called offline solution strategies have been developed based on, e.g., dynamic programming (DP, see, e.g., [67, 1, 90]), Pontryagin's minimum principle (PMP, see, e.g., [120, 18, 110]) or convex optimization (see, e.g., [78, 31]). The offline solution strategies require all disturbances to be known (e.g., the driving cycle) so that the global optimal solution can be computed. Since disturbances are generally unknown, these strategies can, in general, not be implemented in real-time. Still, they do provide a benchmark for online solution methods and are therefore valuable tools.

While some online optimization methods can handle the complexity of the CVEM problem, the aforementioned offline optimal control methods cannot. It should be noted that multi-state energy management problems, e.g., including battery state-of-health [27], battery aging [109], thermal management [72, 65, 92] and the control of a waste heat recovery system [124] are all based on the equivalent consumption minimization strategy (ECMS), meaning that global optimality of the solution cannot be guaranteed. For the offline optimization methods, scalability is poor as the computational complexity of DP increases exponentially with the number of states and solving the two-point boundary value problem resulting from PMP is difficult, particularly when state constraints are present, see, e.g., [72] in the context of thermal dynamics. Finally, a convex approximation of the energy management problem can lead to a globally optimal solution, but still requires a large-scale optimization problem to be solved.

Distributed solutions to the energy management problem aim to remedy/resolve the complexity issue of the underlying optimizations. In [12, 81], an online im-

plementable game-theoretic approach to CVEM is shown. In [83], scalability is obtained by using the Alternating Direction Method of Multipliers (ADMM) while ideas based on ECMS are used to calculate the equivalent costs at a supervisory level. Still, these distributed solutions are all online solution methods for which the global optimal solution is not guaranteed.

In this chapter, we propose to use methods from distributed optimization to solve the convex approximation of the CVEM problem introduced in Chapter 2 and obtain the global optimal solution. This solution will be used to verify the performance of the real-time energy management strategy developed in the next chapter and to analyze the fuel reduction potential of different auxiliaries for energy management. In particular, we use the dual decomposition approach for CVEM that we first introduced in [101] in combination with efficient algorithms to solve the dual functions that we first introduced in [102]. These results have been unified and extended in [99] where the general CVEM problem is presented as a quadratically constrained linear program (QCLP).

This chapter is to a large extent based on the results presented in [99]. The approach is extended with a solution method based on dynamic programming to solve the optimal control problem related to subsystems with on/off decisions (Section 3.3.3). This solution method provides the optimal trade-off between the number of switches and fuel reduction, which will be given for the refrigerated semi-trailer, the air supply system and the climate control system.

The remainder of this chapter is organized as follows. The general optimal control problem and the application of the dual decomposition is given in Section 3.2. In Section 3.3, solution methods are presented to solve the dual functions that result from the dual decomposition. The CVEM problem is casted as an optimal control problem in Section 3.4 and, finally, the results are discussed in Section 3.5.

3.2 Distributed Optimization of Power Nets

In this section, we consider the optimal control of the energy flows in a power net, which is illustrated in Figure 3.1. The power net consists of energy storage devices, e.g., a high-voltage battery, and energy converters, e.g., an electric machine. The storage devices are connected to the converters, while the outputs $y_{m,k}$ and inputs $u_{m,k}$ of the converters are connected to each other via nodes according to

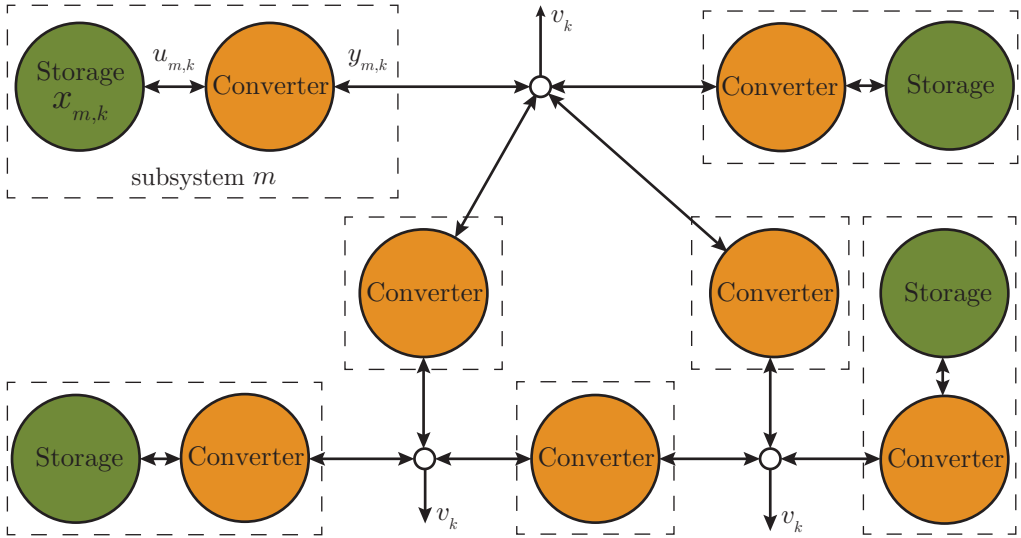


Figure 3.1: Power net with energy storage devices and energy converters.

a specific topology, i.e., energy can be exchanged directly between converters, but not directly between storage devices. At each node $n \in \{1, \dots, N\}$, there is also a known exogenous load signal $v_{n,k}$ given for each time instant k . Subsystems are composed of a combination of a converter, possibly with an energy storage device. The goal of the power net is to minimize the cumulative energy losses of all subsystems, while meeting constraints on the inputs, outputs and states in each subsystem. In this section, we will introduce the optimal control problem for this power net and we will give a dual decomposition approach to solve the optimal control problem. In Section 3.4 we will show that the complete vehicle energy management (CVEM) problem can be represented as a power net, where minimizing the energy losses is equivalent to minimizing the fuel consumption.

3.2.1 Optimal Control Problem

The optimal control problem for the power net is given by

$$\min_{\{u_{m,k}, y_{m,k}\}} \sum_{m \in \mathcal{M}} \sum_{k \in \mathcal{K}} c_m u_{m,k} - d_m y_{m,k}, \quad (3.1a)$$

where $u_{m,k} \in \mathbb{R}$ and $y_{m,k} \in \mathbb{R}$ are the (scalar) inputs and outputs of the converter in subsystem $m \in \mathcal{M} = \{1, \dots, M\}$ with M the number of subsystems and at

time instant $k \in \mathcal{K} = \{0, 1, \dots, K - 1\}$, with K the horizon length. In (3.1a), $c_m \in \mathbb{R}$ and $d_m \in \mathbb{R}_+$ are coefficients that define the energy losses in converter m . Moreover, we use the notation $\{u_{m,k}, y_{m,k}\}$ to indicate $\{u_{m,k}, y_{m,k}\}_{m \in \mathcal{M}, k \in \mathcal{K}}$. This notation will be used throughout the chapter for minimizing over a set. The optimization problem (3.1a) is to be solved subject to a quadratic equality constraint describing the input-output behavior of each converter, i.e.,

$$\frac{1}{2}q_{m,k}u_{m,k}^2 + f_{m,k}u_{m,k} + e_{m,k} + y_{m,k} = 0, \quad (3.1b)$$

with $q_{m,k} \in \mathbb{R}_+$, $f_{m,k} \in \mathbb{R}$ and $e_{m,k} \in \mathbb{R}$ being efficiency coefficients of the converter $m \in \mathcal{M}$ at time instant $k \in \mathcal{K}$, and subject to linear system dynamics of the storage device in subsystem $m \in \mathcal{M}$, i.e.,

$$x_{m,k+1} = A_m x_{m,k} + B_{m,w} w_{m,k} + B_{m,u} u_{m,k}, \quad (3.1c)$$

for all $k \in \mathcal{K}$, where the initial state $x_{m,0}$ and final state $x_{m,K}$ of the storage device are assumed to be given, $w_{m,k}$ is a known load signal at every time instant $k \in \mathcal{K}$ and the input $u_{m,k} \in \mathbb{R}$ is subject to linear inequality constraints, i.e.,

$$\underline{u}_{m,k} \leq u_{m,k} \leq \bar{u}_{m,k}, \quad (3.1d)$$

for all $k \in \mathcal{K}$, $m \in \mathcal{M}$, and the state $x_{m,k}$ is subject to linear inequality constraints, i.e.,

$$\underline{x}_{m,k} \leq x_{m,k} \leq \bar{x}_{m,k}, \quad (3.1e)$$

for all $k \in \mathcal{K}$ and $m \in \mathcal{M}$. Finally, the optimization problem is solved subject to a linear equality constraint describing the power balance in the interconnection of the subsystems, i.e.,

$$\sum_{m \in \mathcal{M}} \mathcal{A}_m u_{m,k} + \mathcal{B}_m y_{m,k} + \frac{1}{M} v_k = \mathbf{0}, \quad (3.1f)$$

for all $k \in \mathcal{K}$, where $\mathcal{A}_m \in \mathbb{R}^N$ and $\mathcal{B}_m \in \mathbb{R}^N$ are vectors with the n -th element being -1 if the power flow to node n is positive, 0 if there is no power flow to node n and 1 if the power flow to node n is negative. Here, N is the number of nodes in the topology where power is aggregated. Furthermore, the load signal

$v_k = [v_{1,k} \dots v_{N,k}]^T \in \mathbb{R}^N$ is assumed to be known at each time instant $k \in \mathcal{K}$. We define the *primal optimal solution* as the solution $\{u_{m,k}^*, y_{m,k}^*\}$ that satisfies (3.1), if it exists, and p^* as the primal optimal value of (3.1). We let $p^* = \infty$ if (3.1) has no solution.

3.2.2 Dual Decomposition and Convex Relaxation

The optimization problem (3.1) can be a large-scale problem (when K and M are large), which is not convex due to the quadratic equality constraint (3.1b). We propose in this chapter to solve (3.1) by decomposing it into several smaller problems and to relax (3.1b). In doing so, we can solve (3.1) efficiently without sacrificing optimality of the solution as we will show below. Problem (3.1a) subject to (3.1b) - (3.1f) cannot be separated due to the complicating constraint (3.1f). Therefore, we decompose the problem via dual decomposition by introducing the following so-called *partial Lagrangian*

$$L(\{u_{m,k}, y_{m,k}, \mu_k\}) = \sum_{m \in \mathcal{M}} \sum_{k \in \mathcal{K}} c_m u_{m,k} - d_m y_{m,k} + \mu_k^T (\mathcal{A}_m u_{m,k} + \mathcal{B}_m y_{m,k} + \frac{1}{M} v_k), \quad (3.2)$$

where $\mu_k \in \mathbb{R}^N$ is a Lagrange multiplier, subject to (3.1b)-(3.1e). Indeed, the partial Lagrangian (3.2) is obtained by adding the complicating constraints (the constraints that act on more than one subsystem) to the objective function in (3.1a). The *partial Lagrange dual function* is now given by

$$g(\{\mu_k\}) = \min_{\{u_{m,k}, y_{m,k}\}} L(\{u_{m,k}, y_{m,k}, \mu_k\}) = \sum_{m \in \mathcal{M}} g_m(\{\mu_k\}), \quad (3.3a)$$

with

$$g_m(\{\mu_k\}) = \min_{\{u_{m,k}, y_{m,k}\}} \sum_{k \in \mathcal{K}} c_m u_{m,k} - d_m y_{m,k} + \mu_k^T (\mathcal{A}_m u_{m,k} + \mathcal{B}_m y_{m,k} + \frac{1}{M} v_k), \quad (3.3b)$$

subject to (3.1b)-(3.1e) and defined for all $m \in \mathcal{M}$. Note again that the argument of g_m is the sequence $\{\mu_k\}_{k \in \mathcal{K}}$. Furthermore, note that each of the Lagrange dual functions (3.3b) subject to (3.1b)-(3.1e) is related to one of the subsystems and

can be solved independently. The dual problem is given by

$$\max_{\{\mu_k\}} g(\{\mu_k\}) = d^*, \quad (3.4)$$

subject to (3.1b)-(3.1e) where d^* is defined as the dual optimal value. The dual problem (3.4) gives a lower bound on the primal optimal value p^* of problem (3.1), i.e.,

$$d^* \leq p^*. \quad (3.5)$$

The dual optimal value d^* will be equal to the primal optimal value p^* , i.e., $p^* = d^*$, if problem (3.1) is strictly convex and the constraints satisfy Slater's constraint qualifications [9]. Problem (3.1), however, is not strictly convex due to the quadratic equality constraint (3.1b). By relaxing this constraint to an inequality constraint, i.e.,

$$y_{m,k} + \frac{1}{2}q_{m,k}u_{m,k}^2 + f_{m,k}u_{m,k} + e_{m,k} \leq 0, \quad (3.1b')$$

for $m \in \mathcal{M}$, $k \in \mathcal{K}$, the optimization problem becomes strictly convex. We define the optimal solution to the dual problem as the solution $\{u_{m,k}^*, y_{m,k}^*, \mu_k^*\}$ that satisfies (3.4) with $g(\{\mu_k\})$ defined in (3.3) with the minimum taken subject to (3.1c)-(3.1e) and (3.1b') instead of (3.1b). The following theorem provides a condition for which the optimal solution to the dual problem leads to the optimal solution to the primal problem.

Theorem 3.2.1. *The optimal solution $\{u_{m,k}^*, y_{m,k}^*, \mu_k^*\}$ to the dual problem (3.4) when (3.1b) is replaced by (3.1b'), solves the primal optimization problem (3.1) with $\{u_{m,k}^*, y_{m,k}^*\}$ (and (3.1b) instead of (3.1b')) if*

- *the optimal solution to the dual problem satisfies $d_m - \mathcal{B}_m^T \mu_k^* > 0$ for all $m \in \mathcal{M}$ and for all $k \in \mathcal{K}$,*
- *there exist a feasible point $\{u_{m,k}, y_{m,k}\}$ for all $m \in \mathcal{M}$ and for all $k \in \mathcal{K}$ satisfying (3.1c) - (3.1e) and (3.1b') with strict inequality.*

Proof. Because the second condition in the hypothesis of the theorem implies that Slater's constraint qualification (see e.g., [9]) holds and that we have strong

duality, we only need to show that the solution to (3.4) subject to (3.1c) - (3.1e) and (3.1b') is achieved with equality if $d_m - \mathcal{B}_m^T \mu_k^* > 0$.

To show that $d_m - \mathcal{B}_m^T \mu_k^* > 0$ for all $m \in \mathcal{M}$, $k \in \mathcal{K}$ implies that the optimal solution to the dual problem yields the optimal solution to the primal problem that satisfies (3.1b), consider the partial Lagrange dual function of problem (3.1) subject to (3.1b') instead of (3.1b), which is given by

$$L(\{u_{m,k}, y_{m,k}, \mu_k\}) = \sum_{m \in \mathcal{M}} \sum_{k \in \mathcal{K}} c_m u_{m,k} - d_m y_{m,k} + \mu_k^T (\mathcal{A}_m u_{m,k} + \mathcal{B}_m y_{m,k} + \frac{1}{M} v_k) + \nu_{m,k} (y_{m,k} + \frac{1}{2} q_{m,k} u_{m,k}^2 + f_{m,k} u_{m,k} + e_{m,k}), \quad (3.6)$$

subject to (3.1c)-(3.1e) and where $\nu_{m,k} \geq 0$ is the (scalar) Lagrange multiplier associated with the (scalar-valued) quadratic inequality constraint (3.1b'). The derivative with respect to $y_{m,k}$ at $\{u_{m,k}^*, y_{m,k}^*, \mu_k^*\}$ of this partial Lagrangian (3.6) (one of the necessary conditions for optimality, see, e.g., [9]) is given by

$$\mathcal{B}_m^T \mu_k^* - d_m + \nu_{m,k}^* = 0. \quad (3.7)$$

Since $d_m - \mathcal{B}_m^T \mu_k^* > 0$ by the hypothesis of the theorem, it follows that $\nu_{m,k}^* > 0$. The positivity of $\nu_{m,k}$ ensures that inequality (3.1b') is satisfied as an equality by complementarity slackness [9], which completes the proof. \square

The first condition of this theorem is in general not mild, but provides an a posteriori check for the optimal solution to the dual problem $\{u_{v,k}^*, y_{v,k}^*, \mu_k^*\}$ that satisfies (3.4) with $g(\{\mu_k\})$ defined in (3.3) with the minimum taken over (3.1c)-(3.1e) and (3.1b') instead of (3.1b), to be equal to the optimal solution to the primal problem to (3.1). Moreover, for the objective function (3.1a) this condition is naturally satisfied as the energy losses in each subsystem $m \in \mathcal{M}$ are defined as $c_m u_{m,k} - d_m y_{m,k}$ for each time instant $k \in \mathcal{K}$, so that the quadratic inequality constraint (3.1b') at the optimal solution implies

$$c_m u_{m,k}^* - d_m y_{m,k}^* \geq d_m (\frac{1}{2} q_{m,k} (u_{m,k}^*)^2 + f_{m,k} u_{m,k}^* + e_{m,k}) + c_m u_{m,k}^*, \quad (3.8)$$

for all $m \in \mathcal{M}$ and $k \in \mathcal{K}$. If the quadratic inequality constraint holds with equality at the optimal solution for all $m \in \mathcal{M}$ and $k \in \mathcal{K}$, then the energy

losses in each subsystem $m \in \mathcal{M}$ are minimal, which is intuitively needed for the solution to be optimal. The second condition in the hypothesis of this theorem is relatively mild (Slater's constraint qualification, see, e.g., [9]) and is satisfied for the numerical example given in Section 3.4. The dual problem (3.4) can be solved efficiently using a subgradient method as will be shown below.

3.2.3 Maximizing the Lagrange Dual Function

Maximizing the Lagrange dual function (3.3) over μ_k can be done with a 'steepest ascent' method, i.e.,

$$\mu_k^{s+1} = \mu_k^s + \alpha_k^s \left(\sum_{m \in \mathcal{M}} \mathcal{A}_m u_{m,k}^s + \mathcal{B}_m y_{m,k}^s + \frac{1}{M} v_k \right), \quad (3.9)$$

for all $k \in \mathcal{K}$ where α_k is a suitably chosen matrix and $s \in \mathbb{N}$ is the iteration counter. In [101], a diagonal matrix with sufficiently small positive constant step sizes on its diagonal was chosen such that the Lagrange dual problem will always converge. However, convergence tended to be slow. A better convergence rate is achieved with a Newton scheme (see e.g., [61]). We will derive this scheme from a primal feasibility perspective. The idea is to update the dual variables μ_k such that for the next iteration primal feasibility for the complicating constraints holds, i.e.,

$$\sum_{m \in \mathcal{M}} \mathcal{A}_m u_{m,k}^{s+1} + \mathcal{B}_m y_{m,k}^{s+1} + \frac{1}{M} v_k = \mathbf{0}. \quad (3.10)$$

To verify this condition, we can approximate the value for $u_{m,k}^{s+1}$ and $y_{m,k}^{s+1}$ by the linear functions

$$u_{m,k}^{s+1} \approx u_{m,k}^s + \left(\frac{\partial u_{m,k}^s}{\partial \mu_k} \right)^T (\mu_k^{s+1} - \mu_k^s), \quad (3.11a)$$

$$y_{m,k}^{s+1} \approx y_{m,k}^s + \left(\frac{\partial y_{m,k}^s}{\partial \mu_k} \right)^T (\mu_k^{s+1} - \mu_k^s), \quad (3.11b)$$

where $\frac{\partial u_{m,k}^s}{\partial \mu_k}$ is a vector with the approximations of the first-order derivatives of $u_{m,k}^s(\mu_k)$ with respect to the dual variables μ_k at iteration s . Similarly, $\frac{\partial y_{m,k}^s}{\partial \mu_k}$ is a vector with the approximations of the first-order derivatives of $y_{m,k}^s(\mu_k)$ with

respect to the dual variables μ_k at iteration s . By substituting (3.11) into (3.10) and solving for μ_k^{s+1} we obtain (3.9) with

$$\alpha_k^s = \left(\sum_{m \in \mathcal{M}} -\mathcal{A}_m \left(\frac{\partial u_{m,k}^s}{\partial \mu_k} \right)^T - \mathcal{B}_m \left(\frac{\partial y_{m,k}^s}{\partial \mu_k} \right)^T \right)^{-1}, \quad (3.12)$$

which can be obtained by calculating the vector with derivatives for each subproblem in a distributed fashion. Note that calculating the derivatives with respect to μ_k in (3.11) can be hard and they may not even exist due to the presence of constraints. To resolve this, the derivatives can be approximated by neglecting the state constraints (3.1e). As a consequence, the iteration (3.9) may not converge. In this case, sufficiently small constant step sizes can be chosen as was done in [101]. The convergence speed might be significantly slower in this case, as will be shown in the simulation study in Section 3.5. Finally, the dual decomposition algorithm consists of iteratively solving (3.3) to obtain $\{u_{m,k}^s, y_{m,k}^s\}$ and updating the Lagrange multipliers by solving (3.9) to obtain $\{\mu_k^{s+1}\}$. In the section below, we will provide methods to efficiently solve the dual functions (3.3b).

3.3 Evaluating the Dual Functions

Each of the Lagrange dual functions (3.3b) related to the subsystems $m \in \mathcal{M}$ can be solved separately and can be written as a linearly constrained quadratic program (LCQP) by substituting (3.1b) into (3.3b). This gives

$$g_m(\{\mu_k\}) = \min_{\{u_{m,k}\}} \sum_{k \in \mathcal{K}} \frac{1}{2} H_{m,k} u_{m,k}^2 + F_{m,k} u_{m,k} + E_{m,k}, \quad (3.13a)$$

with

$$H_{m,k} = (d_m - \mathcal{B}_m^T \mu_k) q_{m,k}, \quad (3.13b)$$

$$F_{m,k} = c_m + \mathcal{A}_m^T \mu_k + (d_m - \mathcal{B}_m^T \mu_k) f_{m,k}, \quad (3.13c)$$

$$E_{m,k} = \mu_k^T \frac{1}{M} v_k + (d_m - \mathcal{B}_m^T \mu_k) e_{m,k}, \quad (3.13d)$$

where the minimization is taken subject to (3.1c) - (3.1e). Note that for strict convexity of (3.13a), it is required that $d_m - \mathcal{B}_m^T \mu_k^* > 0$ for all $k \in \mathcal{K}$, $m \in \mathcal{M}$, at every iteration of the dual decomposition algorithm, which is a more restrictive

condition than in Theorem 3.2.1 for the optimal solution to the dual problem to be equal to the optimal solution to the primal problem. For the simulation study presented in Section 3.4, this condition is satisfied, as will be shown with the numerical example in Section 3.5.

As a result, the dual decomposition allows solving the quadratically constrained quadratic program by solving multiple LCQPs iteratively for all $m \in \mathcal{M}$. However, solving a LCQP for a large horizon length K is still numerically demanding. Therefore, we introduce two solution methods to solve the optimization problem (3.13a), related to each of the subsystems, efficiently. Both methods use the principle of splitting the horizon \mathcal{K} into L disjoint intervals, where each interval is defined as $\mathcal{K}_\ell = \{K_{\ell-1}, \dots, K_\ell - 1\}$ with $0 = K_0 < K_1 < \dots < K_L = K$ and where $\ell \in \mathcal{L} = \{1, \dots, L\}$ with L the number of intervals¹. To decompose the constraints in the optimization problem (3.13a) into smaller optimization problems, we recall that a solution to (3.1c) satisfies

$$x_{m,k+1} = A_m^{k+1-K_{\ell-1}} \tilde{x}_{m,K_{\ell-1}} + \sum_{i \in \{K_{\ell-1}, \dots, k\}} A_m^{k-i} (B_{m,w} w_{m,i} + B_{m,u} u_{m,i}), \quad (3.14a)$$

for all $k \in \mathcal{K}_\ell$, where the local initial condition $\tilde{x}_{m,K_{\ell-1}}$ at each interval $\ell \in \mathcal{L}$ is equal to the final condition at interval $\ell - 1$, i.e.,

$$x_{m,K_{\ell-1}} = \tilde{x}_{m,K_{\ell-1}}, \quad (3.14b)$$

for $\ell \in \mathcal{L}$ and $\tilde{x}_{m,0} = x_{m,0}$ and $\tilde{x}_{m,K_L} = x_{m,K}$, which follow from the initial and final condition of the full horizon. Using these constraints, we can write the dual function (3.13a) as

$$g_m(\{\mu_k\}) = \min_{\{u_{m,k}, \tilde{x}_{m,K_{\ell-1}}\}} \sum_{\ell \in \mathcal{L}} \sum_{k \in \mathcal{K}_\ell} \frac{1}{2} H_{m,k} u_{m,k}^2 + F_{m,k} u_{m,k} + E_{m,k}, \quad (3.15)$$

subject to (3.1d), (3.1e) and (3.14). Note that the problem (3.15) subject to (3.1d), (3.1e) and (3.14) is only coupled by (3.14b).

In the following subsection we will introduce three solution methods to evaluate the dual functions. The first two solution methods can be used to select the

¹Each interval can equivalently be defined as $\mathcal{K}_\ell = [K_{\ell-1}, K_\ell) \cap \mathbb{Z}$; $\ell = 1, \dots, L$ where $0 = K_0 < K_1 < \dots < K_L = K$ and note that $\mathcal{K}_{\ell_1} \cap \mathcal{K}_{\ell_2} = \emptyset$ for all $\ell_1 \neq \ell_2$ and that $\cup_{\ell \in \mathcal{L}} \mathcal{K}_\ell = \mathcal{K}$.

intervals \mathcal{K}_ℓ and the initial state at each interval $\tilde{x}_{m,K_{\ell-1}}$. In the first solution method, based on Alternating Direction Method of Multipliers (ADMM), the horizon is split a priori in a fixed number of intervals. For each interval, an optimization problem is solved that takes the initial state $\tilde{x}_{m,K_{\ell-1}}$ as the decision variable. ADMM is a suitable method as the resulting decomposed problem is not strictly convex, but it is convex, as we will show below. In the second solution method, based on the Lagrangian Method, the horizon is split iteratively and the initial state is fixed on the lower or upper state constraint depending on the solution of the state-unconstrained optimization problem. The Lagrangian Method is only applicable to systems with scalar states, while the ADMM method is applicable to systems with multiple states. Finally, we will introduce a third method based on dynamic programming, that allows solving (3.13) for which some subsystems are only allowed to be turned on or off, i.e., the input power is constrained to

$$u_{m,k} \in \{\underline{u}_{m,k}, \bar{u}_{m,k}\} \text{ for all } k \in \mathcal{K}, \quad (3.16)$$

for those subsystems $m \in \mathcal{M}$ that are only allowed to be turned on or off. In (3.16), $\underline{u}_{m,n|k}$ and $\bar{u}_{m,n|k}$ correspond to the power consumption when the auxiliary is off and on, respectively.

3.3.1 Horizon Splitting with ADMM

For this method, we define a priori the sets $\mathcal{K}_\ell = \{K_{\ell-1}, \dots, K_\ell - 1\}$, $\ell \in \mathcal{L} = \{1, \dots, L\}$. This method is similar to the method proposed in [111] where intervals that contain only one time instant, i.e., $\mathcal{K}_\ell = \{\ell - 1\}$ are used for solving the problem over a short horizon. Contrary to [111], we use intervals containing multiple time instants, thereby making it more applicable for solving the problem over a long horizon as will be demonstrated with the numerical example in Section 3.5. The objective function in (3.15) is separable in variables related to each interval, but is not strictly convex due to the minimization over the local initial state $\tilde{x}_{m,K_{\ell-1}}$, which is an essential assumption for the dual decomposition approach taken in the previous section. Lagrangian methods as used in Section 3.2, however, require convexity of the objective function rather than strict convexity.

Instead, the *partial augmented Lagrangian* for problem (3.15) can be defined as

$$\begin{aligned} \hat{L}_m(\{u_{m,k}, \tilde{x}_{m,K_{\ell-1}}, \nu_{m,\ell}\}) &= \sum_{\ell \in \mathcal{L}} \sum_{k \in \mathcal{K}_\ell} \frac{1}{2} H_{m,k} u_{m,k}^2 + F_{m,k} u_{m,k} + E_{m,k} \\ &+ \nu_{m,\ell-1}^T (\tilde{x}_{m,K_{\ell-1}} - x_{m,K_{\ell-1}}) + \frac{1}{2} (\tilde{x}_{m,K_{\ell-1}} - x_{m,K_{\ell-1}})^T R (\tilde{x}_{m,K_{\ell-1}} - x_{m,K_{\ell-1}}), \end{aligned} \quad (3.17)$$

for all $m \in \mathcal{M}$ in which $\nu_{m,\ell} \in \mathbb{R}^{\dim(x_{m,k})}$ are Lagrange multipliers and where $R \succ 0$ is a diagonal matrix with positive penalty parameters on its diagonal. In this expression, we temporarily omit the constraints that are acting only within one interval, i.e., (3.1d), (3.1e) and (3.14a). We will reintroduce these constraints later in the decomposed problem. The *partial augmented Lagrange dual function* is defined by

$$\hat{g}_m(\{\nu_{m,\ell}\}_{\ell \in \mathcal{L}}) = \min_{\{u_{m,k}, \tilde{x}_{m,K_{\ell-1}}\}} \hat{L}(\{u_{m,k}, \tilde{x}_{m,K_{\ell-1}}, \nu_{m,\ell}\}) = \sum_{\ell \in \mathcal{L}} \hat{g}_{m,\ell}(\nu_{m,\ell-1}, \nu_{m,\ell}), \quad (3.18a)$$

for all $m \in \mathcal{M}$ with

$$\begin{aligned} \hat{g}_{m,\ell}(\nu_{m,\ell-1}, \nu_{m,\ell}) &= \min_{\{u_{m,k}, \tilde{x}_{m,K_{\ell-1}}\}} \sum_{k \in \mathcal{K}_\ell} \frac{1}{2} H_{m,k} u_{m,k}^2 + \frac{1}{2} \tilde{x}_{m,K_{\ell-1}}^T R \tilde{x}_{m,K_{\ell-1}} \\ &+ \hat{G}_{m,k} \tilde{x}_{m,K_{\ell-1}} + \hat{F}_{m,k} u_{m,k} + \hat{E}_{m,k}, \end{aligned} \quad (3.18b)$$

in which

$$\hat{G}_{m,k} = \nu_{m,\ell-1}^T - x_{m,K_{\ell-1}}^T R - \nu_{m,\ell}^T A_m^{K_\ell - K_{\ell-1}}, \quad (3.18c)$$

$$\hat{F}_{m,k} = F_{m,k} - \nu_{m,\ell}^T A_m^{K_\ell - 1 - k} B_{m,u}, \quad (3.18d)$$

$$\hat{E}_{m,k} = E_{m,k} - \nu_{m,\ell}^T A_m^{K_\ell - 1 - k} B_{m,w} \omega_{m,k}, \quad (3.18e)$$

for $\ell \in \mathcal{L}$, with $\nu_{m,L} = \mathbf{0}$ and is to be solved subject to (3.1d), (3.1e) and (3.14a). Expressions (3.18c,d,e) are obtained by substituting (3.14a) for $k = K_\ell - 1$ into (3.17), only for the linear part of the equation, i.e., for $\nu_{m,\ell-1}^T (\tilde{x}_{m,K_{\ell-1}} - x_{m,K_{\ell-1}})$ and *not* for $\frac{1}{2} (\tilde{x}_{m,K_{\ell-1}} - x_{m,K_{\ell-1}})^T R (\tilde{x}_{m,K_{\ell-1}} - x_{m,K_{\ell-1}})$. This gives a more desirable expression for (3.18b), i.e., the product $u_{m,k_1} u_{m,k_2}$ for $k_1 \neq k_2$ is not in the expression. However, as a result, (3.18b) is not separable due to the

term $x_{m,K_{\ell-1}}$ in (3.18b). By minimizing (3.18) sequentially from interval $\ell = 1$ to interval $\ell = L$, as part of the ADMM algorithm (see, e.g., [9]), the minimization problem (3.18), can still be solved efficiently.

To maximize the partial augmented Lagrange dual function (3.18), we use a ‘steepest ascent’ method, i.e.,

$$\nu_{m,\ell}^{t+1} = \nu_{m,\ell}^t + R(\tilde{x}_{m,K_\ell}^t - x_{m,K_\ell}^t) \quad (3.19)$$

for $\ell \in \mathcal{L}$, $m \in \mathcal{M}$ with $t \in \mathbb{N}$ the iteration number and for some given initial condition $\nu_{m,\ell}^0$ for $\ell \in \mathcal{L}$. Finally, the ADMM algorithm consists of iteratively solving (3.18) subject to (3.1c) - (3.1e) to obtain $\{u_{m,k}^t, \tilde{x}_{m,K_{\ell-1}}^t\}$ for $\ell \in \mathcal{L}$, $k \in \mathcal{K}$ and solving (3.14a) for $k = K_\ell - 1$ to obtain x_{m,K_ℓ}^t for $\ell \in \mathcal{L}$, $k \in \mathcal{K}$, followed by an update of the Lagrange multipliers through (3.19) to obtain $\nu_{m,\ell-1}^{t+1}$ for $\ell \in \mathcal{L}$.

3.3.2 Horizon Splitting with the Lagrangian Method

Fixing the interval \mathcal{K}_ℓ *a priori* and using ADMM to solve (3.15) results in a general solution method to solve the LCQP (3.13). We will also develop an iterative procedure that involves splitting the intervals based on solving (3.15) for the particular case where $x_{m,k} \in \mathbb{R}$, i.e., the energy storage device in subsystem $m \in \mathcal{M}$ is a scalar-state system. In Section 3.4, it will be shown that many components in the CVEM problem can be represented by a scalar-state system and, in Section 3.5, we will show that a tailored solution method for these components is more favorable with respect to computation time, which also emphasizes the advantage of using the dual decomposition approach to CVEM where each of the dual functions can be solved with the most suitable solution method.

For this method, we initially take only one interval, i.e. the full horizon, so that $\mathcal{K}_\ell = \{K_{\ell-1}, \dots, K_\ell - 1\} = \{0, \dots, K - 1\}$ and $\ell \in \mathcal{L} = \{1\}$ and solve (3.13a) subject to (3.1d) and (3.14) without considering the state constraints (3.1e). The main reason for this is that the problem without (3.1e) is much easier to solve. Depending on the solution of a state-unconstrained optimization, extra intervals will be added as will be shown later in this section.

First, we define the state unconstrained problem for subsystem $m \in \mathcal{M}$, which is given by (3.15) subject to (3.1d) and (3.14). The Lagrangian of this problem

is given by

$$\begin{aligned}
\hat{L}_m(\{u_{m,k}, \lambda_\ell, \bar{\nu}_k, \underline{\nu}_k\}) &= \sum_{\ell \in \mathcal{L}} \sum_{k \in \mathcal{K}_\ell} \frac{1}{2} H_{m,k} u_{m,k}^2 + F_{m,k} u_{m,k} + E_{m,k} \\
&+ \lambda_\ell \left(A_m^{K_\ell - K_{\ell-1}} \tilde{x}_{m, K_{\ell-1}} - \tilde{x}_{m, K_\ell} + \sum_{i \in \mathcal{K}_\ell} A_m^{K_\ell - 1 - i} (B_{m,w} w_{m,i} + B_{m,u} u_{m,i}) \right) \\
&+ \bar{\nu}_k (u_{m,k} - \bar{u}_{m,k}) + \underline{\nu}_k (\underline{u}_{m,k} - u_{m,k}), \tag{3.20}
\end{aligned}$$

with $\lambda_\ell \in \mathbb{R}$, the Lagrange multiplier associated with the constraint (3.14), $\bar{\nu}_k \in \mathbb{R}$ and $\underline{\nu}_k \in \mathbb{R}$, the Lagrange multipliers associated with the upper and lower input constraints (3.1d), respectively. The Karush-Kuhn-Tucker conditions [9] for minimizing the Lagrangian (3.20) are given by the first-order necessary conditions for optimality, i.e.,

$$\frac{\partial \hat{L}_m(\{u_{m,k}, \lambda_\ell, \bar{\nu}_k, \underline{\nu}_k\})}{\partial u_{m,k}} = H_{m,k} u_{m,k} + F_{m,k} + \bar{\nu}_k - \underline{\nu}_k + \lambda_\ell \sum_{i \in \mathcal{K}_\ell} A_m^{K_\ell - 1 - i} B_{m,u} = 0, \tag{3.21a}$$

for all $k \in \mathcal{K}_\ell$, $\ell \in \mathcal{L}$, feasibility of the constraint (3.14) and the complementary slackness conditions for the inequality constraints

$$\begin{aligned}
\bar{\nu}_k (u_{m,k} - \bar{u}_{m,k}) &= 0, \\
\underline{\nu}_k (\underline{u}_{m,k} - u_{m,k}) &= 0, \tag{3.21b}
\end{aligned}$$

for all $k \in \mathcal{K}_\ell$, $\ell \in \mathcal{L}$ with $\bar{\nu}_k \geq 0$ and $\underline{\nu}_k \geq 0$. Finding a solution for (3.21a) and (3.21b) simultaneously is difficult and often the solution is found with a shooting method and a bisection algorithm over λ_ℓ . This leads to the optimal solution

$$u_{m,k}^* = -H_{m,k}^{-1} (F_{m,k} + \lambda_\ell \sum_{i \in \mathcal{K}_\ell} A_m^{K_\ell - 1 - i} B_{m,u} + \bar{\nu}_k - \underline{\nu}_k), \tag{3.22}$$

for all $k \in \mathcal{K}_\ell$, $\ell \in \mathcal{L}$ for a given λ_ℓ , $\bar{\nu}_k$ and $\underline{\nu}_k$. Instead, we propose a procedure

that aims, for each interval $\ell \in \mathcal{L}$, at solving

$$\lambda_\ell^{t+1} = (1 - \gamma)\lambda_\ell^t + \gamma \hat{H}_m^{-1} \left(A_m^{K_\ell - K_{\ell-1}} \tilde{x}_{m, K_{\ell-1}} - \tilde{x}_{m, K_\ell} + \sum_{i \in \mathcal{K}_\ell} A_m^{K_\ell - 1 - i} \left(B_{m, w} w_{m, i} - B_{m, u} H_{m, i}^{-1} (F_{m, i} + \bar{v}_i^t - \underline{v}_i^t) \right) \right), \quad (3.23a)$$

with relaxation parameter $\gamma \in (0, 1]$ and with

$$\hat{H}_m = \sum_{i \in \mathcal{K}_\ell} A_m^{K_\ell - 1 - i} B_{m, u} H_{m, i}^{-1} \sum_{i \in \mathcal{K}_\ell} A_m^{K_\ell - 1 - i} B_{m, u}, \quad (3.23b)$$

and

$$\bar{v}_k^{t+1} = \max \left\{ 0, -H_{m, k} \bar{u}_{m, k} - F_{m, k} - \lambda_\ell^{t+1} \sum_{i \in \mathcal{K}_\ell} A_m^{K_\ell - 1 - i} B_{m, u} \right\}, \quad (3.23c)$$

$$\underline{v}_k^{t+1} = \max \left\{ 0, H_{m, k} \underline{u}_{m, k} + F_{m, k} + \lambda_\ell^{t+1} \sum_{i \in \mathcal{K}_\ell} A_m^{K_\ell - 1 - i} B_{m, u} \right\}, \quad (3.23d)$$

with $t \in \mathbb{N}$ the iteration index and for $\lambda^0 = 0$ and $\bar{v}_k^0 = \underline{v}_k^0 = 0$ for all $k \in \mathcal{K}$, until (3.14) is satisfied within some desired tolerance. The expressions in (3.23) are obtained by substituting (3.22) into (3.14) and (3.1d). If $H_{m, k}$ is strictly positive and if there exists an optimal solution $u_{m, k}^*$ for which (3.1d) and (3.14) are satisfied, then the solution of iteration (3.23) will converge to the solution of (3.15) (as $t \rightarrow \infty$) subject to (3.1d) and (3.14) for a well chosen relaxation parameter $\gamma \in (0, 1]$.

For solving the state-constrained optimization problem (3.13), we use an idea proposed in [120]. In [120] it is proven that when the relation between λ_ℓ and the final state x_{m, K_ℓ} is monotonic (note that it is linear in this chapter), the time instant at which the state constraint is violated most \hat{K}_ℓ is a contact point of the state-constrained solution, i.e., $x_{m, \hat{K}_\ell} = \bar{x}_{m, k}$ or $x_{m, \hat{K}_\ell} = \underline{x}_{m, k}$. This concept is illustrated in Figure 3.2. This allows us to add \hat{K}_ℓ to the set of splitting instances $\{K_\ell\}_{\ell \in \mathcal{L}}$ and we fix x_{m, \hat{k}_ℓ} at either $\bar{x}_{m, \hat{k}_\ell}$ or $\underline{x}_{m, \hat{k}_\ell}$ depending on whether the upper or lower bound was violated most and solve smaller optimal control problems subject to initial and terminal constraints. Note that due to the particular projection on the state constraints, this method is only suitable for scalar-state systems, i.e., $x_{m, k} \in \mathbb{R}$.

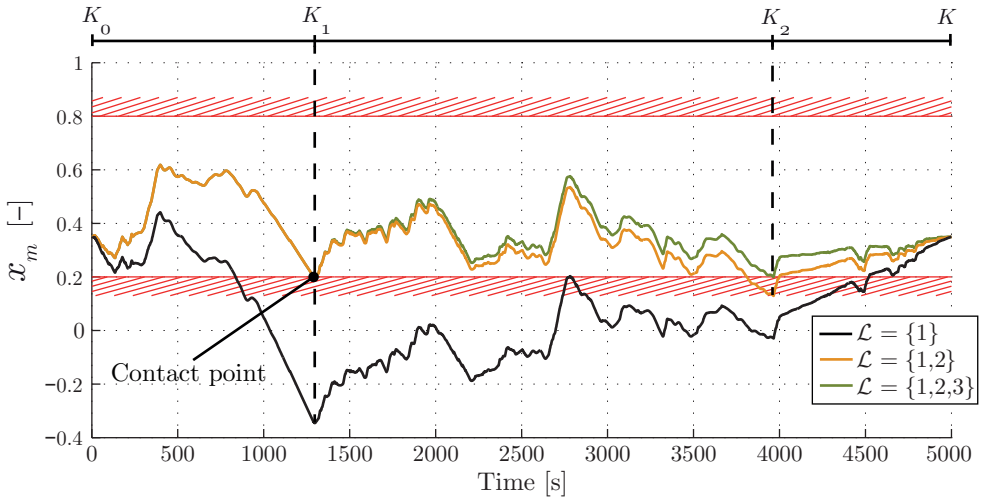


Figure 3.2: Solving the state-constrained optimization problem with the Lagrangian method

As a result of splitting the time horizon \mathcal{K} into L segments using the method outlined before, we might have a large number of ‘contact points’, which makes the method inefficient. We can prove that, under certain conditions, the optimal state trajectory equals either $x_{m,k} = \bar{x}_{m,k}$ or $x_{m,k} = \underline{x}_{m,k}$ for all $k \in \mathcal{K}_\ell$, i.e., it is saturated on the upper or lower bound. This might occur when either $x_{m,K_{\ell-1}} = \bar{x}_{m,K_{\ell-1}}$ and $x_{m,K_\ell} = \bar{x}_{m,K_\ell}$ or $x_{m,K_{\ell-1}} = \underline{x}_{m,K_{\ell-1}}$ and $x_{m,K_\ell} = \underline{x}_{m,K_\ell}$. The following theorem provides conditions, that can be evaluated *a priori*, for which the optimal state trajectory is saturated on the upper or lower bound.

Theorem 3.3.1. *The optimal state trajectory $x_{m,k}$ satisfies $x_{m,k} = \underline{x}_{m,k}$ for all $k \in \mathcal{K}_\ell$ and the corresponding control input satisfies*

$$\underline{u}_{m,k}^* = \frac{1}{B_{m,u}} \left((1 - A_m) \underline{x}_{m,k} + B_{m,w} w_{m,k} \right) \quad (3.24a)$$

if $x_{m,K_{\ell-1}} = \underline{x}_{m,K_{\ell-1}}$ and $x_{m,K_\ell} = \underline{x}_{m,K_\ell}$, and if either one of the following conditions holds for all $k \in \mathcal{K}_\ell$:

- $A_m > 0$, $B_{m,u} < 0$, $H_{m,k+1} \underline{u}_{m,k+1}^* - H_{m,k} \underline{u}_{m,k}^* < 0$, $F_{m,k+1} - F_{m,k} < 0$
- $A_m > 0$, $B_{m,u} > 0$, $H_{m,k+1} \underline{u}_{m,k+1}^* - H_{m,k} \underline{u}_{m,k}^* > 0$, $F_{m,k+1} - F_{m,k} > 0$.

Similarly, the optimal state trajectory $x_{m,k}$ satisfies $x_{m,k} = \bar{x}_{m,k}$ for all $k \in \mathcal{K}_\ell$

and the corresponding control input satisfies

$$\bar{u}_{m,k}^* = \frac{1}{B_{m,u}}((1 - A_m)\bar{x}_{m,k} + B_{m,w}w_{m,k}) \quad (3.24b)$$

if $x_{m,K_{\ell-1}} = \bar{x}_{m,K_{\ell-1}}$ and $x_{m,K_{\ell}} = \bar{x}_{m,K_{\ell}}$, and if either one of the following conditions holds for all $k \in \mathcal{K}_{\ell}$:

- $A_m > 0$, $B_{m,u} < 0$, $H_{m,k+1}\bar{u}_{m,k+1}^* - H_{m,k}\bar{u}_{m,k}^* > 0$, $F_{m,k+1} - F_{m,k} > 0$
- $A_m > 0$, $B_{m,u} > 0$, $H_{m,k+1}\bar{u}_{m,k+1}^* - H_{m,k}\bar{u}_{m,k}^* < 0$, $F_{m,k+1} - F_{m,k} < 0$.

Proof. We only prove the case that $x_{m,k} = \underline{x}_{m,k}$ for all $k \in \mathcal{K}_{\ell}$ and the proof for $x_{m,k} = \bar{x}_{m,k}$ follows mutatis mutandis.

For $\underline{u}_{m,k}^*$ to be a feasible solution it needs to satisfy (3.1d) by definition, such that the Lagrangian of (3.15) subject to (3.14) and (3.1e) on interval ℓ is given by

$$\begin{aligned} \hat{L}_m(\{\underline{u}_{m,k}^*, \lambda_{\ell}, \underline{v}_k\}) &= \sum_{k \in \mathcal{K}_{\ell}} \frac{1}{2} H_{m,k}(\underline{u}_{m,k}^*)^2 + F_{m,k}\underline{u}_{m,k}^* + E_{m,k} + \underline{v}_k(\underline{x}_{m,k} - x_{m,k}) \\ &+ \lambda_{\ell}(A_m^{K_{\ell}-K_{\ell-1}}\tilde{x}_{m,K_{\ell-1}} - \tilde{x}_{m,K_{\ell}} + \sum_{i \in \mathcal{K}_{\ell}} A_m^{K_{\ell}-1-i}(B_{m,w}w_{m,i} + B_{m,u}u_{m,i})), \end{aligned} \quad (3.25)$$

where $x_{m,k}$ is given by (3.14a) for all $k \in \mathcal{K}_{\ell}$. In (3.25), $\underline{v}_k \in \mathbb{R}$ is the Lagrange multiplier associated with the lower state constraint (3.1e). We will show that the lower state is active for all $k \in \mathcal{K}_{\ell}$, which means that the upper state is inactive and can be left out of the Lagrangian. The Karush-Kuhn-Tucker conditions [9] for minimizing the Lagrangian in (3.25) are given by the first-order necessary optimality condition

$$\frac{\partial \hat{L}_m(\{\underline{u}_{m,k}^*, \lambda_{\ell}, \underline{v}_k\})}{\partial \underline{u}_{m,k}^*} = H_{m,k}\underline{u}_{m,k}^* + F_{m,k} + \lambda_{\ell} \sum_{i \in \mathcal{K}_{\ell}} A_m^{K_{\ell}-1-i} B_{m,u} - \underline{v}_k \sum_{i=K_{\ell-1}}^k A_m^{k-i} B_{m,u} = 0, \quad (3.26)$$

for all $k \in \mathcal{K}_{\ell}$, feasibility of the constraint (3.14) and the complementary slackness conditions for the inequality constraint

$$\underline{v}_k(\underline{x}_{m,k} - x_{m,k}) = 0, \quad (3.27)$$

for all $k \in \mathcal{K}_\ell$, for a given $\underline{v}_k \geq 0$. As $\lambda_\ell \sum_{i \in \mathcal{K}_\ell} A_m^{K_\ell-1-i} B_{m,u}$ is a constant in (3.26), we can derive the following relation between the Lagrange multipliers \underline{v}_k at time instant $k+1$ and k

$$\underline{v}_{k+1} = \left(\sum_{i=K_{\ell-1}}^{k+1} A_m^{k-i} B_{m,u} \right)^{-1} \left(\underline{v}_k \sum_{i=K_{\ell-1}}^k A_m^{k-i} B_{m,u} + H_{m,k+1} \underline{u}_{m,k+1}^* - H_{m,k} \underline{u}_{m,k}^* + F_{m,k+1} - F_{m,k} \right), \quad (3.28)$$

for $k \in \mathcal{K}_\ell$ and where $\underline{v}_{K_{\ell-1}} > 0$ if $\tilde{x}_{m,K_{\ell-1}} = \underline{x}_{m,K_{\ell-1}}$, such that if $A_m > 0$, $B_{m,u} < 0$, $H_{m,k+1} \underline{u}_{m,k+1}^* - H_{m,k} \underline{u}_{m,k}^* < 0$ and $F_{m,k+1} - F_{m,k} < 0$ or if $A_m > 0$, $B_{m,u} > 0$, $H_{m,k+1} \underline{u}_{m,k+1}^* - H_{m,k} \underline{u}_{m,k}^* > 0$ and $F_{m,k+1} - F_{m,k} > 0$ then there exist a $\underline{v}_{k+1} > 0$ for all $k \in \mathcal{K}_\ell$, such that the first-order optimality conditions and the complementary slackness conditions are satisfied and $\underline{u}_{m,k}^*$ is optimal for all $k \in \mathcal{K}_\ell$. This completes the proof for $x_{m,k} = \underline{x}_{m,k}$. \square

This theorem provides a priori verifiable conditions when the optimal state trajectory is saturated at the lower bound or upper bound for all $k \in \{K_{\ell-1}, \dots, K_\ell - 1\}$, respectively. The three preceding results, i.e., i) the solution of the optimal control problem without considering the state constraints, ii) the iterative method for splitting the control problem into smaller ones to incorporate state constraints and iii) conditions for which the optimal solution satisfies $x_{m,k} = \bar{x}_{m,k}$ or $x_{m,k} = \underline{x}_{m,k}$ for all $k \in \mathcal{K}_\ell$ allow us to propose the following algorithm for solving (3.13).

Algorithm 3.3.2. Take $\mathcal{K}_1 = \{0, \dots, K-1\}$, $\mathcal{L} = \{1\}$ and let $\tilde{x}_{m,0}$ and $\tilde{x}_{m,K}$ be given.

- For each interval $\ell \in \mathcal{L}$, check if the conditions of Theorem 3.3.1 are satisfied.
 - If the conditions of Theorem 3.3.1 are satisfied, the optimal solution satisfies (3.24a) or (3.24b).
 - If the conditions of Theorem 3.3.1 are not satisfied, compute the input constrained solution using (3.23). Then verify

$$\underline{\varepsilon}_\ell = \max_{k \in \mathcal{K}_\ell} \{\underline{x}_{m,k} - x_{m,k}\}, \quad (3.29a)$$

$$\bar{\varepsilon}_\ell = \max_{k \in \mathcal{K}_\ell} \{x_{m,k} - \bar{x}_{m,k}\}. \quad (3.29b)$$

* If $\underline{\varepsilon}_\ell > 0$ and $\underline{\varepsilon}_\ell > \bar{\varepsilon}_\ell$, the lower state constraint is violated more than the upper state constraint and

$$\hat{K}_\ell = \arg \max_{k \in \mathcal{K}_\ell} \{\underline{x}_{m,k} - x_{m,k}\}, \quad (3.29c)$$

is added to the set of contact points $\{K_\ell\}_{\ell \in \mathcal{L}}$ and re-ordered, i.e., $0 = K_0 \leq \dots \leq K_{\ell-1} \leq \hat{K}_\ell \leq K_\ell \leq K_L$ to define new subsets $\mathcal{K}_\ell = \{K_{\ell-1}, \dots, K_\ell - 1\}$ and $\tilde{x}_{m, \hat{K}_\ell} = \underline{x}_{m, \hat{K}_\ell}$.

* If $\bar{\varepsilon}_\ell > 0$ and $\bar{\varepsilon}_\ell > \underline{\varepsilon}_\ell$, the upper state constraint is violated more than the lower state constraint and

$$\hat{K}_\ell = \arg \max_{k \in \mathcal{K}_\ell} \{x_{m,k} - \bar{x}_{m,k}\}, \quad (3.29d)$$

is added to the set of contact points $\{K_\ell\}_{\ell \in \mathcal{L}}$ and re-ordered, i.e., $0 = K_0 \leq \dots \leq K_{\ell-1} \leq \hat{K}_\ell \leq K_\ell \leq K_L$ to define new subsets $\mathcal{K}_\ell = \{K_{\ell-1}, \dots, K_\ell - 1\}$ and $\tilde{x}_{m, \hat{K}_\ell} = \bar{x}_{m, \hat{K}_\ell}$.

* If both (3.29b) and (3.29a) are nonpositive, the ℓ -th interval does not have to be further divided.

- Repeat until $\max\{\underline{x}_{m,k} - x_{m,k}, x_{m,k} - \bar{x}_{m,k}\} \leq 0$ for all $k \in \mathcal{K}$.

Similarly as the dual decomposition allows the large-scale optimal control problem to be solved by solving smaller optimal control problems on subsystem level, Algorithm 3.3.2 and the ADMM algorithm allow the optimal control problem over a large horizon to be solved through multiple optimal control problems over a smaller horizon. Note that, to ensure convergence of the solution to the dual problem (3.4), the solution to each dual function obtained with Algorithm 3.3.2 or ADMM (3.19) needs to be converged before proceeding with the maximization in (3.9). Still, by combining these solution methods, scalability is significantly improved, which will be demonstrated with the numerical example in Section 3.5.

3.3.3 Dynamic Programming for Subsystems with On/Off Control

The Lagrangian method and the ADMM method presented so far, can only be used to solve the dual functions for which the input $u_{m,k}$ is constrained to an interval as in (3.1d). Only then, (3.1) satisfies the condition on strict convexity and convergence of the dual decomposition is guaranteed. However, in Chapter 2, auxiliaries have been introduced, e.g., the refrigerated semi-trailer, that are only allowed to switch on or off, i.e., $u_{m,k}$ is constrained to

$$u_{m,k} \in \{\underline{u}_{m,k}, \bar{u}_{m,k}\}, \quad (3.30)$$

where $\underline{u}_{m,n|k}$ and $\bar{u}_{m,n|k}$ correspond to the power consumption when the auxiliary is off and on, respectively. Theoretically, the inputs $u_{m,k}$ constrained to an interval as in (3.1d) can be approximated with (3.30) with an infinite number of on/off switches. In practice, however, the number of switches per time horizon is limited and an optimal trade-off exist between the number of switches and the fuel reduction. To find this trade-off, the LCQP (3.13) can be slightly modified, i.e.,

$$g_m(\{\mu_k\}) = \min_{\{u_{m,k}\}} \sum_{k \in \mathcal{K}} \frac{1}{2} H_{m,k} u_{m,k}^2 + F_{m,k} u_{m,k} + E_{m,k} + \sigma \frac{u_{m,k+1} - u_{m|k}}{u_{m,k+1} - u_{m|k}}, \quad (3.31)$$

with $H_{m,k}$, $F_{m,k}$, $E_{m,k}$ as in (3.13b-d), respectively, and subject to (3.1c), (3.1e) and (3.30) instead of (3.1d). In (3.31), σ is a penalty parameter that penalizes the number of switches. Instead of an LCQP, (3.31) is a (non-convex) mixed integer quadratic program (MIQP). Different solution methods exist for solving a MIQP, see, e.g., [45]. In this thesis, we will use the generic dynamic programming tool from [113] for simplicity, although faster solution methods might exist. Note that convergence of the dual decomposition is not guaranteed anymore. Still, the dual decomposition allowed the optimal control problem to be decomposed in (strictly) convex optimization problems and non-convex optimization problems. By updating the decisions of the non-convex optimization problems only at specific iterations in the maximization of the Lagrange dual function (3.9), the dual decomposition converges to a close to optimal solution as will be demonstrated with a numerical example in Section 3.5.

3.4 Application to the CVEM problem

The distributed optimization approach presented in the previous sections will be used to find the optimal solution for energy management of the vehicle model introduced in Chapter 2. The vehicle topology (see Figure 2.1) includes an internal combustion engine (ICE), an electric machine, a high-voltage battery, a refrigerated semi-trailer, an air supply system, an alternator, a DCDC converter, a low-voltage battery and a climate control system (CCS). To find the optimal solution with the distributed optimization approach, we need to make a discrete-time model approximation of the models presented in Chapter 2 and redefine the objective function.

3.4.1 Discrete-Time Model Approximation

We assume that the input power $u_m(t)$ and output power $y_m(t)$ for all $m \in \mathcal{M}$ is constant over the time interval $t \in [k\tau, (k+1)\tau)$ for all $k \in \mathcal{K}$ with τ being the sample time. Then, the input-output behavior for each of the subsystems in the vehicle, as given in Chapter 2, can indeed be described by the quadratic function (3.1b) where the efficiency coefficients are either constant, i.e.,

$$q_{m,k} = q_m, \quad f_{m,k} = f_m, \quad e_{m,k} = e_m, \quad (3.32)$$

for $m \in \{\text{dc, br, hvb, lvb, rst, as}\}$ as given in Chapter 2 or depend on speed, i.e.,

$$q_{m,k} = q_m(\omega_k), \quad f_{m,k} = f_m(\omega_k), \quad e_{m,k} = e_m(\omega_k), \quad (3.33)$$

for $m \in \{\text{ice, em, alt, ccs}\}$ where $q_m(\omega_k)$, $f_m(\omega_k)$ and $e_m(\omega_k)$ are functions parameterizing the efficiency coefficients as function of the piece-wise constant drive line speed ω_k as given in Chapter 2. Note that we have replaced the set $\mathcal{M} = \{1, \dots, M\}$ in the general optimization problem (3.1) by the set $\mathcal{M} = \{\text{ice, em, hvb, rst, as, ccs, dc, lvb, alt, br}\}$, to better indicate the physical origin of the power flows.

Similarly, the input power of the subsystems are bounded by (3.1d) where the upper and lower bounds are either constant, i.e.,

$$\underline{u}_{m,k} = \underline{u}_m, \quad \bar{u}_{m,k} = \bar{u}_m, \quad (3.34)$$

for $m \in \{\text{dc, br, hvb, lvb, rst, as}\}$ as given in Chapter 2 or depend on speed, i.e.,

$$\underline{u}_{m,k} = \underline{u}_m(\omega_k), \quad \bar{u}_{m,k} = \bar{u}_m(\omega_k), \quad (3.35)$$

for $m \in \{\text{ice, em, alt, ccs}\}$ where $\underline{u}_m(\omega_k)$ and $\bar{u}_m(\omega_k)$ are functions parameterizing the lower and upper bound as function of the piece-wise constant drive line speed ω_k .

The dynamics of the high- and low-voltage battery, the refrigerated semi-trailer, the air supply system and the climate control system can be represented by (3.1c) by making a forward Euler approximation of (2.6c) for $m \in \{\text{hvb, lvb, rst, as, ccs}\}$. In particular, the dynamics of the high- and low-voltage battery can be represented by (3.1c) for $m \in \{\text{hvb, lvb}\}$ with $A_m = 1$, $B_{m,w} = 0$ and $B_{m,u} = -\tau$ with τ being the sample time, the dynamics of the refrigerated semi-trailer can be represented by (3.1c) for $m \in \{\text{rst}\}$ with $A_{\text{rst}} = 1 - \frac{\tau h}{C_{\text{rst}}}$, $B_{\text{rst},w} = 0$ and $B_{\text{rst},u} = -\tau$, the dynamics of the air supply system can be represented by (3.1c) for $m \in \{\text{as}\}$ with $A_{\text{as}} = 1$, $B_{\text{as},w} = -\tau$, $B_{\text{as},u} = \tau$ and $w_{\text{rst},k}$ is the power, i.e., $\frac{RT_{\text{out}}\dot{m}_{\text{out}}}{\gamma-1}$ released to the environment at time instant k , and finally the dynamics of the climate control system can be represented by (3.1c) for $m \in \{\text{ccs}\}$ with

$$A_{\text{ccs}} = \begin{bmatrix} 1 - \frac{\tau h_i}{C_r} & \frac{\tau h_i}{C_w} \\ \frac{\tau h_i}{C_r} & 1 - \frac{\tau(h_i + h_o)}{C_w} \end{bmatrix}, \quad B_{\text{ccs},w} = \begin{bmatrix} 0 \\ -\tau \end{bmatrix}, \quad B_{\text{ccs},u} = \begin{bmatrix} -\tau \\ 0 \end{bmatrix}, \quad (3.36)$$

and $w_{\text{rst},k}$ is the latent heat $Q_{1,k}$ at time instant k . A quasi-static approach is generally sufficient for energy management (see, e.g., [40]) such that the sample time is chosen to be 1 second, i.e., $\tau = 1$, which is smaller than the time constants of the dynamics in the subsystems.

Finally, the three exogenous load signals in the topology are assumed to be piece-wise constant as well, i.e., $v_k = [v_{1,k} \ v_{2,k} \ v_{3,k}]^T \in \mathbb{R}^3$, which are the power required to drive a certain drive cycle, the power required for uncontrolled high-voltage auxiliaries and the power required for uncontrolled low-voltage auxiliaries, respectively. These three signals are assumed to be known for every time instant $k \in \mathcal{K}$. Furthermore, we assume that the gearshift strategy is fixed such that the rotational velocity of the drive line ω_k is known (and constant) for every time instant $k \in \mathcal{K}$. The nodes in the topology where power is aggregated described

by (2.5) is given in discrete-time by

$$v_{1,k} - y_{br,k} - y_{ice,k} + u_{em,k} + u_{alt,k} - y_{ccs,k} = 0, \quad (3.37a)$$

$$v_{2,k} - y_{em,k} - y_{hvb,k} - y_{rst,k} - y_{as,k} + u_{dc,k} = 0, \quad (3.37b)$$

$$v_{3,k} - y_{alt,k} - y_{lvb,k} - y_{dc,k} = 0, \quad (3.37c)$$

for every time instant $k \in \mathcal{K}$, which we can write in the form of (3.1f) with

$$\mathcal{A}_{ice} = [0 \ 0 \ 0]^T, \quad \mathcal{B}_{ice} = [-1 \ 0 \ 0]^T, \quad (3.38a)$$

$$\mathcal{A}_{em} = [1 \ 0 \ 0]^T, \quad \mathcal{B}_{em} = [0 \ -1 \ 0]^T, \quad (3.38b)$$

$$\mathcal{A}_{alt} = [1 \ 0 \ 0]^T, \quad \mathcal{B}_{alt} = [0 \ 0 \ -1]^T, \quad (3.38c)$$

$$\mathcal{A}_{dc} = [0 \ 1 \ 0]^T, \quad \mathcal{B}_{dc} = [0 \ 0 \ -1]^T, \quad (3.38d)$$

$$\mathcal{A}_{br} = [0 \ 0 \ 0]^T, \quad \mathcal{B}_{br} = [-1 \ 0 \ 0]^T, \quad (3.38e)$$

$$\mathcal{A}_{hvb} = [0 \ 0 \ 0]^T, \quad \mathcal{B}_{hvb} = [0 \ -1 \ 0]^T, \quad (3.38f)$$

$$\mathcal{A}_{lvb} = [0 \ 0 \ 0]^T, \quad \mathcal{B}_{lvb} = [0 \ 0 \ -1]^T, \quad (3.38g)$$

$$\mathcal{A}_{rst} = [0 \ 0 \ 0]^T, \quad \mathcal{B}_{rst} = [0 \ -1 \ 0]^T, \quad (3.38h)$$

$$\mathcal{A}_{as} = [0 \ 0 \ 0]^T, \quad \mathcal{B}_{as} = [0 \ -1 \ 0]^T, \quad (3.38i)$$

$$\mathcal{A}_{ccs} = [0 \ 0 \ 0]^T, \quad \mathcal{B}_{ccs} = [-1 \ 0 \ 0]^T. \quad (3.38j)$$

3.4.2 Objective Function

The objective in energy management is to minimize the fuel consumption, which is equivalent to minimizing the equivalent fuel energy, i.e.,

$$\min_{\{u_{ice,k}\}} \sum_{k \in \mathcal{K}} \tau u_{ice,k} \quad (3.39)$$

where the equivalent fuel power is given by $u_{ice,k} = H_0 \dot{m}_{f,k}$ with H_0 the lower heating value of the fuel and $\dot{m}_{f,k}$ the fuel consumption rate at sample k . This objective function is only defined in variables related to the internal combustion engine. However, we can obtain an objective function that is defined in variables related to every subsystem in the network, i.e., in the form of (3.1a), which is equivalent to (3.39) for a specific c_m and d_m . In particular, this holds if we choose c_m and d_m for every subsystem such that $\sum_{k \in \mathcal{K}} c_m u_{m,k} - d_m y_{m,k}$

represents the energy losses in the subsystem. The energy losses in each converter are given by the energy flowing into the converter minus the energy flowing out of the converter where the energy flowing into the converter is indicated with the arrow in Figure 2.1. According to this topology, the energy losses in the internal combustion engine, the electric motor, the alternator, the DCDC converter, the high-voltage battery and the low-voltage battery are given by the difference between the input and output power, i.e.,

$$c_m = \tau, \quad d_m = \tau, \quad (3.40a)$$

for $m \in \{\text{ice, em, alt, dc, hvb, lvb}\}$. For the refrigerated semi-trailer, the air supply system, the climate control system and the mechanical brakes, all energy flowing into the subsystem is eventually lost and therefore the energy losses are given for

$$c_m = 0, \quad d_m = \tau, \quad (3.40b)$$

for $m \in \{\text{rst, as, ccs, br}\}$. By substituting (3.40) into (3.1a), we obtain

$$\begin{aligned} \min_{\{u_{m,k}, y_{m,k}\}} \sum_{m \in \mathcal{M}} \sum_{k \in \mathcal{K}} c_m u_{m,k} - d_m y_{m,k} = \\ \min_{\{u_{m,k}, y_{m,k}\}} \tau (u_{\text{ice},k} - y_{\text{ice},k} + u_{\text{em},k} + u_{\text{alt},k} - y_{\text{ccs},k} - y_{\text{br},k} - y_{\text{em},k} - y_{\text{hvb},k} \\ - y_{\text{rst},k} - y_{\text{as},k} + u_{\text{dc},k} - y_{\text{alt},k} - y_{\text{lvb},k} - y_{\text{dc},k} + u_{\text{hvb},k} + u_{\text{lvb},k}). \end{aligned} \quad (3.41a)$$

By using the power balance constraints (3.37), we can reduce this minimization problem to the equivalent problem

$$\min_{\{u_{\text{ice},k}, u_{\text{hvb},k}, u_{\text{lvb},k}\}} \sum_{k \in \mathcal{K}} \tau u_{\text{ice},k} - \tau (v_{1,k} + v_{2,k} + v_{3,k}) + \tau (u_{\text{hvb},k} + u_{\text{lvb},k}). \quad (3.41b)$$

Moreover, as explained in Chapter 2, the high-voltage battery and low-voltage battery satisfy integrator dynamics so that we can write $\sum_{k \in \mathcal{K}} \tau u_{m,k} = x_{m,0} - x_{m,K}$ for $m \in \{\text{hvb, lvb}\}$ and further reduce the minimization problem (3.41b) to

$$\min_{\{u_{\text{ice},k}\}} \sum_{k \in \mathcal{K}} \tau u_{\text{ice},k} - \tau (v_{1,k} + v_{2,k} + v_{3,k}) + x_{\text{hvb},0} - x_{\text{hvb},K} + x_{\text{lvb},0} - x_{\text{lvb},K}. \quad (3.41c)$$

As the load signals are known for all $k \in \mathcal{K}$ and the initial and final states $x_{m,0}$ and $x_{m,K}$ for $m \in \{\text{hvb}, \text{lvb}\}$ are fixed, the optimal value for $u_{\text{ice},k}$ for (3.41c) is equivalent to the optimal value $u_{\text{ice},k}$ for (3.39) for all $k \in \mathcal{K}$. Hence, the optimal control problem (3.1) with objective function (3.1a) and c_m and d_m given by (3.40) provides the optimal solution for which the fuel consumption is minimized over all $k \in \mathcal{K}$ as is indicated in (3.39).

The CVEM problem for a vehicle with an internal combustion engine, an electric machine, a high-voltage battery, a refrigerated semi-trailer, an air supply system, an alternator, a DCDC converter, a low-voltage battery and a climate control system is now fully described by the optimal control problem defined in Section 3.2. In particular, the topology of the vehicle is described through (3.1f) for a given \mathcal{A}_m and \mathcal{B}_m , the objective function, i.e., minimizing fuel consumption, is described by (3.1a) by choosing c_m and d_m appropriately and the behavior of each subsystem is fully described by (3.1b) - (3.1e) by choosing the efficiency coefficients $q_{m,k}$, $f_{m,k}$ and $e_{m,k}$, the state-space matrices A_m , $B_{m,u}$, $B_{m,w}$ describing the dynamics of the subsystems, the lower and upper bound on the inputs $\underline{u}_{m,k}$ and $\bar{u}_{m,k}$, respectively, and the lower and upper bounds on the states $\underline{x}_{m,k}$ and $\bar{x}_{m,k}$, respectively. This allows the CVEM problem to be solved with the solution methods proposed in Section 3.2 and Section 3.3 as will be demonstrated in the next section.

3.5 Simulation Results

In this section, we will demonstrate the distributed optimization approach to complete vehicle energy management (CVEM) by using a simulation study. First, we will give the exogenous signals that we used for the simulation study followed by the results that will be discussed in three subsections. In the first subsection, we will analyze the computational performance and compare it with the state-of-the-art solver CPLEX [45]. In the second subsection, we will discuss the optimal power flows and state trajectories and, in the last subsection, the fuel consumption reduction for CVEM will be discussed.

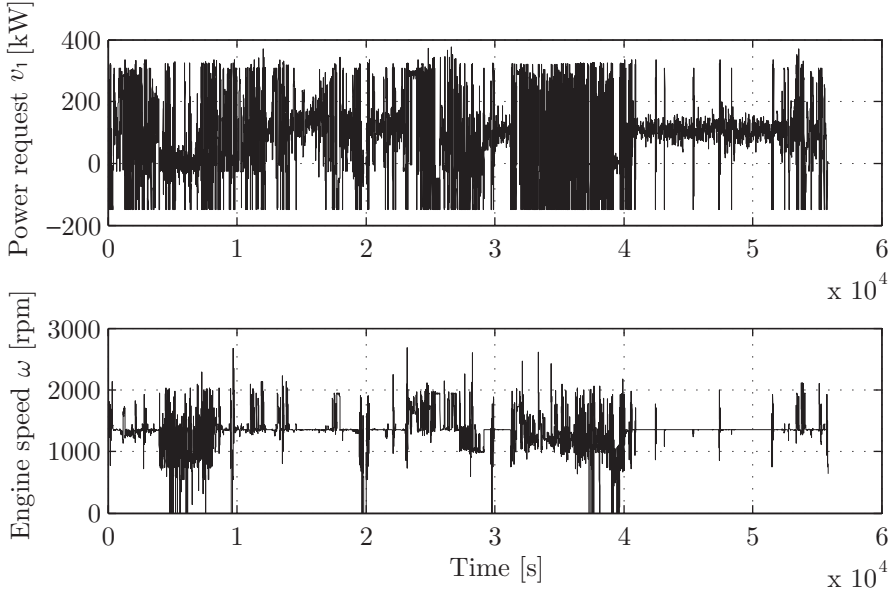


Figure 3.3: Pan European driving cycle.

3.5.1 Exogenous Inputs

The driving cycle is commonly described by a velocity profile over time. If the gear shift strategy is assumed to be known, the velocity profile can be converted to a power required at the wheels and the engine speed. This set of data is derived for a pan European driving cycle and shown in Figure 3.3. The brake power can reach up to -1000 kW. However, only a small part of the total braking power can be recovered by the subsystems. Therefore, the power request used as load signal $v_{1,k}$ is limited to the maximum braking power that can be recovered with all subsystems combined. Furthermore, the uncontrolled high-voltage auxiliaries are assumed to be absent such that $v_{2,k} = 0$ kW for all $k \in \mathcal{K}$ and the power required from uncontrolled low-voltage auxiliaries is assumed to be constant, i.e., $v_{3,k} = 1.5$ kW for all $k \in \mathcal{K}$.

3.5.2 Computational Performance

The local optimization problem related to each component defined in (3.13a) can be solved via different solution methods introduced in Section 3.3. In partic-

Table 3.1: Computation time in seconds for ADMM method with different interval lengths.

Subsystem	$K_\ell - K_{\ell-1}$	$K = 1000$			$K = 5000$		
		min	av	max	min	av	max
HVB	25	0.09	1.40	4.38	2.6	12.3	23.7
	50	0.08	0.69	2.04	1.7	6.15	11.7
	100	0.14	0.69	1.97	2.46	6.62	11.4
	200	0.16	0.41	0.99	0.93	3.94	7.6
	500	0.71	1.73	5.0	4.64	28.0	14.5
RST	25	0.09	1.16	3.7	0.45	6.3	19.8
	50	0.09	0.72	1.94	0.46	4.3	18.3
	100	0.17	0.71	1.54	0.93	5.79	24.3
AS	25	0.09	1.04	8.7	0.42	10.34	46.8
	50	0.09	1.07	8.4	0.40	5.35	41.8
	100	0.15	0.6	7.5	0.74	5.81	62.9
	200	0.18	0.44	4.5	0.85	3.78	36.8
	500	0.99	1.78	5.8	4.5	11.18	87.5
CCS	25	0.1	0.32	1.8	0.49	2.37	20.45
	50	0.1	0.28	1.54	0.5	1.85	12.7
	100	0.12	0.33	1.91	0.61	1.88	12.2
	200	0.14	0.39	2.35	0.7	2.13	13.7

ular, the performance of the ADMM solution method depends on the penalty parameter R in (3.19) and the interval length $K_\ell - K_{\ell-1}$ for $\ell \in \mathcal{L}$. For simplicity, we assume that the interval length is equal for all intervals $\ell \in \mathcal{L}$. The maximum, average and minimum time to compute the solution of the local optimization problem (3.13a) are given in Table 3.1 for the high-voltage battery (HVB), the refrigerated semi-trailer (RST), the air supply system (AS) and the climate control system (CCS) for different values of $K_\ell - K_{\ell-1}$ and two horizon lengths K . The value of the penalty parameter R in (3.19) is manually tuned for each $K_\ell - K_{\ell-1}$, but is kept constant for different lengths K of the drive cycle.

The computation time required to solve the optimization problem strongly depends on the amount of iterations over t in (3.19), required for the ADMM method to converge, which depends on the initial guess of the dual variables. We use the dual variables from the previous iteration s in the dual decomposition,

Table 3.2: Average computation time in seconds per component, per dual decomposition iteration.

Subsystem	Solution method	K				
		1000	2000	3000	4000	5000
HVB	QP	2.81	23.0	93.0	253.8	527.6
	ADMM	0.41	1.22	2.37	3.32	3.94
	LM	2.5e-04	0.066	0.063	0.07	0.09
RST	QP	3.93	29.4	118.4	291.1	562.3
	ADMM	0.72	1.38	1.94	2.60	4.3
	LM	0.045	0.21	0.38	0.74	1.29
AS	QP	4.98	33.9	130.7	366.3	602.6
	ADMM	0.44	0.59	1.15	3.09	3.78
	LM	0.012	0.034	0.046	0.071	0.061
CCS	QP	3.50	40.2	89.6	136.9	159
	ADMM	0.28	0.7	0.93	1.23	1.85

see (3.9), as an initial guess and therefore the amount of ADMM iterations reduces as the dual decomposition converges. As a consequence, the maximum time is significantly larger than the minimum time. The main conclusion drawn from this table is that the optimal $K_\ell - K_{\ell-1}$ differs per component and it should be chosen neither too small nor too large. Moreover, the optimal $K_\ell - K_{\ell-1}$ does not seem to depend on K . For example, the high-voltage battery has the highest performance for $K_\ell - K_{\ell-1} = 200$, which is the optimal trade-off between the size and number of QPs.

With the results of Table 3.1, we choose $K_\ell - K_{\ell-1} = 200$ for the high-voltage battery, $K_\ell - K_{\ell-1} = 50$ for the refrigerated semi-trailer, $K_\ell - K_{\ell-1} = 200$ for the air supply system and $K_\ell - K_{\ell-1} = 50$ for the climate control system. These results are compared with other solution methods in Table 3.2. This table shows the average computation time to solve the local optimization problem (3.13a) over all iterations s in the dual decomposition. Here, QP indicates the computation time for solving the local optimization problem (3.13a) with the QP solver CPLEX [45] directly, ADMM corresponds with Section 3.3.1 and LM corresponds with the Lagrangian Method introduced in Section 3.3.2. This table shows that ADMM offers a large improvement compared to QP, especially for

Table 3.3: Case studies with problem size defined in number of inputs, states and quadratic constraints.

Case	Description	Inputs	States	Quadratic constraints
Case 1	Truck with ICE, EM and a HVB	$4K$	K	K
Case 2	Case 1 with a RST	$5K$	$2K$	K
Case 3	Case 2 with an AS	$6K$	$3K$	K
Case 4	Case 3 with a CCS	$7K$	$5K$	$2K$
Case 5	Case 4 with an ALT and a LVB	$9K$	$6K$	$3K$
Case 6	Case 5 with a DCDC converter	$10K$	$6K$	$3K$

large horizons K . The LM method (with relaxation parameter $\gamma = 1$) reduces the computation time even further and depends on the number of intervals L required for the LM method. For $K = 3000$, the amount of intervals are 2, 6 and 53 for the high-voltage battery, the air supply system and the refrigerated semi-trailer, respectively. Note that this method cannot be used for the climate control system as this method is only suitable for scalar-state systems, i.e., $x_{m,k} \in \mathbb{R}$. Due to the absence of state constraints, the optimization problem for the internal combustion engine, electric machine, alternator, DCDC converter and mechanical brakes can be solved explicitly and are not shown in the table. Since the dynamics of the low-voltage battery are similar to the dynamics of the high-voltage battery, we conjecture that LM is also best for the low-voltage battery.

To assess the computational performance of solving the energy management problem for different vehicle configurations, we define six case studies with increasing complexity. These case studies are introduced in Table 3.3. To demonstrate that the conditions in Theorem 3.2.1 hold, we show in Table 3.4 the minimum value of the dual variables $\min_{k \in \mathcal{K}} \min_s \{\mu_{i,k}^s\}$, where $\mu_{i,k}^s$ denotes the i -th element of the vector μ_k^s at time $k \in \mathcal{K}$ and iteration s , i.e., $\mu_k^s = [\mu_{1,k}^s \mu_{2,k}^s \mu_{3,k}^s]^T \in \mathbb{R}^3$. Note that with $\mathcal{B}_m = -1$ for all $m \in \mathcal{M}$ and $d_m = \tau$ for all $m \in \mathcal{M}$, the condition in Theorem 3.2.1 is satisfied if and only if $\mu_{i,k}^s > -\tau$ for all $k \in \mathcal{K}$, $i \in \{1, 2, 3\}$ and s , which is always satisfied as shown in Table 3.4 for $\tau = 1$. Theorem 3.2.1 is satisfied for all simulations and is not further demonstrated in this section. Moreover, this table also shows the reduced iterations of the dual Newton update strategy compared with an update strategy with fixed step sizes,

Table 3.4: Number of iterations and minimum of the dual variables over all iterations for $K = 5000$.

	Case 1	Case 2	Case 3	Case 4	Case 5	Case 6
iter. (α_s^k constant)	105	122	119	228	221	384
iter. (Newton)	26	30	31	131	134	117
$\min_{k \in \mathcal{K}} \min_s \{\mu_{1,k}^s\}$	0.416	0.430	0.431	-0.03	-0.03	-0.03
$\min_{k \in \mathcal{K}} \min_s \{\mu_{2,k}^s\}$	0.621	0.622	0.626	0.616	0.623	0.612
$\min_{k \in \mathcal{K}} \min_s \{\mu_{3,k}^s\}$	N.A.	N.A.	N.A.	N.A.	0.522	0.628

i.e., with α_k^s being a constant. The Newton strategy always converged, which implies that the derivatives in (3.12) are sufficiently well approximated.

The computation times are given in Table 3.5 for each configuration. For these simulations, the optimal control problems related to each subsystem are solved in series, which is more straightforward to implement and, moreover, this results already in sufficient computational benefits for offline energy management. The computation time of the Distributed Optimization (DO) method introduced in this chapter are compared with the computation time of the QCQP solver CPLEX [45]. The CPLEX solver cannot handle quadratic constraints written in vector format and every quadratic constraint needs to be programmed separately. This requires a large amount of assembly time, which is not used for solving the actual optimization problem. Therefore, the computation times of CPLEX with and without assembling the optimization problem are given. If we compare only the time required to solve the optimization problem, DO is still 1825 times faster for Case 1 with $K = 5000$ and 64 times faster for Case 6 with $K = 3000$. Scalability of DO in the horizon length K is superior compared with CPLEX. Scalability in the number of components is not always better with DO, but only in the rare case with small K and many more components, CPLEX could be better than DO. The flexibility of adding and removing components with CPLEX remains poor though.

3.5.3 Optimal Input and State Trajectories

The optimal power flows as function of time are shown in Figure 3.4 for the complete vehicle and with a drive cycle length of only $K = 3000$ for clarity. Both, the results from DO, as well as the results from solving the optimization

Table 3.5: Computation times of DO and CPLEX in seconds.

Case	Solution method	K				
		1000	2000	3000	4000	5000
Case 1	CPLEX ¹	8.1	80	300	727	1259
	CPLEX ²	46	389	1405	3403	6509
	DO	0.035	0.24	0.21	0.74	0.69
Case 2	CPLEX ¹	20.3	369	1186	2355	6464
	CPLEX ²	90	924	3085	6946	15422
	DO	0.14	0.99	1.19	1.96	3.25
Case 3	CPLEX ¹	45	334	2014	6650	$> 10^4$
	CPLEX ²	146	1177	4863	13528	$> 10^4$
	DO	0.34	1.72	1.69	2.74	7.0
Case 4	CPLEX ¹	71	454	3112	$> 10^4$	$> 10^4$
	CPLEX ²	357	2721	10770	$> 10^4$	$> 10^4$
	DO	4.35	10.5	18.6	24.2	40.1
Case 5	CPLEX ¹	76	958	2834	$> 10^3$	$> 10^3$
	CPLEX ²	791	6835	22213	$\gg 10^4$	$\gg 10^4$
	DO	9.6	23.1	43.8	60.9	120.3
Case 6	CPLEX ¹	79	965	3285	$> 10^4$	$> 10^4$
	CPLEX ²	1003	8304	28202	$\gg 10^4$	$\gg 10^4$
	DO	11.3	31.5	51.4	73.2	150.7

¹ Computation times without assembly time

² Computation times with assembly time

problem with CPLEX are shown. This figure demonstrates that both methods converge to the same solution (within a desired tolerance). Moreover, the fuel consumption of DO is 0.019 % smaller compared with CPLEX, which is negligible. Two important observations can be made from this figure, i) all auxiliaries are used to store (brake) energy and ii) the DCDC converter is generally used to supply the low-voltage auxiliaries, except when free brake energy is available, then the alternator supplies the low-voltage auxiliaries and charges the low-voltage battery. The first observation can also be seen from the state trajectories given in Figure 3.5 where $\tilde{x}_{hvb} = \frac{x_{hvb}}{E_{hvb}}$ is the high-voltage battery energy normalized with respect to the maximum battery capacity E_{hvb} , $\tilde{x}_{lvb} = \frac{x_{lvb}}{E_{lvb}}$ is the low-voltage

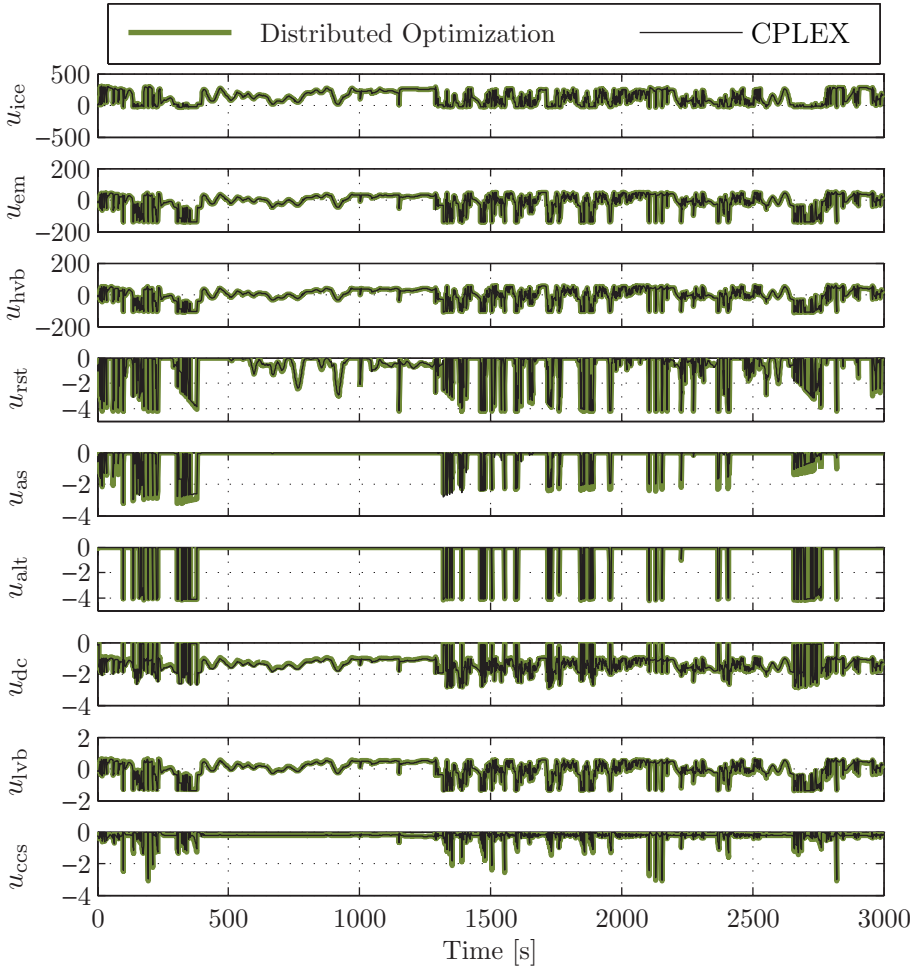


Figure 3.4: Optimal power flows (in kW) for DO and CPLEX.

battery energy normalized with respect to the maximum battery capacity E_{lbb} , T_{rst} is the air temperature in the refrigerated trailer, p_{as} is the air pressure in the air supply system and T_{ccs} is the wall temperature in the climate control system. This figure shows that all state constraints are met, where for the climate control system, only the constraint on the wall temperature is shown. The optimal state trajectories over the full pan European driving cycle are given in Appendix A, which requires solving the CVEM problem with over 500.000 input constraints, 300.000 state constraints and 150.000 quadratic constraints.

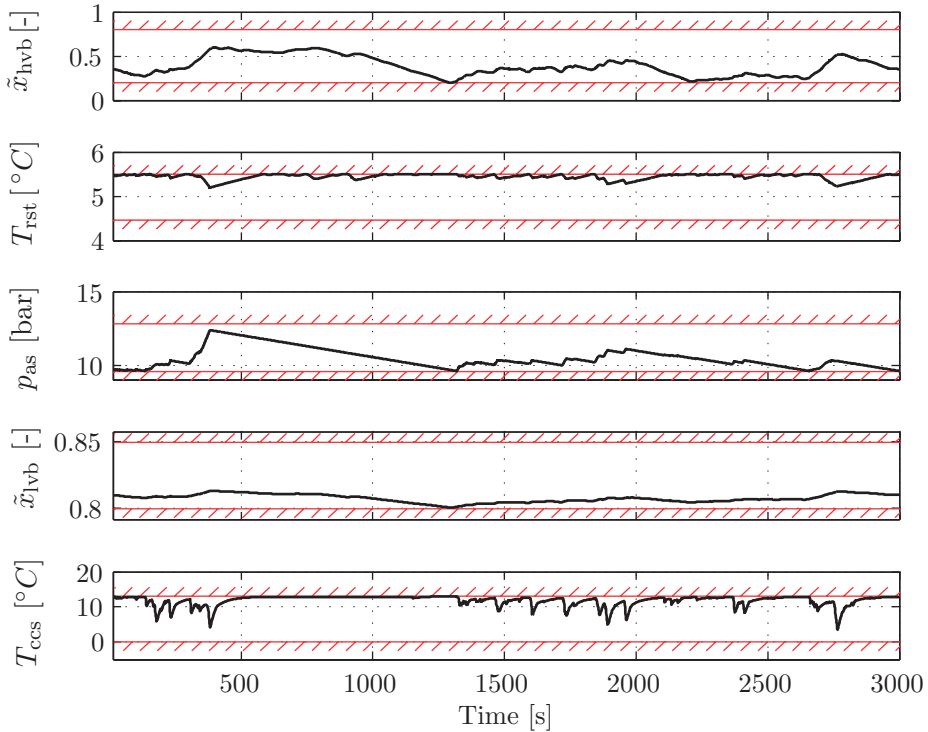


Figure 3.5: Optimal state trajectories for distributed optimization.

3.5.4 Fuel Consumption Reduction

To analyze the fuel consumption for different parts of the complete drive cycle, the drive cycle is split into three parts. The first part is given by $k \in \{0, \dots, 19999\}$, the second part by $k \in \{20000, \dots, 39999\}$ and the third part by $k \in \{40000, \dots, 55579\}$. The fuel consumption reduction for each of the cases and for each of these drive cycles are given in Table 5.1. For the first case, the baseline is a non-hybrid truck with the air temperature in the refrigerated semi-trailer kept at its upper bound, the air pressure in the air supply system kept at its lower bound and the temperature in the climate control system kept at its upper bound. For the next cases, the baseline is the previous case to emphasize the potential of each auxiliary. Results are shown without aging constraints on the high-voltage battery, as presented in [99], and results with aging constraints. The results with aging constraints are obtained with the method presented in [55]. This method applies the same dual decomposition, but the optimal con-

Table 3.6: Fuel reduction results.

Case	Without battery aging				With battery aging			
	Part 1	Part 2	Part 3	Full	Part 1	Part 2	Part 3	Full
1	6.00%	10.93%	2.33%	6.64%	5.35%	9.77%	2.02%	5.91%
2	0.08%	0.12%	0.03%	0.07%	0.32%	0.57%	0.13%	0.35%
3	0.02%	0.03%	0.01%	0.02%	0.10%	0.12%	0.04%	0.09%
4	0.01%	0.04%	0.02%	0.03%	0.01%	0.04%	0.02%	0.03%
5	0.07%	0.11%	0.02%	0.06%	0.07%	0.15%	0.03%	0.08%
6	0.34%	0.32%	0.25%	0.34%	0.40%	0.44%	0.38%	0.41%

control problem related to the high-voltage battery system is solved as a sequential quadratic program to satisfy the aging constraint. The aging constraint penalizes the use of the high-voltage battery, which is more realistic, and causes a drop in fuel reduction compared to an unrestricted high-voltage battery. The CVEM strategy recognizes this and stores more energy in the buffers of the auxiliaries, thereby recovering some of the lost fuel reduction. Overall, the DCDC converter (Case 6) is the most potential auxiliary for reducing fuel with 0.41 %. Overall, the fuel reduction obtained with smart control of all auxiliaries, i.e., Case 6 compared with Case 1, is 0.52 % without taking into account battery aging and 0.96 % by taking into account battery aging.

3.5.5 Optimal trade-off between number of switches and fuel reduction

The current trend in automotive applications is to electrify the auxiliaries in the vehicle, which do allow for continuous control (see, e.g., [95]). Still, the refrigerated semi-trailer, the air supply system and the climate control system are often attached to the engine via a clutch and, therefore, can only be switched on or off. Therefore, the optimal control problem related to the refrigerated semi-trailer, the air supply system and the climate control system is also solved with the dynamic programming solution method presented in Section 3.3.3.

The amount of switches is controlled with the penalty parameter σ . These on/off decision variables are not convex so that the dual decomposition is not guaranteed to converge. Still, the optimal control problem related to the on/off

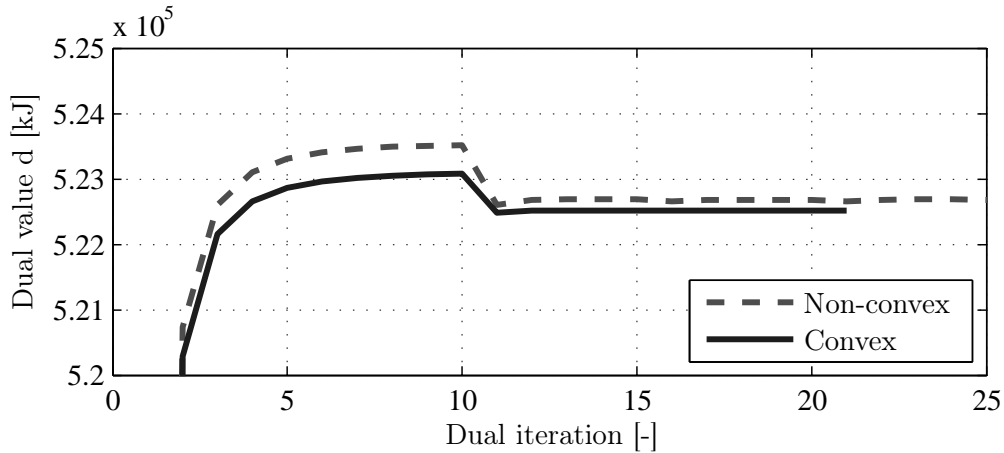


Figure 3.6: Convergence of the dual value for the convex optimal control problem and the non-convex optimal control problem.

controlled subsystem is only solved every n -th iteration. This allows the algorithm to converge for the remaining $n-1$ iterations while the non-convex decisions are fixed. This is demonstrated in Figure 3.6 for $n = 5$. In this figure, the dual value d defined by (3.4) as function of the dual iterations is given for the convex optimal control problem and non-convex optimal control problem with on/off decisions. Although, the global optimal solution is not guaranteed and choosing n can be difficult, the solution seems to give a good approximation of the global optimal solution. Moreover, solving the CVEM problem with many on/off auxiliaries is still efficient as the optimal control problem associated with the on/off subsystems is only solved at a limited number of iterations.

This solution method for on/off control allows us to solve the CVEM problem with different switching penalties for the refrigerated-semitrailer, the air supply system and the climate control system. The results are shown in Figure 3.8 for Part 1 and Part 2 of the pan European driving cycle and where battery aging is taken into account. For each of the auxiliaries and each part of the driving cycle, two hatched regions are shown, i.e., an infeasible region and a default region. The boundary of the infeasible region is given by the optimal trade-off between the number of switches and the fuel reduction and obtained with the method presented in this chapter.

Furthermore, the default controller turns on the auxiliary when the lower en-

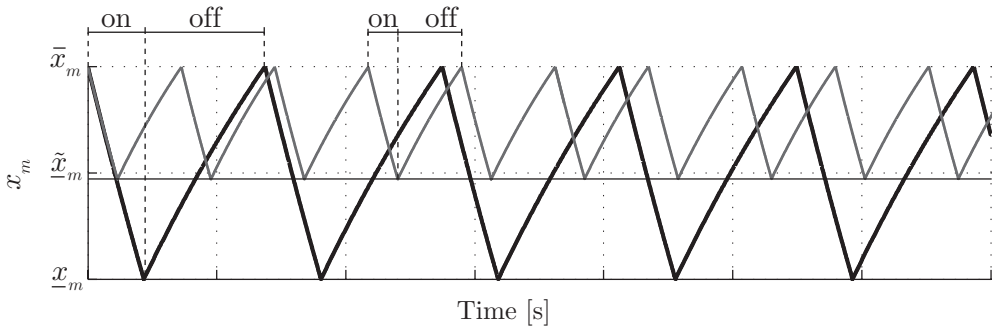


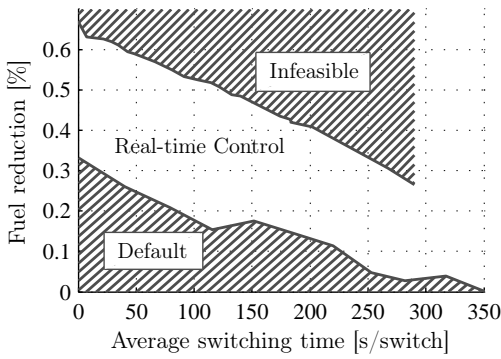
Figure 3.7: Default control of a subsystem that can only be turned on or off for two different lower bounds.

ergy limit is violated and turns the auxiliary off when the upper energy limit is violated, which is illustrated in Figure 3.7. For these auxiliaries, it holds that the more energy is stored, the higher is the rate of energy dissipation to the environment. To show this, let us consider for example the refrigerated semi-trailer where a larger difference between the air temperature inside and the ambient temperature leads to a larger energy dissipation. By decreasing the upper energy limit, the number of switches with default control will increase, but also the energy dissipation decreases leading to a fuel reduction. This trade-off defines the boundary of the default region. A proper real-time energy management strategy operates preferably close to the infeasible region, but definitely not in the default region. This can be rather challenging for the climate control system as the default region is close to the infeasible region leaving a very narrow band for real-time control.

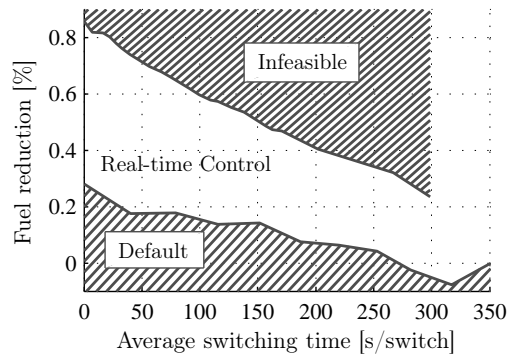
The fuel reduction obtained with continuous control is given at the average switching time of 0 seconds, i.e., with infinite switching. For the climate control system, this leads to a jump, which is a result of the 1 second sample time that is used to solve the optimal control problem. This leads to a minimum average switching time of 5 seconds. Another observation from these results is that the fuel reduction shown in Figure 3.8 with continuous control for the refrigerated semi-trailer, the air supply system and the climate control system is much larger than the fuel reduction given in Table 5.1. This is a result of a different default control strategy, i.e., the default control strategy used for Table 5.1 is a continuous control strategy that keeps the energy in the subsystem at the upper bound. By

comparing the smart continuous control strategy to the default switched control strategy, a fuel reduction of 1.42 % can be obtained instead of 0.96 %.

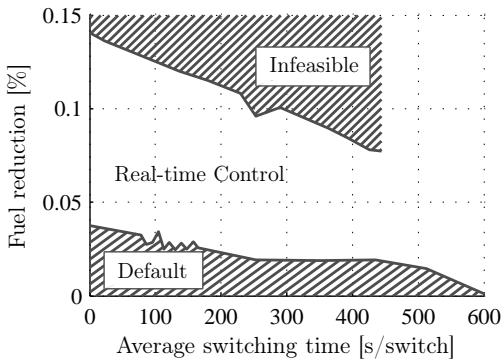
Obtaining a fuel reduction by smart control of some auxiliaries, e.g., the climate control system, can be challenging and integration of those auxiliaries into the energy management strategy might not outweigh the additional cost and complexity. However, the main result of the distributed optimization approach presented in this chapter is that the energy management problem is decomposed into smaller energy management problems related to each subsystem. Each of the energy management problems on subsystem level is much easier to solve and can be solved with different algorithms, e.g., an ADMM method, Lagrangian method or even dynamic programming. Extensions to more sophisticated models will also be easier. A very interesting example is the extension to higher-order battery models and battery aging in [55] where only the smaller energy management problem related to the high-voltage battery had to be modified. Finally, developing optimal control algorithms for different subsystems can be done in parallel, e.g., thermal management of the internal combustion engine can be included in the internal combustion engine optimization problem, while at the same time thermal management of the high-voltage battery can be included in the high-voltage battery optimization problem.



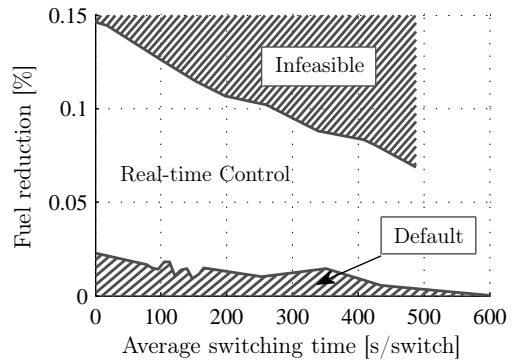
(a) Refrigerated semi-trailer, part 1



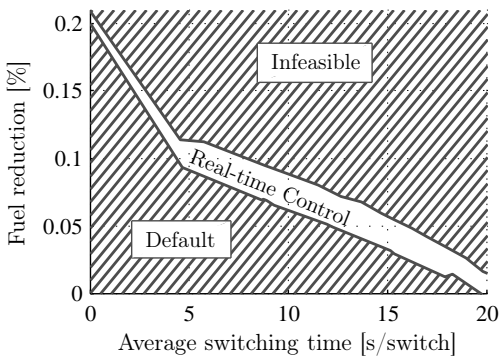
(b) Refrigerated semi-trailer, part 2



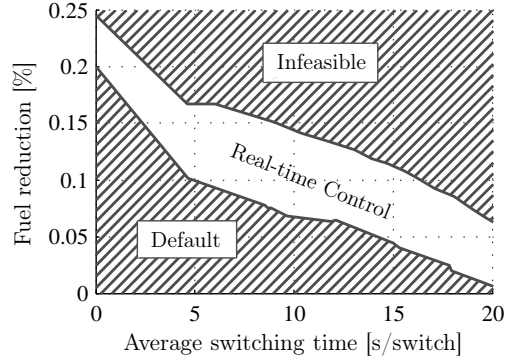
(c) Air supply system, part 1



(d) Air supply system, part 2



(e) Climate control system, part 1



(f) Climate control system, part 2

Figure 3.8: Fuel reduction potential for smart on/off control of the refrigerated semi-trailer, the air supply system and the climate control system.

3.6 Conclusions and Discussion

In this chapter, a distributed optimization approach has been proposed to solve the complete vehicle energy management problem of a hybrid truck with auxiliaries. Conclusions will be drawn and a discussion on the results will be given in this section.

3.6.1 Conclusions

The approach presented in this chapter applies first a dual decomposition to the optimal control problem such that the problem related to each subsystem can be solved separately. Then, either an ADMM method, a Lagrangian Method or a solution method based on dynamic programming has been used to efficiently solve the optimal control problem for every subsystem in the vehicle. The proposed approach has been demonstrated by solving the complete vehicle energy management problem of a hybrid truck with a refrigerated semi-trailer, an air supply system, an alternator, a DCDC converter, a low-voltage battery and a climate control system. Simulation results have shown that the computation time is reduced by a factor of 64 up to 1825, compared to solving the problem with the CPLEX solver, depending on the vehicle configuration and driving conditions. The fuel consumption can be reduced up to 1.42 % by including auxiliaries in the energy management problem. This requires however, that the auxiliaries are continuous controlled or that the number of switches is unbounded.

3.6.2 Discussion

The distributed optimization approach presented in this chapter recovers the global optimal solution by solving the CVEM offline. This requires that all disturbances are known on forehand, e.g., the driving cycle. As disturbances are never exactly known, the solution cannot be implemented in real-time and moreover, the computational complexity is still too high for real-time control. Rule-based strategies have a low computational complexity and have been proposed in literature for control of the hybrid electric system [17, 42, 47, 122]. These rules can be derived from the optimal offline solution, e.g., from the optimal output powers as function of the power request v_1 at the wheels, which is given in Figure 3.9 for the electric motor output power and for the (continuous) refrigerated

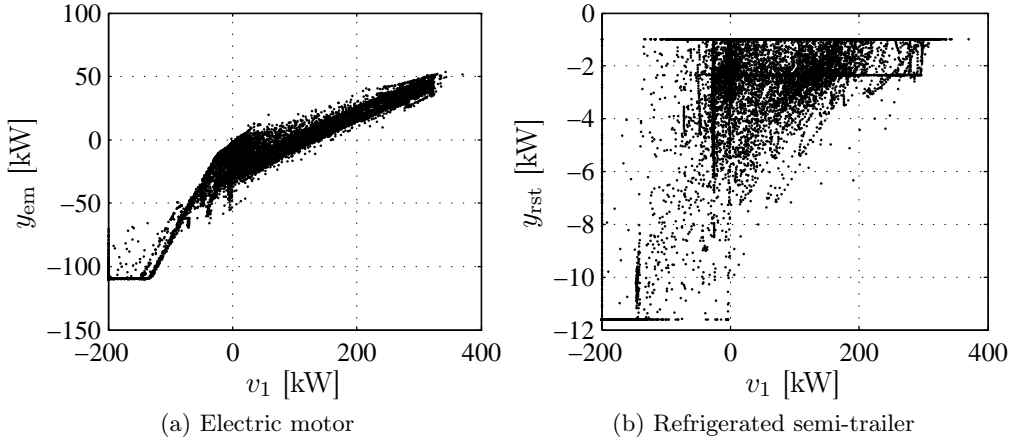


Figure 3.9: Optimal output power versus power request.

semi-trailer output power. This figure shows that the relation between power request and the electric motor power is better defined than the relation between the power request and the refrigerated semi-trailer power. Finding a rule-based strategy for the refrigerated semi-trailer (and the other auxiliaries) is therefore not straightforward.

More advanced strategies based on optimal control can lead to close to optimal decisions, but are often restricted by their computational complexity. Still, the approach presented in this chapter can be modified to be used for real-time control. To do so, the optimal control problem needs to be defined over a shorter (receding) horizon. After dual decomposition, this results in small Linearly Constrained Quadratic Programs (LCQP) for each of the subsystems, which can be solved in real-time with embedded LCQP solvers. The optimal control problem is then solved at each time instant k after which only the decisions at the first time instant are implemented. The so-called distributed model predictive control approach will be presented in the next chapter for real-time CVEM.

4

Distributed Economic MPC for Online Energy Management

Abstract - *In this chapter, a real-time distributed economic model predictive control approach to Complete Vehicle Energy Management (CVEM) is presented using a receding control horizon in combination with a dual decomposition. The dual decomposition allows the CVEM optimization problem to be solved by solving several smaller optimization problems. The receding horizon control problem is formulated with variable sample intervals, allowing for large prediction horizons with only a limited number of decision variables and constraints in the optimization problem. Furthermore, a novel on/off control concept for control of the refrigerated semi-trailer, the air supply system and the climate control system is introduced. Simulation results on a low-fidelity vehicle model show that close to optimal fuel reduction performance can be achieved. The fuel reduction for the on/off controlled subsystems strongly depends on the number of switches allowed. By allowing up to 15 times more switches, a fuel reduction of 1.3 % can be achieved.*

4.1 Introduction

The previous chapter provides an offline solution strategy to solve the Complete Vehicle Energy Management (CVEM) problem. The offline solution strategy requires all disturbances to be known (e.g., the driving cycle) so that the global optimal solution can be computed. This solution strategy cannot be used in real-time as these disturbances are generally not known. Still, it does provide a benchmark for online solution strategies and is therefore a valuable tool. Examples of online solution strategies that are real-time implementable are rule-based strategies (see, e.g., [17, 42]), equivalent consumption minimization strategies (ECMS, see, e.g., [107, 88, 89]) and solution strategies based on model predictive control (MPC, see, e.g., [3, 53, 84]).

The MPC strategies are interesting as they naturally take into account prediction information. The prediction information can be stochastic as in [25, 129] or deterministic as in [3, 53, 84, 104, 7, 116]. The deterministic MPC strategies either predict the future power demand as a function of the current power demand, e.g., the power demand is exponentially decaying, as in [104, 7] or held constant as in [116], or the future power demand is predicted with a vehicle model and road preview information, as in [3] or it is assumed that the future power demand is exactly known, as in [53, 84]. The choice of the cost function also leads to many variations in MPC strategies. The cost function generally weights the fuel consumption, with or without additional terms penalizing the final state, the state deviations and the size of the control inputs, which leads to many penalizing parameters.

While the aforementioned online solution strategies might be able to handle the complexity of the CVEM problem, the flexibility of these strategies is poor. Rule-based strategies require a new set of rules for every subsystem that is added to the CVEM problem, ECMS requires tuning of an equivalence factor for each additional state in the CVEM problem and MPC requires reformulating the optimal control problem, the cost function and tuning of the penalizing parameters each time a subsystem is added.

To enhance the flexibility of the online energy management strategy, a distributed solution strategy can be taken. In [11], an online game-theoretic approach to CVEM is presented, but prediction information is not taken into ac-

count. In [81], an online game-theoretic approach in combination with MPC is presented, which does utilize prediction information, but requires solving a nonlinear program. In [83], flexibility is obtained by using the Alternating Direction Method of Multipliers (ADMM), while ideas based on ECMS are used to calculate the equivalent costs at a supervisory level. While each of these solution strategies is interesting and provides a certain degree of flexibility, they require still a significant amount of tuning while a real-time implementability is not guaranteed.

In this chapter, which is based on [103, 100], we propose to use distributed economic MPC to solve the CVEM problem introduced in Chapter 2. In particular, we define the optimal control problem as in Chapter 3 over a shorter (receding) horizon. After applying a dual decomposition, this results in small Linearly Constrained Quadratic Programs (LCQP) for each of the subsystems, which can be efficiently solved in real-time with embedded LCQP solvers. The optimal control problem is then solved at each time instant $k \in \mathbb{N}$ over a horizon with length N after which only the decisions at the time instant k are implemented. The conventional cost function in MPC is generally chosen as a quadratic performance index, which is a measure of the predicted deviation of the error between the states and inputs from their corresponding steady-state values, as was done in the context of energy management in, e.g., [104, 7, 116]. For CVEM, the cost function follows from the desire to minimize the energy losses in the vehicle. Therefore, we will adopt the terminology as in [32], which uses economic MPC as forcing the system to operate around a pre-specified steady-state value is not necessarily the most efficient.

Choosing the length of the prediction horizon for economic MPC is difficult. On the one hand, the need for soft final state constraints to be added to the cost function, as is done in, e.g., [104], can be avoided by taking a long prediction horizon. On the other hand, the number of decision variables is typically proportional to the length of the prediction horizon, which leads to a preference for short prediction horizons to allow for real-time implementation. Therefore, we will use variable prediction time intervals that allows long prediction horizons with a limited number of decision variables. These were first introduced in [103]. Furthermore, we will incorporate the control concept first introduced in [100] that allows the control of auxiliaries that can only be turned on or off. This

concept relaxes the use of binary (on/off) decision variables to continuous decision variables over the entire horizon, except for the first time instant, where the decision variable is actually binary. Recall that in MPC this is the only control input that is actually implemented. This allows the relaxed control problem to be formulated as the minimization of two solutions to a LCQP, where one LCQP is solved under the assumption that the first decision being "on" and one LCQP is solved under the assumption that the first decision being "off". The solution with the lowest total cost of the two is then the optimal solution.

In this chapter, we will formalize such an optimization strategy. In doing so, the disturbances over the prediction horizon are assumed to be known exactly and the solution strategy is evaluated on the low-fidelity vehicle model presented in Chapter 2. This excludes the influence of faulty prediction information and allows a thorough analysis of the algorithm. In the next chapter, the solution strategy will be implemented on a high-fidelity vehicle model and future disturbances are predicted to truly demonstrate the fuel reduction potential of the algorithm in a realistic simulation environment.

The outline of this chapter is as follows. The distributed model predictive control approach is given in Section 4.2. In Section 4.3, the prediction method for the disturbances is given and the simulation results on the low-fidelity vehicle model are given in Section 4.4. Some important conclusions will be drawn in Section 5.5.

4.2 Distributed Economic Model Predictive Control

In this section, we propose to use a distributed economic model predictive control (DEMPC) approach to efficiently solve the CVEM problem over a receding horizon. The solution is found by decomposing the optimal control problem with a dual decomposition, which results in a smaller optimization problem related to each component, which can be solved efficiently. This section first presents the receding horizon control problem, then the distributed solution approach followed by a method to handle on/off-controlled subsystems. Finally, we will discuss the stability and recursive feasibility properties.

4.2.1 Receding Horizon Optimal Control Problem

The objective for CVEM is minimizing the cumulative fuel consumption, which is equivalent to minimizing the cumulative fuel energy given by (2.4). In this chapter, the CVEM is solved in a receding horizon fashion, for which we approximate the objective function (2.4), at each given time instant $k \in \mathbb{N}$ by

$$\{u_{ice,n|k}\}_{n \in \mathcal{N}} = \arg \min_{\{u_{ice,n|k}\}_{n \in \mathcal{N}}} \sum_{n \in \mathcal{N}} \tau_n u_{ice,n|k} \quad (4.1)$$

with prediction time instant $n \in \mathcal{N} = \{0, 1, \dots, N-1\}$ where N is the prediction horizon length and where the engine input power $u_{ice,n|k}$ is constant over the length of the sample interval τ_n . In MPC, (4.1) is solved over the horizon N at each given time instant $k \in \mathbb{N}$ and only the first decision is implemented, i.e., $u_{ice,0|k} = u_{ice}(k\tau_0)$ is implemented at time $k\tau_0$. At the next time instant $k+1$, this process is repeated and results in $u_{ice,0|k+1} = u_{ice}((k+1)\tau_0)$ as the implemented control action at time $(k+1)\tau_0$. Note that the objective function (4.1) is only defined in variables related to the internal combustion engine. However, in Section 3.4.2, it has been shown that an objective function can be defined in variables related to every subsystem in the network, i.e., in the form of

$$\{u_{m,n|k}, y_{m,n|k}\} = \arg \min_{\{u_{m,n|k}, y_{m,n|k}\}} \sum_{m \in \mathcal{M}} \sum_{n \in \mathcal{N}} c_{m,n} u_{m,n|k} - d_{m,n} y_{m,n|k}, \quad (4.2a)$$

where $u_{m,n|k} \in \mathbb{R}$ and $y_{m,n|k} \in \mathbb{R}$ are the inputs and outputs of the converter in subsystem $m \in \mathcal{M} = \{\text{ice, em, hvb, rst, as, ccs, dc, lvb, alt, br}\}$, which are constant over the length of the sample interval τ_n . In particular, the objective in (4.2a) is equivalent to (4.1) for $d_{m,n} = \tau_n$ for all $m \in \mathcal{M}$, $c_{m,n} = \tau_n$ for $m \in \{\text{ice, em, alt, dc, hvb, lvb}\}$ and $c_{m,n} = 0$ for $m \in \{\text{rst, as, ccs, br}\}$ as was shown in Section 3.4.2. Note that, in (4.2a) we use the notation $\{u_{m,n|k}, y_{m,n|k}\}$ to indicate $\{u_{m,n|k}, y_{m,n|k}\}_{m \in \mathcal{M}, n \in \mathcal{N}}$. This notation will be used throughout the chapter for minimizing over a set.

The receding horizon optimal control problem aims at solving (4.2a) at each time instant $k \in \mathbb{N}$ subject to a quadratic equality constrained describing the

input-output behavior of each converter, i.e.,

$$q_{m,n|k} u_{m,n|k}^2 + f_{m,n|k} u_{m,n|k} + e_{m,n|k} + y_{m,n|k} = 0, \quad (4.2b)$$

for $m \in \mathcal{M}$ and $n \in \mathcal{N}$ and subject to linear system dynamics of the energy in the storage device in subsystem m , i.e.,

$$x_{m,n+1|k} = A_{m,n} x_{m,n|k} + B_{m,n}^w w_{m,n|k} + B_{m,n}^u u_{m,n|k}, \quad (4.2c)$$

for $m \in \mathcal{M}$ and $n \in \mathcal{N}$ and where $x_{m,0|k}$ is the measured current state of the storage device m , $x_{m,N|k}$ is a desired final state of the storage device m at the end of the prediction horizon, $w_{m,n|k}$ is a predicted disturbance at every prediction time instant $n \in \mathcal{N}$ at time $k \in \mathbb{N}$ for storage device m and subject to linear inequality constraints on the inputs of each converter, i.e.,

$$\underline{u}_{m,n|k} \leq u_{m,n|k} \leq \bar{u}_{m,n|k}, \quad (4.2d)$$

for all $n \in \mathcal{N}$ and $m \in \mathcal{M}$ and subject to linear inequality constraints on the states of each storage device, i.e.,

$$\underline{x}_{m,n|k} \leq x_{m,n|k} \leq \bar{x}_{m,n|k}, \quad (4.2e)$$

for all $n \in \mathcal{N}$ and $m \in \mathcal{M}$. Finally, the optimization problem is solved subject to a linear equality constraint describing the interconnection of the subsystems, i.e.,

$$v_{n|k} + \sum_{m \in \mathcal{M}} \mathcal{A}_m u_{m,n|k} + \mathcal{B}_m y_{m,n|k} = \mathbf{0} \quad (4.2f)$$

for all $n \in \mathcal{N}$, where $\mathcal{A}_m \in \mathbb{R}^L$ and $\mathcal{B}_m \in \mathbb{R}^L$ are vectors with the ℓ -th element being -1 if the power flow to the node ℓ is positive, 0 if there is no power flow to the node ℓ and 1 if the power flow to the node is negative. Here, L is the number of nodes in the topology where power is aggregated. Indeed, the power balance constraints in (2.5) are given by (4.2f) for well chosen matrices \mathcal{A}_m and \mathcal{B}_m . Furthermore, it is assumed that the disturbance $v_{0|k}$ can be measured at each time instant $k \in \mathbb{N}$, while $v_{n|k}$ for $n \in \{0, \dots, N-1\}$ has to be predicted at each time instant $k \in \mathbb{N}$ with the prediction algorithm presented in Section 4.3.

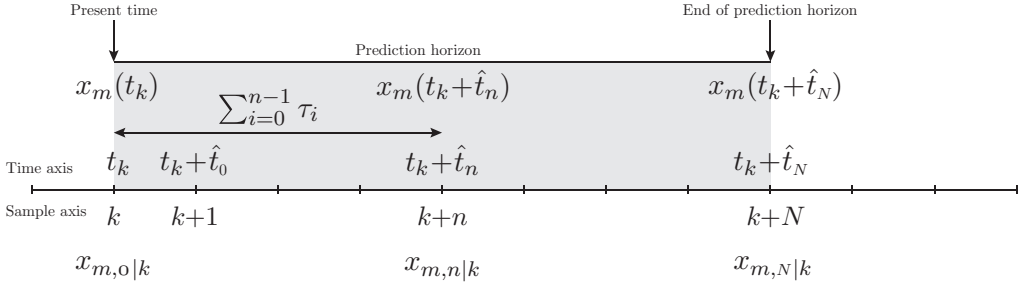


Figure 4.1: Prediction of $x_{m,n|k} = x_m(t_k + \hat{t}_n)$ at some future time $t_k + \hat{t}_n$.

It should be noted that the efficiency coefficients $q_{m,n|k}$, $f_{m,n|k}$ and $e_{m,n|k}$ and the lower and upper bounds $\underline{u}_{m,n|k}$ and $\bar{u}_{m,n|k}$, respectively, that depend on speed, as is the case for the internal combustion engine, the electric machine and alternator, are obtained by evaluating these coefficients and bounds at the predicted speed $\omega_{n|k}$ for $n \in \mathcal{N}$ at each time instant $k \in \mathbb{N}$. Moreover, the dynamics of the high- and low-voltage battery, the refrigerated semi-trailer, the air supply system and the climate control system given in Chapter 2 can all be formulated as a linear differential equation, i.e.,

$$\frac{d}{dt}x_m(t) = \tilde{A}_m x_m(t) + \tilde{B}_{m,w} w_m(t) + \tilde{B}_{m,u} u_m(t), \quad (4.3)$$

for $m \in \{\text{hvb}, \text{lvb}, \text{rst}, \text{as}, \text{ccs}\}$. This differential equation allows us to make a prediction of $x_{m,n|k} = x_m(t_k + \hat{t}_n)$ at some future time $t_k + \hat{t}_n$ (see Figure 4.1), where $\hat{t}_n = \sum_{i=0}^{n-1} \tau_i$, given a measurement of the state $x_{m,0|k} = x_m(t_k)$ at present time t_k and a piecewise constant u_m , i.e., $u_m(t_k + t)$ for $t \in [\hat{t}_n, \hat{t}_{n+1})$ and $n \in \mathcal{N}$. This prediction is made by making a discrete approximation of (4.3), leading to (4.2c) with

$$A_{m,n} = e^{\tilde{A}_m \tau_n}, \quad B_{m,n}^w = \Gamma_{m,n} \tilde{B}_m^w, \quad B_{m,n}^u = \Gamma_{m,n} \tilde{B}_m^u, \quad (4.4)$$

in which $\Gamma_{m,n} = \int_0^{\tau_n} e^{\tilde{A}_m s} ds$ and τ_n is the sample time used in (4.3).

In [103], we proposed to take variable prediction time intervals τ_n to allow for a long prediction horizon using only a limited amount of prediction instants N . This is necessary to keep the optimal control problem small in the number of decision variables and real-time solvable. This method is similar to move blocking

strategies [10] except that it does not only assume that the control inputs over the prediction time intervals are constant, it also assumes that it is sufficient to only constrain the dynamics at the beginning and end of each interval through (4.2c).

4.2.2 Distributed Solution using a Dual Decomposition

The optimal control problem (4.2a) subject to (4.2b) - (4.2f) is a quadratically constrained linear program, which cannot be easily solved using embedded solvers, e.g., CVXgen [71] or QPoases [34]. We therefore apply ideas from distributed optimization and will show that this leads to several linearly constrained quadratic programs (LCQPs). It should be noted that the subsystems in (4.2) are only connected by (4.2f).

To decompose the problem, we will employ the dual decomposition approach, as was done in the previous chapter. Using the notation of this chapter, we again augment the objective function (4.2a) with the complicating constraints (i.e., the constraints that act on more than one subsystem), which is (4.2f) in this case. This leads to the following so-called *partial Lagrangian*:

$$L(\{u_{m,n|k}, y_{m,n|k}, \mu_{n|k}\}) = \sum_{n \in \mathcal{N}} \mu_{n|k}^T v_{n|k} + \sum_{m \in \mathcal{M}} c_{m,n} u_{m,n|k} - d_{m,n} y_{m,n|k} + \mu_{n|k}^T (\mathcal{A}_m u_{m,n|k} + \mathcal{B}_m y_{m,n|k}), \quad (4.5)$$

where $\mu_{n|k} \in \mathbb{R}^L$ is a Lagrange multiplier, which is to be solved subject to (4.2b)-(4.2e). The partial Lagrange dual function is given by

$$\begin{aligned} g(\{\mu_{n|k}\}) &= \min_{\{u_{m,n|k}, y_{m,n|k}\}} L(\{u_{m,n|k}, y_{m,n|k}, \mu_{n|k}\}) \\ &= \sum_{n \in \mathcal{N}} \mu_{n|k}^T v_{n|k} + \sum_{m \in \mathcal{M}} g_m(\{\mu_{n|k}\}), \end{aligned} \quad (4.6a)$$

with

$$\begin{aligned} g_m(\{\mu_{n|k}\}) &= \min_{\{u_{m,n|k}, y_{m,n|k}\}} \sum_{n \in \mathcal{N}} c_{m,n} u_{m,n|k} - d_{m,n} y_{m,n|k} \\ &\quad + \mu_{n|k}^T (\mathcal{A}_m u_{m,n|k} + \mathcal{B}_m y_{m,n|k}), \end{aligned} \quad (4.6b)$$

subject to (4.2b)-(4.2e). Note that each of the Lagrange dual functions (4.6b)

subject to (4.2b)-(4.2e) is related to one of the subsystems $m \in \mathcal{M}$ and can be solved independently. To solve the dual optimization problem, the dual function (4.6) has to be maximized over $\mu_{n|k}$. This can be done using a ‘steepest ascent’ method by iteratively solving

$$\mu_{n|k}^{s+1} = \mu_{n|k}^s + \alpha_k^s \left(v_{n|k} + \sum_{m \in \mathcal{M}} \mathcal{A}_m u_{m,n|k}^s + \mathcal{B}_m y_{m,n|k}^s \right), \quad (4.7)$$

where α_k^s is a suitably chosen matrix. It has been shown in Section 3.2.2 that under very mild and verifiable conditions, the solutions to the dual optimization problem (4.6) and (4.7) and the primal optimization problem (4.2) are the same.

Each of the Lagrange dual functions (4.6b) related to one of the subsystems can be solved separately and can be written as an LCQP by substituting (4.2b) into (4.6b), which gives

$$g_m(\{\mu_{n|k}\}) = \min_{\{u_{m,n|k}\}} \sum_{n \in \mathcal{N}} \frac{1}{2} H_{m,n|k} u_{m,n|k}^2 + F_{m,n|k} u_{m,n|k} + E_{m,n|k} \quad (4.8a)$$

with

$$H_{m,n|k} = (d_{m,n} + \mathcal{B}_m^T \mu_{n|k}) q_{m,n|k}, \quad (4.8b)$$

$$F_{m,n|k} = c_{m,n} + \mathcal{A}_m^T \mu_{n|k} + (d_{m,n} + \mathcal{B}_m^T \mu_{n|k}) f_{m,n|k} \quad (4.8c)$$

$$E_{m,n|k} = (d_{m,n} + \mathcal{B}_m^T \mu_{n|k}) e_{m,n|k} \quad (4.8d)$$

and subject to (4.2c) - (4.2e). Note that for convexity of (4.8a), it is required that $d_{m,n} + \mathcal{B}_m^T \mu_{n|k} > 0$ for all $k \in \mathcal{K}$, $m \in \mathcal{M}$. Under this condition, the dual decomposition allows solving the quadratically constrained linear program by solving multiple LCQPs iteratively. These LCQPs can be solved efficiently in real-time using, e.g., CVXgen [71] or QPoases [34].

The dual decomposition leads to a distributed economic model predictive control approach for CVEM that can be summarized in the following algorithm where $\epsilon > 0$ is a well chosen convergence criteria, $s \in \{0, \dots, s_{\max}\}$ is the iteration counter and s_{\max} is the maximum number of iterations.

Algorithm 4.2.1. Take $k = 0$ and initialize $\{\mu_{n|0}^0\}_{n \in \mathcal{N}}$

- Measure $x_{m,0|k}$ for all $m \in \mathcal{M}$ and $v_{0|k}$ and predict $v_{n|k}$ for all $n \in \mathcal{N}$

- *repeat until* $\|\mu_{n|k}^{s+1} - \mu_{n|k}^s\| \leq \epsilon$ for all $n \in \mathcal{N}$ or $s > s_{\max}$
 - Solve (4.8) subject to (4.2c) - (4.2e) for all $m \in \mathcal{M}$
 - Update the Lagrange dual variables using (4.7) for all $n \in \mathcal{N}$
- Implement the first element of the decision variables, i.e., $u_{m,0|k}$ for all $m \in \mathcal{M}$.
- Initialize the dual variables at $k + 1$ with the optimal dual variables at k , i.e., $\{\mu_{n|k+1}^0\}_{n \in \mathcal{N}} = \{\mu_{n|k}^*\}_{n \in \mathcal{N}}$
- Set $k = k + 1$

4.2.3 Modified Lagrange Dual Function for On/Off Control

For the optimal control problem presented so far, it has been assumed that the decision variables $u_{m,n|k}$ for all $n \in \mathcal{N}$ and all $m \in \mathcal{M}$ are constrained to an interval given by (4.2d). However, for some subsystems $m \in \mathcal{M}_{\text{bin}} \subset \mathcal{M}$ introduced in Chapter 2, the power can only be turned on or off, i.e.,

$$u_{m,n|k} \in \{\underline{u}_{m,n|k}, \bar{u}_{m,n|k}\}, \quad (4.9)$$

for all $n \in \mathcal{N}$ and $m \in \mathcal{M}_{\text{bin}}$ where $\underline{u}_{m,n|k}$ and $\bar{u}_{m,n|k}$ correspond to the power consumption when the auxiliary is off and on, respectively. The optimal control problem (4.2) subject to (4.9) instead of (4.2d) for $m \in \mathcal{M}_{\text{bin}}$ is hard to solve due to the binary decision variables. To still allow on/off control for some of the subsystems, we approximate the solution of (4.2) subject to (4.9) instead of (4.2d) for $m \in \mathcal{M}_{\text{bin}}$ by a solution for which we only take (4.9) for $n = 0$ and take (4.2d) for $n > 0$, i.e., (4.9) is relaxed to being an element of a continuous interval for the tail of the horizon. This approximation is justified as only the first element of the decision variables is actually used as a setpoint for the power to a subsystem. To do so, we augment (4.8) with a penalty for switching from on to off and vice versa, i.e.,

$$g_m(\{\mu_{n|k}\}) = \min_{\{u_{m,n|k}\}_{n \in \mathcal{N}}} \sum_{n \in \mathcal{N}} \frac{1}{2} H_{m,n|k} u_{m,n|k}^2 + F_{m,n|k} u_{m,n|k} + E_{m,n|k} + \sigma(x_{m,0|k}) \|u_{m,0|k} - u_{m,0|k-1}\| \quad (4.10a)$$

where the Lagrange dual function for which $u_{m,0|k} = \bar{u}_{m,n|k}$ is given by

$$\begin{aligned} \bar{g}_m(\{\mu_{n|k}\}) = & \\ & \frac{1}{2}H_{m,0|k}\bar{u}_{m,0|k}^2 + F_{m,0|k}\bar{u}_{m,0|k} + E_{m,0|k} + \sigma(x_{m,0|k})\|\bar{u}_{m,0|k} - u_{m,0|k-1}\| \\ & + \inf_{\{u_{m,n|k}\}_{n \in \mathcal{N} \setminus \{0\}}} \sum_{n \in \mathcal{N} \setminus \{0\}} \frac{1}{2}H_{m,n|k}u_{m,n|k}^2 + F_{m,n|k}u_{m,n|k} + E_{m,n|k} \end{aligned} \quad (4.10b)$$

and where the Lagrange dual function for which $u_{m,0|k} = \underline{u}_{m,n|k}$ is given by

$$\begin{aligned} \underline{g}_m(\{\mu_{n|k}\}) = & \\ & \frac{1}{2}H_{m,0|k}\underline{u}_{m,0|k}^2 + F_{m,0|k}\underline{u}_{m,0|k} + E_{m,0|k} + \sigma(x_{m,0|k})\|\underline{u}_{m,0|k} - u_{m,0|k-1}\| \\ & + \inf_{\{u_{m,n|k}\}_{n \in \mathcal{N} \setminus \{0\}}} \sum_{n \in \mathcal{N} \setminus \{0\}} \frac{1}{2}H_{m,n|k}u_{m,n|k}^2 + F_{m,n|k}u_{m,n|k} + E_{m,n|k} \end{aligned} \quad (4.10c)$$

with $H_{m,n|k}$, $F_{m,n|k}$ and $E_{m,n|k}$ as defined in (4.8b,4.8c,4.8d), subject to (4.2c) - (4.2e) and subject to (4.9) instead of (4.2d) for $n = 0$. In (4.10), $u_{m,0|k-1}$ indicates whether the subsystem is currently on or off and $\sigma(x_{m,0|k})$ is a (state-dependent) penalty parameter. This penalty parameter is used to achieve a desired switching frequency.

The optimization problem (4.10) can now be solved by solving the two LCQPs (4.10b) and (4.10c) and the optimal decision at the first time instant ($n = 0$) is given by

$$u_{m,0|k} = \begin{cases} \underline{u}_{m,0|k} & \text{if } \underline{g}_m \leq \bar{g}_m \\ \bar{u}_{m,0|k} & \text{if } \bar{g}_m \leq \underline{g}_m. \end{cases} \quad (4.11)$$

It is this control action that is implemented at time instant $k \in \mathbb{N}$ for this subsystem $m \in \mathcal{M}_{\text{bin}}$. It has to be noted that the optimal control problem (4.2) subject to (4.9) for $n = 0$ and (4.2d) for $n > 0$ is not convex and consequently it is not guaranteed that the dual solution d^* will converge to the primal solution p^* . However, in case that the power of the on/off (non-convex) subsystems is small compared to the continuous (convex) subsystems, the dual solution will still converge for most time instances $k \in \mathbb{N}$ and a close to optimal performance can be achieved as will be demonstrated in Section 4.4.

4.2.4 Stability and Feasibility

Stability and feasibility are generally important properties that need to be addressed for MPC. Stability, however, is not a concern for the economic MPC approach presented in this chapter. Namely, the objective is not to control the states to a steady-state value, but to find a solution that minimizes the energy losses in the vehicle while satisfying the upper and lower state constraints over a finite horizon.

Still, feasibility does need to be addressed. The following three causes can lead to an infeasible solution:

1. The CVEM problem becomes infeasible if the power of the internal combustion engine is not sufficient to provide power to all subsystems and disturbances in the vehicle.
2. The optimal control problem related to one of the subsystems becomes infeasible if the final state cannot be reached due to limitations on the control inputs and a horizon that is not sufficiently long.
3. The optimal control problem related to one of the subsystems becomes infeasible if the initial state at time instant $k \in \mathcal{N}$ violates the state constraints as a result of unpredicted disturbances and modeling errors.

The first cause for infeasibility can be avoided by having a sufficiently powerful internal combustion engine that can always provide enough power to all subsystems and disturbances in the vehicle. In practice, it can occur that the engine power is limited, which eventually would lead to a smaller acceleration than requested.

The second cause for infeasibility can be avoided by taking a sufficiently long horizon. An indicative measure for the minimal length of the horizon for each of the dynamic subsystems can be obtained by maximizing the lower bound on the required control horizon τ . This lower bound should be such that there exists an input $u_m(t) \in [\underline{u}_m, \bar{u}_m]$ for $t \in [0, \tau)$ such that

$$x_{m,N|k} = e^{\tilde{A}_m \tau} x_m + \tilde{B}_m^w \bar{w}_m \int_0^\tau e^{\tilde{A}_m s} ds + \tilde{B}_m^u \int_0^\tau e^{\tilde{A}_m s} u_m(s) ds, \quad (4.12)$$

for both $x_m \in \{\underline{x}_m, \bar{x}_m\}$ and (an estimate of) the worst-case disturbance \bar{w}_m and

the given final state $x_{m,N|k}$. With the variable prediction time intervals proposed in this chapter, the horizon τ can be taken sufficiently long, so as to satisfy (4.12), without the need for many decision variables.

The third and final cause for infeasibility can be solved by projecting the initial state into the feasible set and contracting the input constraint (4.2d) for $n = 0$ to ensure feasibility for the next time instant. Note that, as a result, it is not guaranteed that the state constraints will not be violated. For CVEM, this is not a concern as the state constraint are already chosen conservatively from practical considerations and small violations of the state constraints is allowed.

4.3 Prediction of Disturbance Signals

In order to solve the receding horizon problem, accurate predictions of the disturbances $w_{m,n|k}$, $m \in \mathcal{M}$, and $v_{n|k} = [v_{1,n|k} \ v_{2,n|k} \ v_{3,n|k}]^T$, as in (4.2c) and (4.2f), are needed, as well as time varying efficiency constants in (4.2b), which requires and accurate prediction of the engine speed $\omega_{n|k}$. In this chapter, we assume that all disturbances at the energy storage buffers $w_{m,n|k}$ are constant (i.e. $w_{m,n|k} = w_{m,k}$ for all $m \in \mathcal{M}$ and $n \in \mathcal{N}$) and measurable, e.g., the ambient temperature of the refrigerated semitrailer, see Chapter 2. Furthermore, we assume that the high-voltage network has no disturbances, i.e., $v_{2,n|k} = 0$ for all $n \in \mathcal{N}$ and $k \in \mathbb{N}$ and the disturbance power on the low-voltage network (consisting of e.g., the power needed for the head lights) is constant, i.e., $v_{3,n|k} = 1.5$ kW for all $n \in \mathcal{N}$ and $k \in \mathbb{N}$. As a result of these assumptions, we only need to propose a method to obtain an accurate prediction of the propulsion power $v_{1,n|k}$, i.e., the power needed at the wheels for tracking a reference velocity.

The propulsion power $v_{1,n|k}$ and the engine speed $\omega_{n|k}$ at prediction step $n \in \mathcal{N}$ at time $k \in \mathbb{N}$ are obtained by averaging the prediction of the propulsion power and engine speed, i.e.,

$$v_{1,n|k} = \frac{1}{\tau_n} \int_{\hat{t}_n}^{\hat{t}_{n+1}} P_r(t + t_k) dt, \quad (4.13a)$$

$$\omega_{n|k} = \frac{1}{\tau_n} \int_{\hat{t}_n}^{\hat{t}_{n+1}} \omega_r(t + t_k) dt, \quad (4.13b)$$

for $n \in \mathcal{N}$ with $t_k = k\tau_0$ for $k \in \mathbb{N}$ and $\hat{t}_n = \sum_{i=0}^{n-1} \tau_i$, where P_r is the propul-

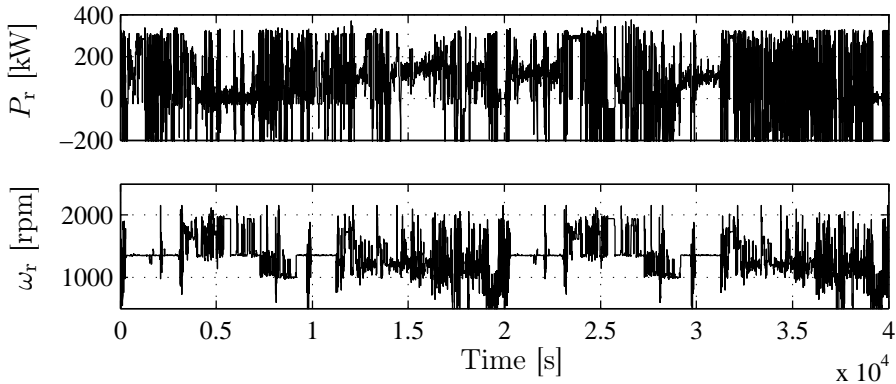


Figure 4.2: Part 1 ($t \in [0, 20000)$) and Part 2 ($t \in [20000, 40000)$) of a pan European driving cycle.

sion power and ω_r is the engine speed. In the next chapter, we will present a method that can predict the propulsion power and engine speed as function of the predicted velocity, the predicted road slope with an eHorizon sensor, e.g., ADASIS [98] and the predicted gear.

In this chapter, we will only focus on the analysis of the solution strategy, where we assume that the predicted propulsion power and engine speed is exact. In particular, the propulsion power and engine speed are obtained with the high-fidelity vehicle model presented in the next chapter for a pan European driving cycle. The propulsion power and engine speed are shown in Figure 4.2 where we define Part 1 by $t \in [0, 20000)$ and Part 2 by $t \in [20000, 40000)$. Indeed, the first and the second part in Figure 4.2 correspond with the first and second part used in Section 3.5.4 for the analysis of the fuel consumption with the offline solution strategy.

4.4 Simulation Results

In this section, the results of the DEMPC approach to CVEM will be presented. The energy management problem is solved in a receding horizon as in Section 4.2, and at each time instant $k \in \mathbb{N}$ the first input is implemented on the simplified power-based vehicle model introduced in Chapter 2. The vehicle model runs at a frequency of 1 Hz where the exogenous disturbances, e.g., the drive cycle $P_r(t)$ are constant at each time interval $t \in [k\tau, (k+1)\tau)$ with $\tau = 1$ second, $k \in \mathbb{N}$.

We will first analyze the influence of the prediction horizon. Then the results on the control of auxiliaries that can only be turned on or off will be given. Finally, the influence of the number of iterations on the fuel reduction will be given.

4.4.1 Influence of Prediction Horizon

A key element in the proposed algorithm is variable prediction time intervals to allow for large control horizons with a few decision variables. Choosing the length of these variable prediction time intervals is not straightforward, but we will demonstrate that choices can be made based on practical limitations and intuition, while close to optimal performance can be achieved. To do so, we first consider the case of a hybrid electric truck without auxiliaries and predict the power at the wheels, i.e., $v_{1,n|k}$ for all $n \in \mathcal{N}$ at time instant k and the engine speed $\omega_{n|k}$ for all $n \in \mathcal{N}$ at time instant k with (4.13) for three different cases with decreasing accuracy in prediction information, i.e.,

- **Case 1:** In this case, we do not take variable prediction time intervals, but take intervals of 1 second, i.e., $\sum_{n \in \mathcal{N}} \tau_n = N$. Because the simulation model has a sample time of 1 second, we have that the prediction is exact over the length of the interval $[t_n, t_{n+1})$. This also means that N is large to obtain a large control horizon. Real-time implementation is therefore not feasible and this case can only be solved for a hybrid truck without taking the auxiliaries into account in the energy management strategy.
- **Case 2:** In this case, we do take variable sample intervals with $(\tau_0, \dots, \tau_{N-1}) = (1, 1, 2, 4, 6, 8, 10, 12, 16, 20, \tau_{N-1})$ and predict the propulsion power and engine speed with (4.13). We choose $\sum_{n \in \mathcal{N}} \tau_n - \tau_{N-1} = 80$ from a practical point of view as 80 seconds corresponds to about 2 km of preview information at cruise control speed (88 km/h). This is the maximum distance over which preview information is available in the heavy-duty vehicle. To still allow for a larger control horizon, we can choose τ_{N-1} for which in this case the power at the wheels and the engine speed is calculated with (4.13) as well.
- **Case 3:** This case is a small adaptation to Case 2. Namely, as preview information is not available after 80 seconds (in practice), the propulsion

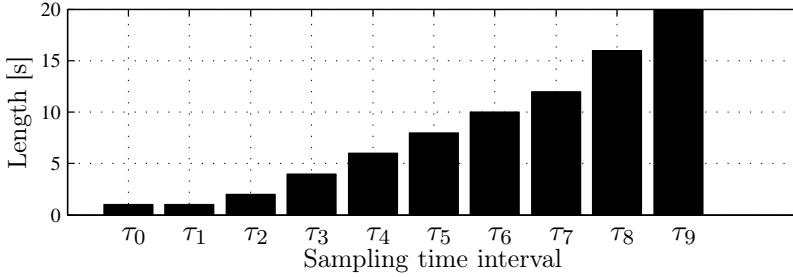


Figure 4.3: Length of the sampling time intervals.

power and the engine speed for $N - 1$, i.e., $v_{1,N-1|k}$ and $\omega_{N-1|k}$, cannot be predicted and are therefore assumed to be fixed to a pre-specified value after 80 seconds.

The choice for the sampling time intervals for Case 2 and Case 3 is plotted in Figure 4.3 and is based on three considerations, i.e., i) $\sum_{n \in \mathcal{N}} \tau_n - \tau_{N-1} = 80$ seconds, ii) The first interval is 1 second as this decision is implemented, iii) The intervals should increase in size for $n \rightarrow N - 1$ as nearby prediction information is likely to be more accurate. These considerations do not lead to too many significant different choices for the sequence τ_n , $n \in \mathcal{N}$ and the results in Figure 4.4 show that good performance can be achieved with the one proposed. In this figure, the fuel reduction is shown as function of the horizon length $\sum_{n \in \mathcal{N}} \tau_n$ for each of the three cases and for the two parts of the drive cycle. The horizon length for Case 1 is changed by changing N while for Case 2 and Case 3, the horizon length is changed by changing τ_N . Moreover, the global optimal solution is calculated with the approach presented in Chapter 3 and shown as a constraint. Note that for Case 3, the power request after 80 s is fixed to a pre-specified value. Therefore, it is not useful to choose the horizon very long for Case 3 as this results in a lower fuel reduction. Figure 4.5 shows the simulation results for Case 3 for three different horizon lengths and where $v_{1,N|k}$ is varied from 10 kW to 90 kW and $\omega_{N|k} = 1250$ rpm. The main conclusion drawn from these two figures is that Case 3, which is closest to practice, can achieve good fuel reduction performance and sensitivity to the length of the control horizon and the choice for $v_{1,N|k}$ is not significant. For the remaining simulations, we choose $\sum_{n \in \mathcal{N}} \tau_n = 280$, $v_{1,N|k} = 30$ kW and $\omega_{N|k} = 1250$ rpm.

These settings also fully define the smart control of the continuous controlled

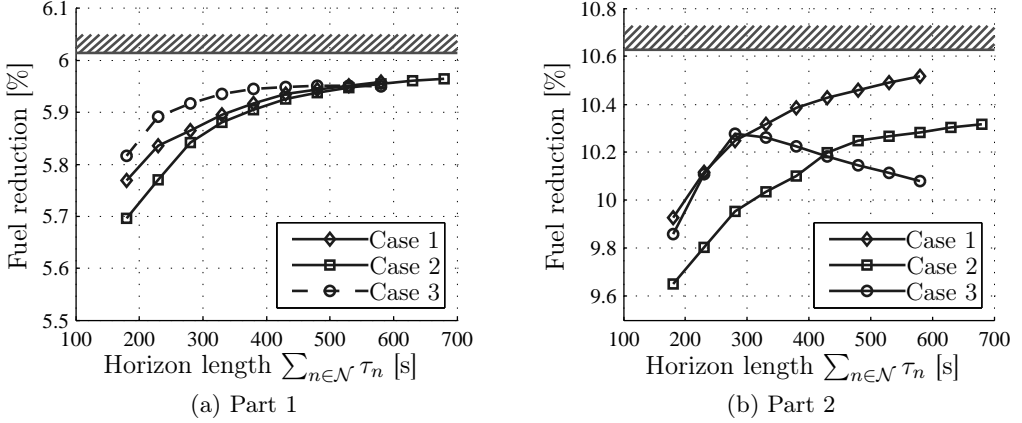


Figure 4.4: Fuel reduction of a hybrid heavy-duty vehicle for two parts of the drive cycle and various cases.

alternator and DCDC converter. Smart control of the alternator (without a DCDC converter) leads to a fuel reduction of 0.09 % and 0.24 % fuel reduction for Part 1 and Part 2, respectively. By adding smart control of the DCDC converter, the fuel reduction is increased to 0.47 % and 0.6 % for Part 1 and Part 2, respectively. Smart control of the auxiliaries with on/off control will be discussed in the next section.

4.4.2 Auxiliaries with On/Off Control

Next, we consider the analysis of the on/off controlled auxiliaries. The simulation results are obtained by taking only the hybrid vehicle with one additional switching subsystem, e.g., the refrigerated semi-trailer. Note that this requires solving two QPs for every switched system at each time instant k . We have defined three different switching strategies, i.e.,

- **Strategy 1:** For this strategy, the penalty parameter for switching $\sigma(x_{m,0|k}) = \sigma > 0$ is a constant value.
- **Strategy 2:** Inspired by [15], the penalty parameter for switching is for this strategy defined by $\sigma = (x_{m,0|k} - \hat{x}_m)\delta$ where \hat{x}_m is a target state and δ is a positive weight. The target state is the lower energy bound if

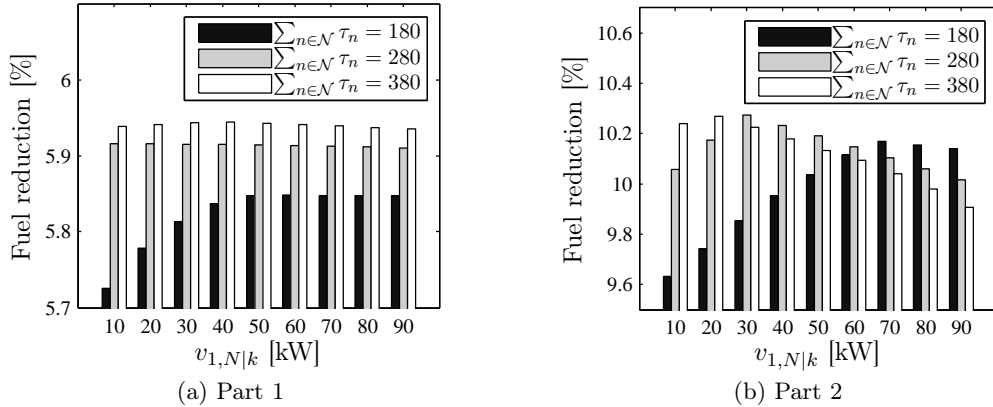


Figure 4.5: Sensitivity to the pre-specified value of $v_{1,N|k}$.

the subsystem is off and the target state is the upper energy bound if the subsystem is on.

- **Strategy 3:** This strategy is a small adaptation of Strategy 2 and only used for the refrigerated semi-trailer and air supply system. Here, the desired final state in the energy storage device is adapted as a linear function of the average value of the dual variables, i.e., $x_{m,N} = a\bar{\mu}_{2,n} + b$ for some a and b and where the average value of the dual variables over the prediction horizon is given by $\bar{\mu}_{2,n} = \frac{1}{\sum_{n \in \mathcal{N}} \tau_n} \sum_{n \in \mathcal{N}} \mu_{2,n}$. This can improve the performance of subsystems with a default switching time much larger than the prediction horizon, such as the refrigerated semi-trailer and air supply system.

The results for each of these strategies and each of the subsystems are shown in Figure 4.6 for Part 1 (a,c,e) and Part 2 (b,d,f) of the drive cycle. Different penalty parameter settings are used, which result in a different average switching time. The fuel reductions are obtained by comparing to a default controller, which switches between an upper and lower bound, as in Section 3.5.5. The results are plotted on top of the results given in Figure 3.8, which showed the feasible region for real-time control in between the two hatched areas, i.e., an infeasible region and a default controller region. The upper boundary of the feasible region is given by the optimal trade-off between the number of switches and the fuel reduction and obtained with the offline solution method presented in Chapter 3. The default

controller turns on the auxiliary when the lower energy limit is violated and turns the auxiliary off when the upper energy limit is violated. For these auxiliaries, it holds that the more energy is stored, the higher is the rate of energy dissipation to the environment. To show this, let us consider the example of a refrigerated semi-trailer, where a larger difference between the air temperature inside and the ambient temperature leads to a larger energy dissipation. By decreasing the upper energy limit, the number of switches with default control will increase, but also the energy dissipation decreases leading to a fuel reduction. This trade-off defines the lower boundary of the feasible region, which lowers fuel benefit by smart on/off control for these auxiliaries. Still, a significant amount of fuel can be saved with the refrigerated semi-trailer, the air supply system and the climate control system, but the average switching time is also significantly lower.

For the refrigerated semi-trailer and the air supply system, it is very difficult to obtain a large average switching time as this time easily exceeds the maximum length of accurate prediction information. The climate control system is difficult to optimize as the fuel reduction for the default strategy with a shorter switching time is already high compared to the maximum obtainable fuel reduction.

4.4.3 Limiting the Number of Iterations

The number of iterations for all the simulations so far does not have an upper bound. However, at each iteration, 8 LCQPs need to be solved so that limiting the amount of iterations reduces the computation time and thereby improves the real-time properties. Therefore, smart control of the hybrid vehicle with all auxiliaries is simulated subject to a maximum on the number of iterations. The fuel reduction results by smart control of the auxiliaries are shown in Figure 4.7 for Part 1 and Part 2 of the drive cycle. Only the fuel reduction of the smart auxiliaries are shown to demonstrate the potential of CVEM. The average switching time for the refrigerated semi-trailer is 35 and 22 seconds for Part 1 and Part 2, respectively, for the air supply system 52 and 31 seconds, for Part 1 and Part 2, respectively, and for the climate control system 7 seconds for both parts of the drive cycle. With a very low number of iterations, fuel reduction performance is indeed sacrificed. However, with an upper limit of 50 iterations, around 99 % of the maximum fuel reduction is already obtained and with 25 iterations, around 97 % of the maximum fuel reduction is obtained.

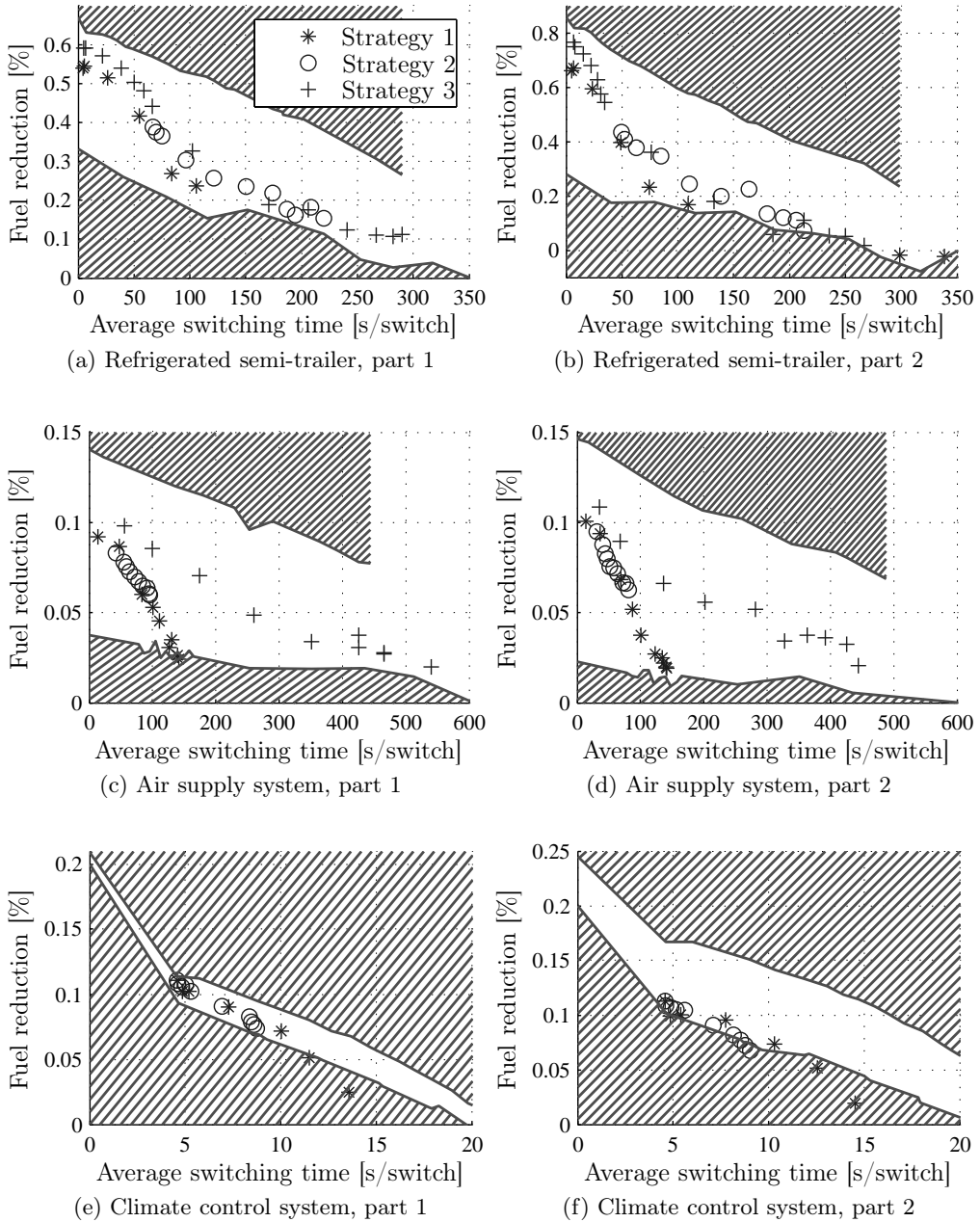


Figure 4.6: Fuel reduction with real-time on/off control of the refrigerated semi-trailer, the air supply system and the climate control system for three different switching strategies.

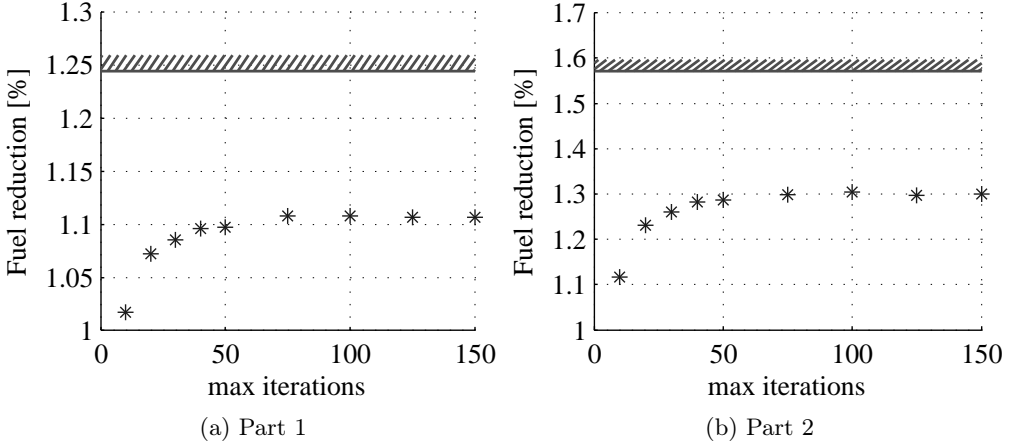


Figure 4.7: Fuel reduction as a result of smart control of auxiliaries with number of iterations being limited.

4.4.4 State Trajectories

The state trajectories for Part 1 of the driving cycle are shown in Figure 4.8. Here, $\tilde{x}_{hvb} = \frac{x_{hvb}}{E_{hvb}}$ is the high-voltage battery energy normalized with respect to the maximum battery capacity E_{hvb} , $\tilde{x}_{lvb} = \frac{x_{lvb}}{E_{lvb}}$ is the low-voltage battery energy normalized with respect to the maximum battery capacity E_{lvb} , T_{rst} is the air temperature in the refrigerated trailer, p_{as} is the air pressure in the air supply system and T_{ccs} is the wall temperature of the climate control system. This figure shows that all state constraints are satisfied. The state trajectories for the complete pan European driving cycle, as in Chapter 3, are given in Appendix A.2.

4.5 Conclusions and Discussion

In this chapter, a real-time and distributed solution for complete vehicle energy management is presented using a receding horizon in combination with a dual decomposition. Conclusions will be drawn and a discussion on the results will be given in this section.

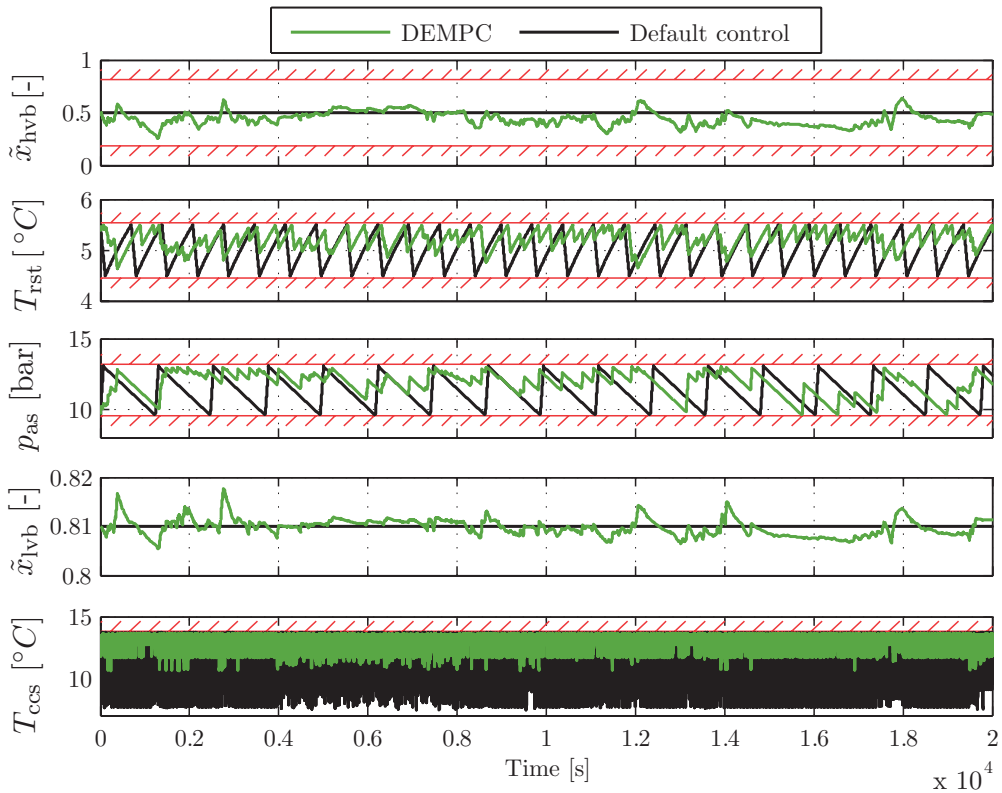


Figure 4.8: State trajectories for Part 1 of the pan European driving cycle.

4.5.1 Conclusions

The approach presented in this chapter first applies a dual decomposition to the receding horizon optimal control problem, so that the problem related to each subsystem can be solved separately. Each sub-problem related to each subsystem is a linearly constrained quadratic program that can be solved efficiently with embedded quadratic programming solvers. Variable prediction time intervals are used to obtain a long control horizon with a limited number of decision variables. As a result, the final state constraint can be used as a constraint, instead of a ‘soft’ constraint, which avoids the need for tuning parameters.

Furthermore, a novel on/off control concept for control of the refrigerated semi-trailer, the air supply system and the climate control system is introduced. The concept requires solving the linearly constrained quadratic program twice, one

with the first decision being on and one with the first decision being off. The solution with the lowest cost is taken as the optimal solution.

The only parameters for the solution strategy proposed in this chapter are the variable prediction time intervals and the penalty parameters for switching. The variable sample times can be chosen intuitively and simulation results on a low-fidelity vehicle model show that close to optimal fuel reduction performance can be achieved without carefully tuning these sample times. The fuel reduction of the on/off controlled subsystems strongly depends on the number of switches allowed. The fuel reduction for the on/off controlled subsystems can be close to optimal, but the number of switches needs to be increased significantly. Particularly for the refrigerated semi-trailer and the air supply system, it is very difficult to obtain a large average switching time as this time easily exceeds the maximum length of accurate prediction information. Still, by allowing more switches, a fuel reduction of up to 1.3 % can be achieved.

4.5.2 Discussion

The variable sample times are chosen intuitively and simulation results on the low-fidelity vehicle model show that close to optimal fuel reduction performance can be achieved without carefully tuning these sample times. However, not having to rely on intuition, these variable sample times can be adapted based on the prediction information.

The simulation results on the low-fidelity vehicle model presented in this chapter provide valuable insights in the sensitivities of the parameters and performance of the algorithm in a simple and predictable environment. Indeed, the control-oriented model used for the DEMPC approach to optimize the setpoints is exactly the same as the vehicle model on which the setpoints are implemented. The control-oriented model is a (convex) approximation of high-fidelity vehicle model (see Chapter 2), which induces an error between the predicted behavior and the actual behavior. Although the simulation results are promising, it is necessary to implement the setpoints on the high-fidelity vehicle model to assess the sensitivity of this approximation.

Furthermore, the prediction of the propulsion power and engine speed in this chapter is exact to exclude the influence of faulty prediction information. To predict the propulsion power and engine speed of the high-fidelity vehicle model, a

preview functionality needs to be developed that leads to an accurate prediction, but the computational load must be limited to allow for real-time implementation. The predicted propulsion power and engine speed is therefore always an approximation and the influence of the accuracy of the prediction needs to be taken into account.

Finally, the real-time aspects of the solution strategies have not been demonstrated. The variable sample times do allow for a small number of decision variables, thereby greatly enhancing the real-time properties, but the solution strategy needs to be implemented on an embedded platform to fully demonstrate the real-time feasibility of the solution strategy.

5

Validation on a High-Fidelity Vehicle Model

Abstract - *In this chapter, the distributed economic model predictive control approach is validated on a high-fidelity vehicle model of the heavy-duty vehicle. The propulsion power needed for driving and the engine speed is predicted by assuming that the vehicle follows a reference speed set by the cruise control or the downhill speed control, which is valid for long-haul driving. This allows the vehicle speed to be predicted over a trajectory with a road slope predicted by an e-horizon sensor, e.g., ADASIS, leading to a prediction of the propulsion power and engine speed. The prediction algorithm is validated with measured ADASIS information on a public road around Eindhoven, which demonstrates that sufficiently accurate prediction of the propulsion power and engine speed is feasible if the vehicle follows the most probable path. Simulations with the high-fidelity vehicle model show that a fuel reduction of 0.58 % can be obtained compared to the best default control strategy and 0.98 % compared with the worst default control strategy. The control strategy is implemented on a dSpace Autobox and shows that the maximum computation time is only 3.2 ms per iteration, which demonstrates that real-time implementation is feasible.*

5.1 Introduction

The previous chapter provides an online solution strategy to solve the complete vehicle energy management (CVEM) problem. The online solution strategy requires a prediction of the future disturbances and solves optimal control with a distributed economic model predictive control (DEMPC) approach. In particular, the dual decomposition is applied, which results in small linearly constrained quadratic programs (LCQP) for each of the subsystems, which can be efficiently solved in real-time with embedded LCQP solvers. The optimal control problem is solved at each time instant $k \in \mathbb{N}$ after which only the decisions at the first time instant are implemented. This online solution strategy is validated with the low-fidelity vehicle model presented in Chapter 2. The results provide key insights in the performance and sensitivities of the DEMPC strategy. The low-fidelity vehicle model however, has a restricted complexity and does not capture all nonlinear behavior and power restrictions of the heavy-duty vehicle.

A prototype vehicle has been built for the CONVENIENT project (see Figure 5.1), which is a research project part of the 7th framework programme of the European Commission. The prototype has a hybrid drive train with an internal combustion engine and an electric machine attached to a high-voltage battery system and all auxiliaries are electrified. At the moment of developing the DEMPC strategy, the prototype vehicle is not approved to be tested on the public road, but only on designated test tracks. This constrains the validation of the online solution strategy as prediction information is not available for driving on the test track. Namely, prediction information is essential to demonstrate the fuel reduction potential of the DEPMC strategy. Therefore, the DEMPC strategy is validated on a high-fidelity vehicle model of the heavy-duty vehicle. The vehicle model is developed by the Institute für Kraftfahrzeuge Aachen (IKA) [28, 76]. It consists of a detailed vehicle model describing the longitudinal dynamics of the vehicle and the dynamics of all (nonlinear) components in the vehicle.

The DEMPC strategy provides a setpoint to all subsystems in the vehicle, including the electric machine and internal combustion engine. However, control of the electric motor and internal combustion engine is difficult as safety is critical for a vehicle that weighs up to 40.000 kg. Control of the hybrid system is therefore not feasible in the prototype vehicle. Therefore, it is decided to validate the



Figure 5.1: CONVENIENT prototype truck.

strategy without control of the hybrid system in the high-fidelity vehicle model as well. Still, the other subsystems, i.e., the refrigerated semi-trailer, the air supply system, the climate control system, the DCDC converter and the alternator can receive setpoints from the online solution strategy. This still allows validation of the fuel reduction potential for most of the subsystems in the heavy-duty vehicle.

The outline of this chapter is as follows. In Section 5.2, the high-fidelity vehicle model and the integration of the online solution strategy will be discussed. In Section 5.3, prediction of the disturbances will be discussed and, finally, in Section 5.4, the simulation results will be presented.

5.2 High-fidelity Simulation Model

The high-fidelity vehicle model is developed by the Institute für Kraftfahrzeugen (IKA) to evaluate the fuel reduction potential for complete vehicle energy management, see [28, 76]. The vehicle model simulates the behavior of the prototype truck and is shown in Figure 5.2. The vehicle model consist of three large subsystems, i.e., the dSpace autobox that contains all the control functionality, the driver model and the vehicle model. The vehicle model and drive model will be discussed briefly followed by the integration of the DEMPC approach presented in Chapter 3.

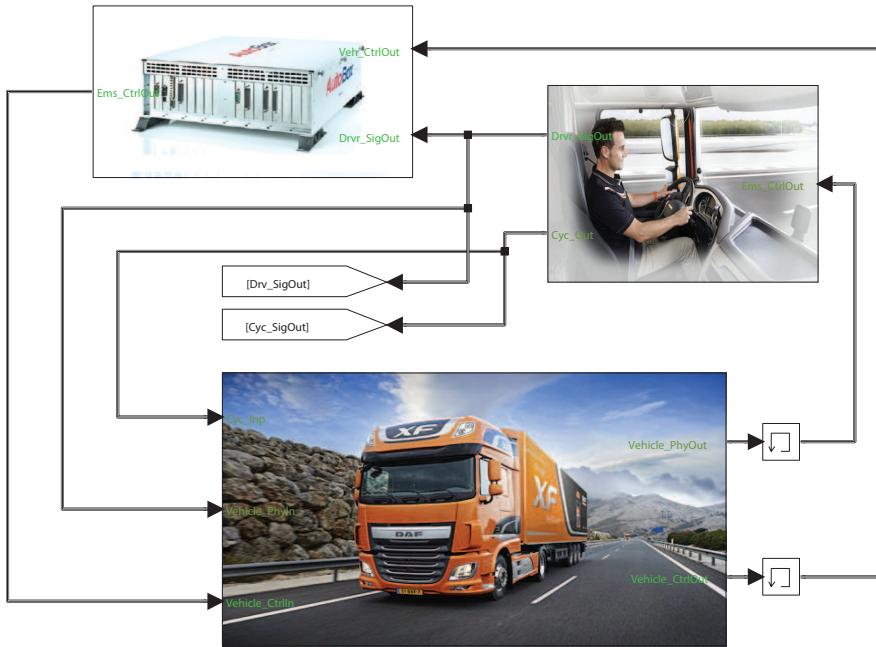


Figure 5.2: High-fidelity vehicle model.

5.2.1 Vehicle and Driver Model

All the components in the heavy-duty vehicle and their interaction are modeled in the vehicle subsystem. In this subsystem, the internal combustion engine, the electric machine, the clutch, the gearbox and the differential are modeled to simulate the powertrain of the vehicle. The torque delivered by the power train results in a movement, velocity and acceleration of the truck. The high-voltage battery is connected via a multi-mode inverter to the electric motor, the refrigerated semi-trailer, and the air supply system, which makes up the high-voltage network in the truck. The alternator is connected to the engine and delivers power to the low-voltage network consisting of the low voltage batteries, the electric steering pump and the constant low-voltage auxiliaries, e.g., the head lights. A DCDC converter is also present that connects the high-voltage network to the low-voltage network. A mechanical compressor from the climate control system is connected to the engine via a clutch. The setpoints for each of the components, e.g, the engine torque, are given externally from the Autobox or

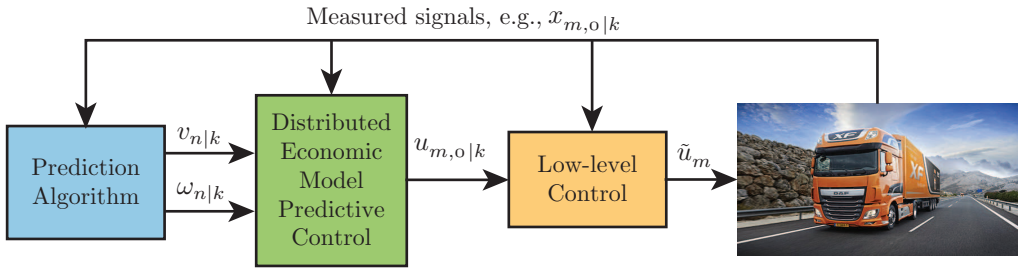


Figure 5.3: Integration of distributed model predictive control approach

driver subsystem. The main responsibility of the driver subsystem is tracking a velocity profile that is defined by the drive cycle. Some setpoints are first sent to the Autobox, e.g., the drive torque request, and then further processed and some are directly sent to the truck, e.g., the blower level of the climate control system. The interested reader is referred to [28, 76] for more details on the high-fidelity vehicle model.

5.2.2 Integration of the DEMPC approach

The DEMPC approach presented in the previous chapter is integrated in the dSpace autobox subsystem together with the control system for the hybrid drive train. An schematic overview of the implementation is given in Figure 5.3 and consists of the prediction algorithm, the DEMPC and the low-level controllers. The prediction algorithm provides a prediction of the disturbance $v_{n|k}$ and engine speed $\omega_{n|k}$ for all $n \in \mathcal{N}$ for which more details will be given in the next section.

The DEMPC is as presented in Chapter 4. It was envisioned in [52] to have an energy management system operator (EMSO) and for each subsystem a smart algorithm that optimizes its own power setpoints based on information from the EMSO. In particular, the EMSO defines the prices for which components can buy or sell energy and each of the subsystems maximizes their own profit based on these prices. This provides the necessary flexibility for adding new subsystems and maximizing the profit for each of the subsystems can even be done in a distributed fashion on different electronic control units.

Indeed, the solution strategy presented in Chapter 4 can be integrated along the lines of [52], as is shown in Figure 5.4. Here, the Lagrange dual functions related to each subsystem $m \in \mathcal{M}$ are solved independently given the dual variables $\mu_{n|k}$

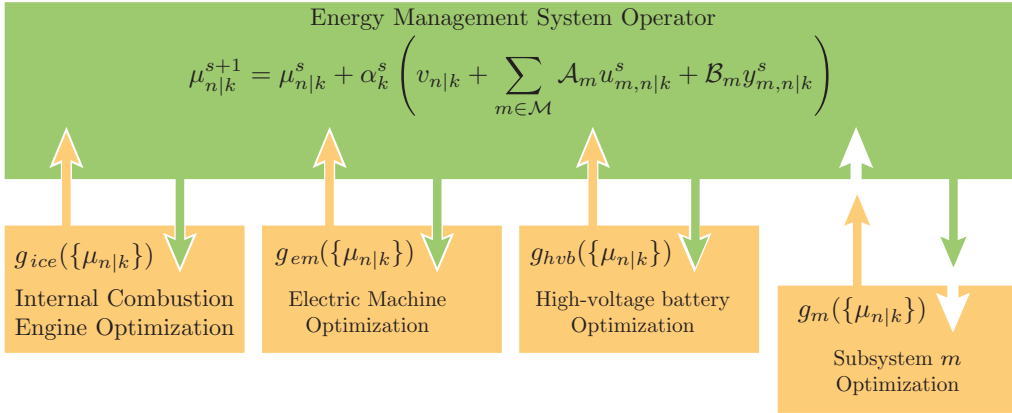


Figure 5.4: Flexible control interface.

for node $n \in \mathcal{N}$ at time $k \in \mathcal{N}$, i.e., the prices from the EMSO. Depending on the power request of each subsystem, the EMSO performs a price update, i.e., by updating the dual variables. This solution strategy can be implemented by having a separate electronic control unit for solving the optimization problem for each of the subsystems and the EMSO. This requires communication of the decisions and dual variables over a communication bus, e.g., CAN. This implementation is challenging as each of the subsystems needs to share N decisions with N being the length of the prediction horizon and the communication needs to be synchronized. Alternatively, the EMSO and the optimization problem related to each subsystem can be implemented on the same electronic control unit. This approach is taken here by integrating the entire DEMPC strategy on a dSpace Autobox.

The low-level control in Figure 5.3 transforms the power setpoints from the DEMPC solution to setpoints suitable for each of the components, e.g., the alternator and DCDC converter require a voltage setpoint. To do so, the voltage setpoint for the alternator, is controlled with a PI controller, i.e.,

$$\tilde{u}_{\text{alt}}(t) = K_{\text{alt}}^{\text{p}}(u_{\text{alt},0|k} - U_{\text{LV}}(t)I_{\text{alt}}(t)) + K_{\text{alt}}^{\text{i}} \int_0^t u_{\text{alt}}(s) - U_{\text{LV}}(s)I_{\text{alt}}(s)ds, \quad (5.1)$$

where $u_{\text{alt},0|k}$ is the desired alternator input power, U_{LV} is the measured voltage of the low-voltage network, I_{alt} is the measured alternator current and $K_{\text{alt}}^{\text{p}}$ and $K_{\text{alt}}^{\text{i}}$ are the proportional gain and integral gain of the PI controller, respectively. The

voltage setpoint of the DCDC converter is controlled with another PI controller, i.e.,

$$\tilde{u}_{\text{dc}}(t) = K_{\text{dc}}^{\text{p}}(u_{\text{dc},0|k} - U_{\text{LV}}(t)I_{\text{dc}}(t)) + K_{\text{dc}}^{\text{i}} \int_0^t u_{\text{dc}}(s) - U_{\text{LV}}(s)I_{\text{dc}}(s)ds, \quad (5.2)$$

where $u_{\text{dc},0|k}$ is the desired DCDC converter input power, U_{HV} is the measured voltage of the high-voltage network, I_{dc} is the measured DCDC current and K_{dc}^{p} and K_{dc}^{i} are the proportional gain and integral gain of the PI controller, respectively. Note that providing power with the alternator and DCDC converter simultaneously can lead to problems with two separate PI controllers. Therefore, either only the alternator will be used to provide power to the low-voltage network or only the DCDC converter will be used.

The refrigerated semi-trailer, the air supply system and the climate control system are turned on or off with a binary signal, i.e, they are turned on when they receive a ‘1’ and are turned off when they receive a ‘0’. To do so, the power setpoint from the DEMPC approach is transformed to a binary signal with

$$\begin{aligned} \tilde{u}_m &= 1, & \text{if } |u_{m,0|k}| > 0 \\ \tilde{u}_m &= 0, & \text{if } |u_{m,0|k}| = 0 \end{aligned} \quad (5.3)$$

for $m \in \{\text{rst, as, ccs}\}$. As stated in the introduction, control of the hybrid system is not feasible in the prototype vehicle as well as in the high-fidelity vehicle model. Instead, the hybrid system is controlled with a black box rule-based strategy. The hybrid system is still an essential part of the DEMPC strategy, as the auxiliaries need the decisions from the hybrid system to optimize their own decisions. By doing so, the algorithm predicts the behavior of the hybrid system by assuming that the hybrid system will make the optimal decisions along the objective function in the optimal control problem.

5.3 Prediction of Disturbance Signals with ADASIS

In order to solve the CVEM problem with the DEMPC approach, accurate predictions of the disturbances $w_{m,n|k}$, $m \in \mathcal{M}$, and $v_{n|k} = [v_{1,n|k} \ v_{2,n|k} \ v_{3,n|k}]^T$, as in (4.2c) and (4.2f), are needed, as well as time varying efficiency constants

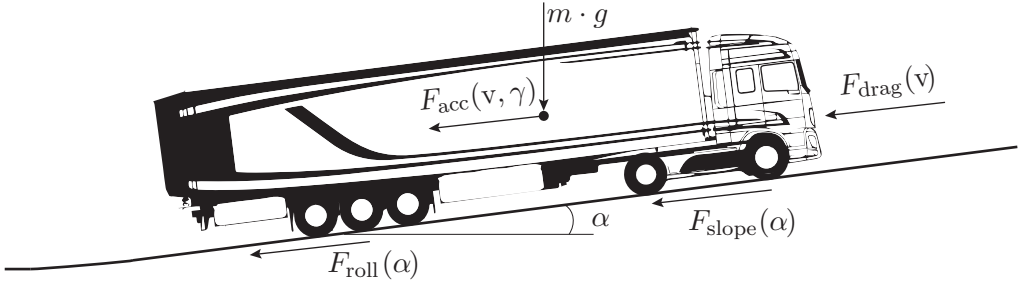


Figure 5.5: Longitudinal forces acting on a moving vehicle.

in (4.2b), which requires an accurate prediction of the engine speed $\omega_{n|k}$. As was done in the previous chapter, we assume that all disturbances at the energy storage buffers are constant (i.e. $w_{m,n|k} = w_{m,k}$ for all $m \in \mathcal{M}$ and $n \in \mathcal{N}$) and measurable, e.g., the ambient temperature of the refrigerated semitrailer, see Chapter 2. Furthermore, the high-voltage network has no disturbances, i.e., $v_{2,n|k} = 0$ for all $n \in \mathcal{N}$ and $k \in \mathbb{N}$ and the disturbance power on the low-voltage network (consisting of e.g., the power needed for the head lights) is identified online. The latter is done by considering the optimal solution at time instant $k \in \mathbb{N}$ and finding the value $v_{3,0|k}$ that satisfies (2.5). This value is assumed to remain constant over the prediction horizon, i.e., $v_{3,n|k} = v_{3,0|k}$ for $n \in \mathcal{N}$. As a result, we only need a method to obtain an accurate prediction of the propulsion power $v_{1,n|k}$, i.e., the power needed at the wheels for tracking a reference velocity and the engine speed $\omega_{n|k}$.

5.3.1 Power Required at the Wheels

The propulsion power $v_{1,n|k}$ and the engine speed $\omega_{n|k}$ at prediction step $n \in \mathcal{N}$ at time $k \in \mathcal{K}$ are obtained by averaging the prediction of the propulsion power and engine speed, i.e.,

$$v_{1,n|k} = \frac{1}{\tau_n} \int_{\hat{t}_n}^{\hat{t}_{n+1}} P_{\text{r}}(v(t_k + t), \alpha(t_k + t), \gamma(t_k + t)) dt, \quad (5.4a)$$

$$\omega_{n|k} = \frac{1}{\tau_n} \int_{\hat{t}_n}^{\hat{t}_{n+1}} \omega_{\text{r}}(v(t_k + t), \gamma(t_k + t)) dt, \quad (5.4b)$$

for $n \in \mathcal{N}$ with $t_k = k\tau_0$, $k \in \mathbb{N}$, and $\hat{t}_n = \sum_{i=0}^{n-1} \tau_i$. The propulsion power and engine speed mainly depend on the road slope $\alpha(t)$, the vehicle speed $v(t)$ and the selected gear $\gamma(t)$ and can be predicted using a simple longitudinal vehicle model (see, e.g., [40]). In particular, we predict these quantities using

$$P_r(v, \alpha, \gamma) = (F_{\text{acc}}(v, \gamma) + F_{\text{slope}}(\alpha) + F_{\text{roll}}(\alpha) + F_{\text{drag}}(v)) v, \quad (5.5a)$$

$$\omega_r(v, \gamma) = \frac{r_{\text{gb}}(\gamma)}{r_{\text{dyn}}} v, \quad (5.5b)$$

where $r_{\text{gb}}(\gamma)$ is the combined gearbox and differential ratio that depends on the selected gear $\gamma \in \{1, \dots, 12\}$, r_{dyn} is the dynamic wheel radius, v is the (predicted) vehicle speed, F_{acc} is the force required to accelerate the vehicle, F_{slope} is the force required to drive the vehicle up or down a slope, F_{roll} the rolling resistance of the tyres and F_{drag} is the air resistance of the vehicle. These forces are schematically shown in Figure 5.5 and are given by

$$F_{\text{acc}}(v, \gamma) = \left(m + \frac{J_{\text{eq}}(\gamma)}{r_{\text{dyn}}^2} \right) \frac{dv}{dt}, \quad (5.5c)$$

$$F_{\text{slope}}(\alpha) = mg \sin \alpha, \quad (5.5d)$$

$$F_{\text{roll}}(\alpha) = mg C_{\text{roll}} \cos \alpha, \quad (5.5e)$$

$$F_{\text{drag}}(v) = \frac{1}{2} \rho_{\text{air}} C_{\text{drag}} A v^2, \quad (5.5f)$$

where m is the vehicle mass, J_{eq} is the equivalent inertia of the drive line at the wheels as function of the selected gear, g is the gravitational constant, C_{roll} rolling resistance coefficient of the tires, A is the frontal area, C_{drag} is the air drag coefficient and ρ_{air} is the air density. It is assumed that all constants are known, or can be estimated online using techniques presented in [68, 126, 117, 33]. The time-dependent road slope $\alpha(t)$, vehicle speed $v(t)$ and gear selection $\gamma(t)$, however, need to be predicted for $t > 0$.

5.3.2 Prediction Algorithm

The road slope can be predicted with an e-horizon system, e.g., ADASIS [98], which gives a vector of road slopes over the relative distance $s(t)$ to the current position of the vehicle, i.e., $\alpha(t) = \alpha(s(t))$. Prediction of the velocity $v(t)$ is more difficult. Nevertheless, since we consider long-haul heavy-duty vehicles,

which spend most of their time on the highway, we can assume that the cruise control (CC) or the downhill speed control (DSC) is active during most of the driving. In this case, the desired velocity of the vehicle is regulated towards v_{cc} for cruise control and towards v_{dsc} for downhill speed control. Typically, it holds that $v_{dsc} > v_{cc}$, i.e., the DSC speed is larger than the CC speed, which allows some of the potential energy to be stored as kinetic energy. Finally, a rule-based gear shift strategy is assumed that satisfies

$$\gamma(v) = \max\{\{1, \dots, 12\} \mid \underline{\omega}_r \leq \omega_r(v, \gamma)\}, \quad (5.6)$$

where $\underline{\omega}_r$ is the constant lower threshold for gear shifting, respectively. This strategy seeks always the highest gear for which the minimum engine speed is satisfied, which corresponds generally with the most efficient gear shift strategy. The propulsion power is constrained as well

$$\underline{P}_r(v, \gamma) \leq P_r(v, \alpha, \gamma) \leq \overline{P}_r(v, \gamma), \quad (5.7a)$$

where $\underline{P}_r(v, \gamma)$ and $\overline{P}_r(v, \gamma)$ are the lower and upper bound that depend on the vehicle speed, the selected gear and whether CC or DSC is active. In particular, the maximum power is always constrained to the maximum engine power, i.e.,

$$\overline{P}_r(v, \gamma) = \eta_{gb}(\gamma) \overline{u}_{ice}(\omega_r(v, \gamma)), \quad (5.7b)$$

where $\eta_{gb}(\gamma)$ is the efficiency of the gearbox and differential as function of the selected gear. The minimum power is constrained to

$$\underline{P}_r(v, \gamma) = \begin{cases} \frac{\underline{u}_{ice}(\omega_r(v, \gamma))}{\eta_{gb}(\gamma)} & \text{if } v < v_{dsc} \\ -\infty & \text{otherwise.} \end{cases} \quad (5.7c)$$

This constraint means that braking with the electric motor and friction brakes is only allowed when the vehicle speed exceeds the desired downhill speed.

Solving (5.5) subject to (5.6) and (5.7a) is hard due to the nonlinear vehicle dynamics, the appearance of the derivative $\frac{dv}{dt}$ and the constraints (5.7) and because the road slope is given as function of distance and not as function of time. Therefore, we propose to make a forward Euler approximation of (5.5) over the time horizon $t \in [t_k, t_k + \sum_{i=0}^{N-1} \tau_i)$ at time instants $\tilde{t}_\ell = \frac{\ell}{L-1} \sum_{i=0}^{N-1} \tau_i$,

$\ell \in \{0, \dots, L-1\}$. This includes approximating

$$\left. \frac{dv}{dt} \right|_{t=t_k+\tilde{t}_\ell} \approx \frac{v(t_k+\tilde{t}_{\ell+1}) - v(t_k+\tilde{t}_\ell)}{\tilde{t}_{\ell+1} - \tilde{t}_\ell}. \quad (5.8)$$

We then find a solution for (5.5) subject to (5.6) and (5.7a) sequentially over the interval $[t_k, t_k + \sum_{i=0}^{N-1} \tau_i)$ and at each time instant $t_k + \tilde{t}_\ell$ we switch, if necessary, between CC and DSC and select a different gear. The algorithm to predict the power request at the wheels is then given by

Algorithm 5.3.1.

Initialize $s(t_k) = 0$ and measure $v(t_k)$, $\gamma(t_k)$.

For $\ell \in \{0, \dots, L-1\}$,

- Obtain the road slope from ADASIS $\alpha(s(t_k + \tilde{t}_\ell))$
- Calculate the engine speed with (5.5b) and, if necessary, shift gears according to (5.6) to obtain $\gamma(t_k + \tilde{t}_\ell)$ and $\omega_r(t_k + \tilde{t}_\ell)$
- If $v(t_k + \tilde{t}_\ell) > v_{cc}$, set DSC active, otherwise set CC active
- **if CC active:** Calculate the power request with (5.5a) for the desired $\frac{dv}{dt} = \frac{v_{cc} - v(t_k + \tilde{t}_\ell)}{\tilde{t}_{\ell+1} - \tilde{t}_\ell}$ to obtain $P_r(t_k + \tilde{t}_\ell)$
- **if DSC active:** Calculate the power request with (5.5a) for the desired $\frac{dv}{dt} = \frac{v_{dsc} - v(t_k + \tilde{t}_\ell)}{\tilde{t}_{\ell+1} - \tilde{t}_\ell}$ to obtain $P_r(t_k + \tilde{t}_\ell)$
- If $P_r(t_k + \tilde{t}_\ell) \geq \overline{P}_r(v, \gamma)$, set $P_r \Rightarrow \overline{P}_r(v, \gamma)$, if $P_r(t_k + \tilde{t}_\ell) \leq \underline{P}_r(v, \gamma)$, set $P_r \Rightarrow \underline{P}_r(v, \gamma)$ and compute $\frac{dv}{dt}$ satisfying (5.5)
- Update vehicle speed: $v(t_k + \tilde{t}_{\ell+1}) = v(t_k + \tilde{t}_\ell) + \frac{dv}{dt}(\tilde{t}_{\ell+1} - \tilde{t}_\ell)$
- Update distance: $s(t_k + \tilde{t}_{\ell+1}) = s(t_k + \tilde{t}_\ell) + v(t_k + \tilde{t}_\ell)(\tilde{t}_{\ell+1} - \tilde{t}_\ell)$

This algorithm predicts the power request $P_r(v, \alpha, \gamma)$ and engine speed $\omega_r(v, \gamma)$ over the prediction horizon $[t_k, t_k + \sum_{i=0}^{N-1} \tau_i)$, which is used in (5.4) to obtain the average propulsion power and the average engine speed over the variable prediction time intervals τ_i for $i \in \mathcal{N}$. This allows the optimal control problem (4.2) to be solved with the distributed model predictive control approach, as will be demonstrated in the next section.

5.4 Simulation Results

In this section, the results of the DEMPC approach to CVEM will be presented. Prediction information is a key element in the proposed approach and in the first section, results will be given on predicting the power request and engine speed with Algorithm 5.3.1 and ADASIS. In the next section, the fuel reduction for CVEM on the high-fidelity vehicle model will be presented followed by a detailed analysis of the energy flows. Finally, to demonstrate the real-time aspects of the algorithm, we will show the computational performance of the algorithm for a dSpace Autobox.

5.4.1 Power Request and Engine Speed Prediction with ADASIS

In the prototype vehicle, the road slope is predicted by the ADASIS protocol, which gives the road slope as function of the relative distance from the current position of the vehicle. ADASIS measurements are gathered for a highway cycle of 19 km driven in the region of Eindhoven (Netherlands). ADASIS provides the road slope at non-uniform distances from the current position depending on the future road slope. Moreover, the road slopes are not instantly available but new predictions are gradually added and old predictions are gradually removed based on the most probable path predicted by ADASIS.

The amount of predicted road slopes, indicated with N_{ADASIS} therefore changes all the time as shown in Figure 5.6. The upper plot in this figure shows the number of predictions as function of the distance driven by the vehicle in the high-fidelity simulation environment. The number of predictions sometimes goes to zero, which happens when the vehicle takes an exit, which is different from the most probable path predicted by the ADASIS protocol. After the exit, the ADASIS protocol notices that a different path is taken and all erroneous predictions are discarded. This happens three times on the drive cycle under consideration. The measured road slope and four examples of a road slope prediction by ADASIS are shown in the second plot. For the green labeled cases, plenty of predictions are available and no unpredicted exit is taken, which lead to very accurate prediction of the road slope. For the red labeled cases however, unpredicted exits are taken in the future, which result in a faulty prediction of the road slope. As

a consequence, the velocity, the power request and the engine speed predicted with Algorithm 5.3.1, is sufficiently accurate for the green examples but faulty for the red examples. This is also shown by the plot with the average root mean square error (RMSE) of the difference between the predicted power request and the measured power request over the entire prediction horizon. This plot clearly shows that if the vehicle follows the most probable path, a sufficiently accurate prediction of the future power request can be made with Algorithm 5.3.1 in combination with the ADASIS protocol. As heavy-duty vehicles often tend to drive the same route, the protocol can and will be improved in coming years by taking this information into account for predicting the most probable path.

The drive cycle for which ADASIS information is available is very short and the region around Eindhoven is very flat so that differences in road slope are mainly caused by driving up and down flyovers. The differences in road slope are not even significant to reach the downhill speed control (DSC) reference speed after which the vehicle starts to actively recover brake energy with the hybrid system. This cycle will therefore not show the true potential of the DEMPC. Instead the fuel reduction is analyzed with the high-fidelity vehicle model by driving the same drive cycle as used for the low-fidelity vehicle model for which the reference vehicle speed and road slope is given in Figure 5.7. We will assume that the vehicle always follows the most probable path, i.e, the road slope prediction is exact. This leads to an average RMSE of 29 kW for the power prediction, which is similar to the RMSE made with the ADASIS protocol and Algorithm 5.3.1.

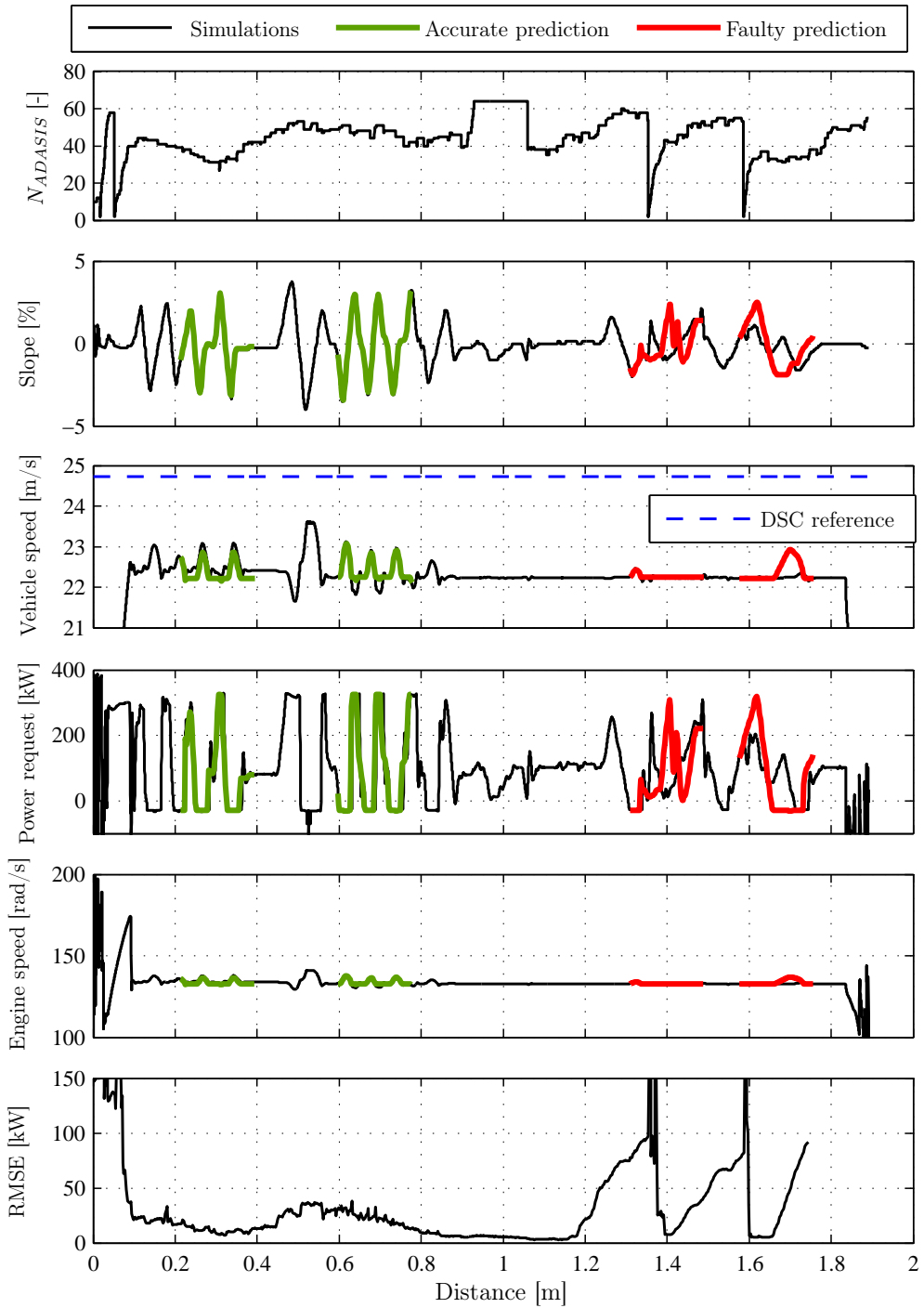


Figure 5.6: Road load prediction with Algorithm 5.3.1 and ADASIS.

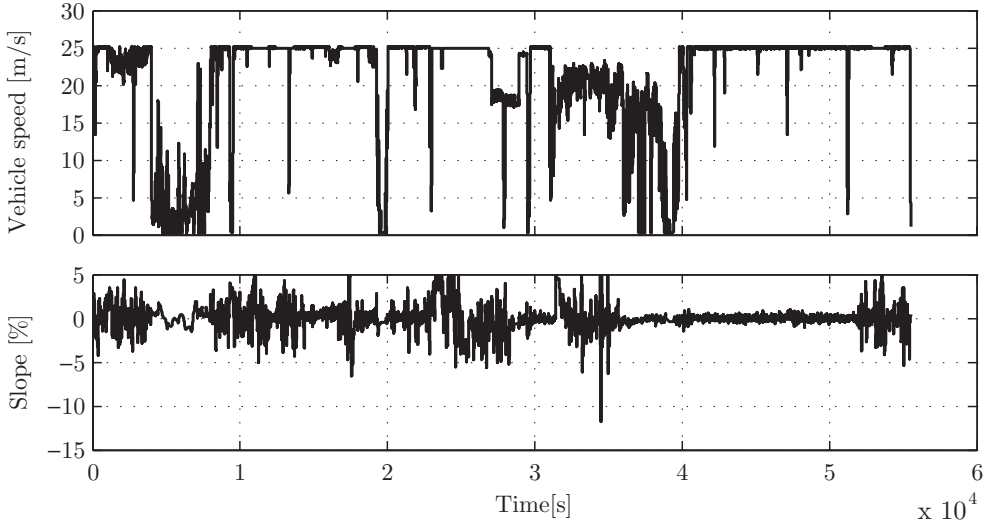


Figure 5.7: Reference vehicle speed on the PAN European driving cycle.

5.4.2 Fuel Reduction for CVEM

The fuel consumption for the high-fidelity vehicle model with CVEM is compared with the fuel consumption of the high-fidelity vehicle model with two default control strategies. The first default strategy (D1) is as follows

- **Refrigerated semi-trailer:** The temperature in the refrigerated trailer cycles between the lower and upper temperature bound, i.e, between $4.5\text{ }^{\circ}\text{C}$ and $5.5\text{ }^{\circ}\text{C}$.
- **Air supply system** The air pressure in the air supply system cycles between the lower and upper pressure bound, i.e, between 9.6 bar and 13.1 bar. Each time that the pressure hits the upper bound, some of the pressure is released through the desiccant cartridge to remove the water build up inside the cartridge.
- **Climate control system** The wall temperature of the evaporator cycles between the lower and upper temperature bound, i.e, between $5\text{ }^{\circ}\text{C}$ and $7\text{ }^{\circ}\text{C}$.
- **Alternator** A fixed voltage setpoint is sent to the alternator such that the initial amount of energy in the low-voltage battery is equal to the final

amount of energy.

- **DCDC converter** The DCDC converter is not used on the default control strategy.

This strategy is the same default control strategy as used in [11]. The following default control strategy (D2) is an adaptation to D1 with a different control strategy for the air supply system and the climate control system, i.e.,

- **Air supply system** Recent developments made it possible to only remove the water from the desiccant cartridge after a certain amount of cycles. This reduces the amount of air released to the environment and thereby improves the efficiency of the air supply system.
- **Climate control system** Automotive climate control systems generally cycle between a very low upper and lower temperature bound as in default strategy D1. The cold air is mixed with warm air heated by the internal combustion engine to supply the right air temperature to the cabin. This is very inefficient and recent trends increased the upper and lower temperature bound. For this default control strategy the wall temperature of the evaporator cycles between $9\text{ }^{\circ}\text{C}$ and $13.5\text{ }^{\circ}\text{C}$.

This strategy is the same as the default strategy used in Chapter 4 for the low-fidelity vehicle model, except that the alternator receives a constant voltage setpoint instead of a constant power setpoint, which results in a slightly different alternator power.

The fuel reduction results with CVEM compared to the two baseline strategies are given in Table 5.1. To analyze the fuel reduction contribution of each of the subsystems, the results of various simulations are shown for which only one subsystem is being controlled with the CVEM algorithm. For completeness, the fuel reductions are given for Part 1, i.e., for $t \in [0, 20000)$, for Part 2, i.e., for $t \in [20000, 40000)$ and for the complete driving cycle. Part 1 and Part 2 are the same parts used in Chapter 4 to evaluate the control strategy on the low-fidelity vehicle model. For a complete analysis, the difference in stored energy inside the energy storage systems at the start and end of the cycle must be taken into account. However, as each of these drive cycles is very long, the effect on the overall fuel consumption is small and neglected in this table.

Table 5.1: Fuel reduction results on the high-fidelity vehicle model

Subsystem	Default D1	Default D2		
	Complete	Part 1	Part 2	Complete
Refrigerated semi-trailer	0.30 %	0.43 %	0.30 %	0.30 %
Air supply system	0.26 %	0.07 %	0.04 %	0.05 %
Climate control system	0.19 %	0.07 %	0.00 %	0.02 %
Alternator	0.07 %	0.13 %	0.04 %	0.07 %
DCDC converter	0.20 %	0.15 %	0.22 %	0.20 %
CVEM	0.98 %	0.63 %	0.56 %	0.58 %

The fuel reduction is strongly related to the average switching time for the refrigerated semi-trailer, the air supply system and the climate control system. These times are shown in Figure 5.8 for the two default control strategies and for the smart CVEM control strategy. Indeed, compared with the second default control strategy, the average switching time is decreased with a factor 8.5, 8.2 and 1.5 for the refrigerated semi-trailer, the air supply system and the climate control system, respectively.

For the average switching times given in Figure 5.8, the fuel reduction obtained with CVEM in the high-fidelity vehicle model is around half the fuel reduction obtained with CVEM in the low-fidelity vehicle model. We will present some analysis on the energy flows in the next section to obtain a better understanding on this result.

5.4.3 Energy Flows in the Vehicle

The CVEM strategy utilizes the energy buffers in all subsystems to store energy. This is shown in Figure 5.9 for only $t \in [0, 10000)$ and shown for the complete driving cycle in Appendix A.3. Here, $\tilde{x}_{hvb} = \frac{x_{hvb}}{E_{hvb}}$ is the high-voltage battery energy normalized with respect to the maximum battery capacity E_{hvb} , $\tilde{x}_{lvb} = \frac{x_{lvb}}{E_{lvb}}$ is the low-voltage battery energy normalized with respect to the maximum battery capacity E_{lvb} , T_{rst} is the air temperature in the refrigerated trailer, p_{as} is the air pressure in the air supply system and T_{ccs} is the wall temperature of the climate control system. Note that the control of the hybrid system is rule-based in the high-fidelity vehicle model, which can be observed from the energy

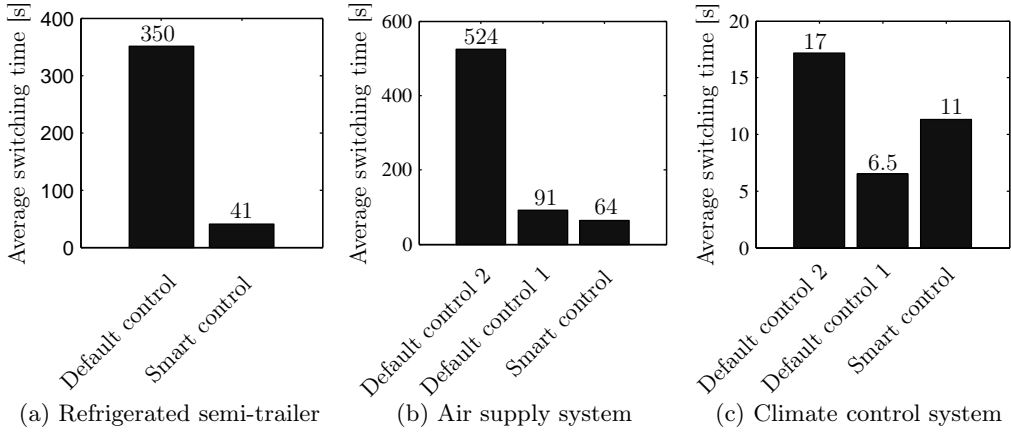


Figure 5.8: Average switching times.

in the high-voltage battery. In particular, regenerative braking energy stored in the high-voltage battery, i.e, the peaks where $\tilde{x}_{hvb} = 0.55$, is directly used for boosting leading to a sharp drop in energy. This figure shows, indeed, that most subsystems are used at these moments to store energy as the temperature in the refrigerated semi-trailer is lowered, the air pressure is increased and the energy in the low-voltage battery is increased. Only the climate control system hardly lowers its temperature.

The amount of regenerative energy that is stored in the subsystems relative to their total energy consumption is given in Figure 5.10 for the two default control strategies and for the smart control strategy evaluated on the high-fidelity vehicle model (HF) and on the low-fidelity vehicle model (LF). The amount of regenerative energy harvested on the low-fidelity vehicle model is for all subsystems larger than for the high-fidelity vehicle model, which can explain some of the differences in the fuel reduction. In particular, the energy harvested by the electric machine in the high-fidelity vehicle model is 25.8 % lower than in the low-fidelity vehicle model due to, e.g., not taking into account gear shifting in the low-fidelity vehicle model. This has a significant impact on the fuel reduction potential of CVEM. Furthermore, comparing percentages is difficult as the fuel consumption for the default control strategy is 10.7 % higher in the high-fidelity vehicle model than in the low fidelity vehicle model.

Finally, to put the fuel reduction potential in perspective, the energy losses in

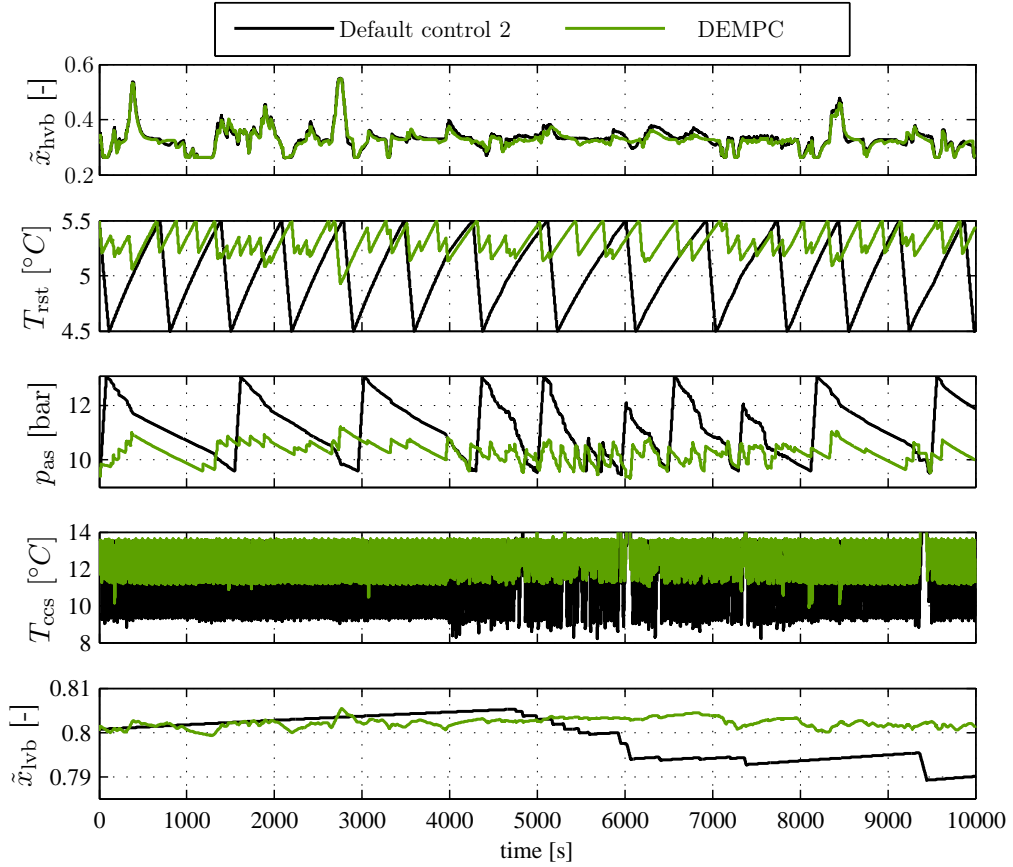


Figure 5.9: State trajectories for $t \in [0, 10000)$ of the PAN European driving cycle.

each subsystem are given as percentage of the total fuel energy in Figure 5.11 for the two default control strategies and for the smart control strategy evaluated on the high-fidelity vehicle model. An interesting observation is that only 1 % of the fuel energy is used for the refrigerated semi-trailer with the default control strategy, which is slightly reduced with the smart control strategy. A fuel reduction of 0.3 % as given in Table 5.1 is then actually a 30 % improvement on subsystem level. The majority of the energy losses in the vehicle are in the internal combustion engine and other energy losses as a result of air drag, friction brakes, etc., which is shown in Figure 5.12. It is remarkable that the other energy losses, which include the energy losses in the friction brakes, are only reduced

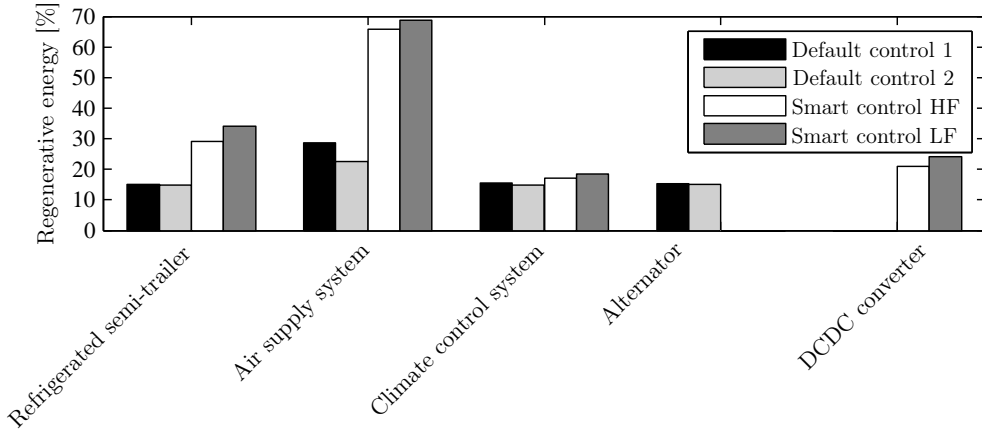


Figure 5.10: Regenerative energy stored in the subsystems relative to their total energy consumption.

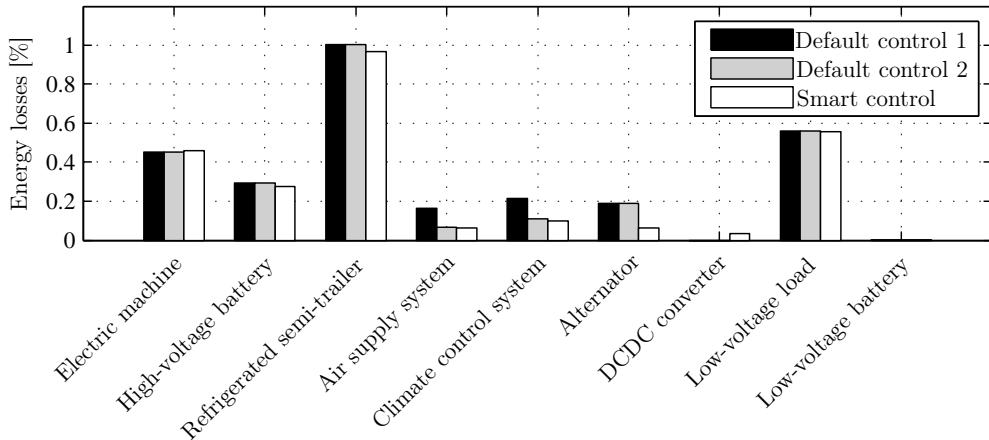


Figure 5.11: Energy losses for each subsystem as percentage of the total fuel energy.

with 0.2 %. This means that the electric machine is not used to significantly recover more braking energy as with the default control strategy and this can be an opportunity for improving the fuel reduction. Still, with CVEM, the energy losses in the internal combustion engine are reduced with 1.2 %, which indicates that energy from the internal combustion engine is used more efficiently.

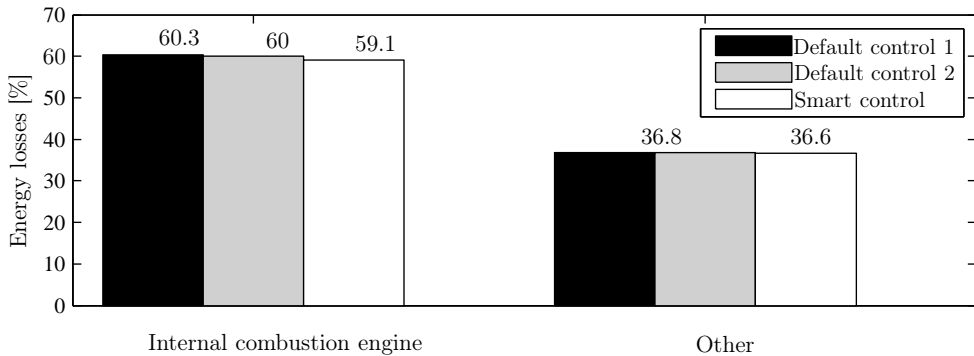


Figure 5.12: Energy losses in the internal combustion engine and other energy losses as a result of air drag, friction brakes, etc.

5.4.4 Implementation on a dSpace Autobox

As a final step to prove feasibility of the DEMPC approach to CVEM, the algorithm is implemented on a dSpace Autobox. The prototype vehicle is equipped with a dSpace autobox with a DS1005 PPC Board that features a PowerPC 750GX processor running at 1 GHz. To test the real-time aspects of the control algorithm proposed in this paper, the algorithm is implemented onto the DS1005. The algorithm is running in open loop, i.e., the inputs for the control algorithm, e.g., the vehicle velocity, distance are not following from the vehicle model, which is too large to run in real-time, but follow from lookup tables. Similarly, the setpoints generated by the control algorithm are not implemented on the vehicle model but are discarded. Still, the ADASIS information is processed

Table 5.2: Case studies for implementation on a dSpace Autobox.

Case	Description	Number of QPs solved at each iteration
1	Only hybrid system	1
2	Case 2 with the refrigerated semi-trailer	3
3	Case 3 with the air supply system	5
4	Case 3 with the climate control system	7
5	Case 4 with the low-voltage battery	8

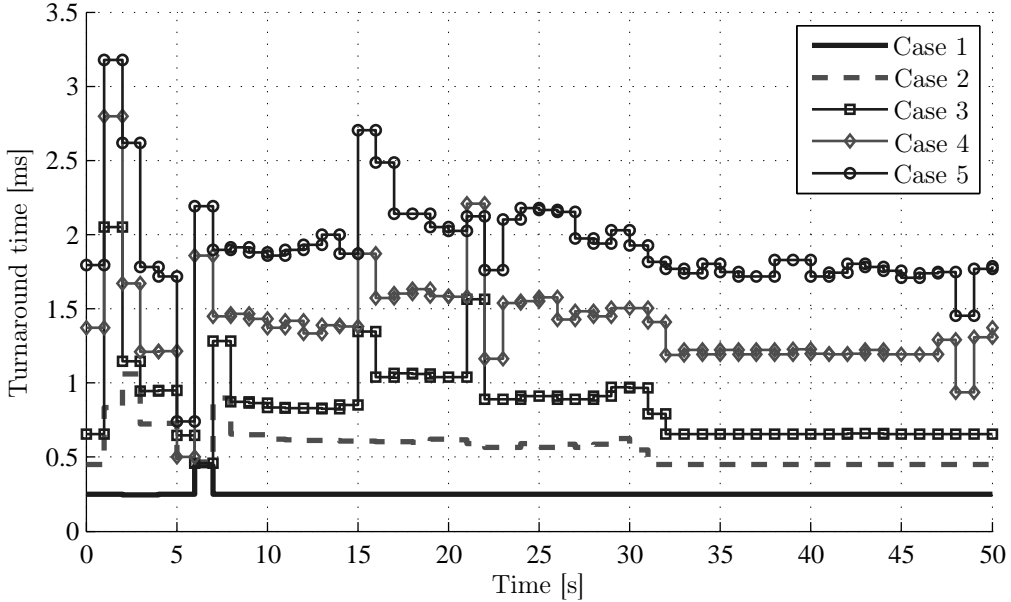


Figure 5.13: Turnaround times.

in real-time as function of the distance driven by the heavy-duty vehicle. This approach allows us to isolate the computational performance of the previewer and the control algorithm only.

Five cases are given in Table 5.2 to analyze the scalability properties. The algorithm is running at 50 Hz and at each sampling period, one iteration of the dual decomposition algorithm is executed, i.e., the number of QPs as given in Table 5.2 are solved and the dual variables are updated once. This allows for 50 iterations as the setpoints for the subsystems are updated with a frequency of 1 Hz. The turnaround times of the algorithm are given in Figure 5.13 for each of the cases over the first 50 seconds of the drive cycle given in Fig. 5.6. It is shown that by smart control of all subsystem (Case 5), the worst case execution time still only occupies 16% ($\frac{3.2 \text{ ms}}{20 \text{ ms}} 100\%$) of the sampling period. The remaining time can be used for other tasks or the update frequency of the setpoints can be lowered.

5.5 Conclusions and Discussion

In this chapter, a distributed economic model predictive control (DEMPC) approach to complete vehicle energy management is validated on a high-fidelity vehicle model. Conclusions will be drawn and a discussion on the results will be given in this section.

5.5.1 Conclusions

Prediction of the disturbances is essential for DEMPC. The propulsion power needed for driving and the engine speed have been predicted by assuming that the vehicle follows a reference speed set by the cruise control or the downhill speed control, which is valid for high-way driving. This allowed the vehicle speed to be predicted over a trajectory with a road slope predicted by an e-horizon sensor, e.g., ADASIS, leading to a prediction of the propulsion power and engine speed. The prediction algorithm has been validated with measured ADASIS information on a public road around Eindhoven, which demonstrated that sufficiently accurate prediction of the propulsion power and engine speed is feasible if the vehicle follows the most probable path.

The fuel reduction for the DEMPC approach to CVEM has been validated for a PAN European driving cycle. A fuel reduction of 0.58 % can be obtained compared to the best default control strategy and 0.98 % compared with the worst default control strategy. This is indeed lower than estimated with the low-fidelity vehicle model, which can partly be related to the 25 % less braking energy that is recovered in the high-fidelity vehicle model and the absolute fuel consumption of the default control strategy is 10 % higher.

The DEMPC approach applies first a dual decomposition to the receding horizon optimal control problem such that the problem related to each subsystem can be solved separately, e.g., on a separate electronic control unit. To avoid a heavy communication load, all subproblems have been solved on the same platform. This type of implementation has been demonstrated by implementing the DEMPC approach on a dSpace Autobox. The results showed that the maximum computation time is only 3.2 ms per iteration, which demonstrated that real-time implementation is feasible.

5.5.2 Discussion

In this chapter, the DEMPC approach has been implemented and validated on the high-fidelity vehicle model. The results demonstrated that the fuel consumption can indeed be reduced by smart control of all the subsystems in the vehicle. However, to obtain this fuel reduction, the switching frequency of the refrigerated semi-trailer, the air supply system and the climate control system need to be increased with up to factor 9. These subsystems can be modified to be controlled with a continuous setpoint, e.g., with an electric motor that runs at variable speeds. This avoids a compromise between the number of switches and the fuel reduction for these components and fuel efficiency can be further improved.

The DEMPC approach is only validated on the high-fidelity vehicle model. To fully demonstrate the approach, the solution strategy needs to be implemented on the heavy-duty vehicle and tested on a road with significant fluctuations in road slope. This also requires that other disturbances, e.g., the ambient temperature need to be measured. An interesting extension to this field is to use online parameter estimation to update the parameters that are used to predict and optimize the decisions and states of each subsystem.

6

Conclusions

As stated in the introduction of this thesis, reducing the emission of the greenhouse gas CO₂ and developing competitive heavy-duty vehicles are the main drivers for reducing the fuel consumption. This has led to many technological developments that improved the efficiency of each of the subsystems in the vehicle. However, optimizing all these subsystems individually does not automatically guarantee global optimal fuel efficiency at the vehicle level. Therefore, a new energy management strategy that takes into account all the energy flows and energy buffers in the vehicle, i.e., a complete vehicle energy management (CVEM), is needed. The research question posed in the introduction was to assess the fuel reduction potential of a CVEM strategy that takes into account all energy flows and energy buffers in the vehicle. Key objectives in this assessment are that the CVEM is required to be flexible with respect to adding auxiliaries, scalable for real-time purposes and suitable for on/off controlled devices. This assessment led to the two main objectives in this thesis, i.e.,

- Objective 1: The development of a flexible and scalable optimal control concept for CVEM with on/off controlled auxiliaries*
- Objective 2: The development of a flexible and scalable real-time energy management strategy for CVEM with on/off controlled auxiliaries*

The conclusions of the research along the lines of these objectives will be given in Section 6.1. The research has also led to inspiration and directions for further research, which will be given in Section 6.2 and, finally, this thesis will be concluded with some implications in Section 6.3.

6.1 Conclusions

The main conclusions of this thesis are summarized below.

Convex approximation of the behavior of a heavy-duty vehicle: The distributed optimization approach to CVEM requires a model that is suitable for a model-based energy management approach. This low-fidelity vehicle model has been obtained in Chapter 2 by making a convex approximation of the behavior of the subsystems in the heavy-duty vehicle considered in this thesis. The behavior of each of the subsystems has been defined in their input and output power and the stored energy inside the subsystems. This general framework in terms of powers and energies allows any vehicle topology to be fully described by the power balances on the networks in the vehicle, e.g., the mechanical, the high-voltage and the low-voltage network. The input-output power behavior of all subsystems is approximated with a strictly convex quadratic equality constraint. The dynamics for some subsystems in the vehicle, i.e., the energy in the high-voltage battery, the low-voltage battery, the refrigerated semi-trailer, the air-supply system and climate control system are described by a linear differential equation. The low-fidelity vehicle model allows the CVEM problem to be formulated as an optimal control problem that can be solved with a distributed optimization approach.

Flexible and scalable optimal control concept for CVEM with on/off controlled auxiliaries: In Chapter 3, the distributed optimization approach has been presented to solve the complete vehicle energy management problem offline. The offline solution strategy requires all disturbances (such as the driving cycle) to be known, so that the global optimal solution can be computed. This computation has been performed in a two step procedure. In the first step, a dual decomposition has been applied that allowed the underlying optimal control problem to be solved for every subsystem separately. The second step amounts to solving the optimization problem for every subsystem separately, yielding a distributed implementation of the optimization. Three methods have been proposed for the latter. The first two methods rely on splitting the control horizon into several smaller horizons. The first method uses Alternating Direction Method of Multipliers and divides the horizon a priori, while the second method divides the horizon iteratively by solving unconstrained optimization problems analytically.

The third method, based on dynamic programming, is used to solve the optimal control problem related to subsystems with on/off control. The approach has been demonstrated by solving the complete vehicle energy management problem for a PAN European driving cycle. Simulation results have shown that the fuel consumption can be reduced up to 1.42 %, assuming that the auxiliaries are continuous controlled. This requires, however, that the auxiliaries are continuous controlled or that the number of switches is unbounded. More interestingly, the computation time has been reduced by a factor of 64 up to 1825, when compared to solving a centralized convex optimization problem.

Flexible and scalable real-time energy management strategy for CVEM with on/off controlled auxiliaries: The offline solution strategy cannot be used in real-time as the disturbances, e.g., the driving cycle, are generally not known a priori. In Chapter 4, the optimal control problem has been formulated as a receding horizon optimal control problem and has been solved with a distributed economic model predictive control (DEMPC) approach. In particular, a dual decomposition has been applied to this receding horizon optimal control problem such that the problem related to each subsystem can be solved separately. All of the optimization problems related to each subsystem are linearly constrained quadratic programs that can be solved efficiently with embedded quadratic programming solvers. Variable prediction time intervals have been used to obtain a long control horizon with a limited number of decision variables. As a result, the final state constraint can be used as a constraint, instead of a ‘soft’ constraint, which avoids the need for tuning parameters.

To deal with auxiliaries that can only be turned on or off, a novel on/off control concept has been developed for control of the refrigerated semi-trailer, the air supply system and the climate control system. The concept requires solving the linearly constrained quadratic program twice, one with the first decision being on and one with the first decision being off. The solution with the lowest cost is taken as the optimal solution.

The only parameters for the solution strategy proposed in Chapter 4 are the variable prediction time intervals and the penalty parameters for switching. The variable sample times have been chosen intuitively and simulation results on a low-fidelity vehicle model show that close to optimal fuel reduction performance can be achieved without carefully tuning these sample times. The fuel reduction

of the on/off controlled subsystems strongly depends on the number of switches that are allowed. The fuel reduction for the on/off controlled subsystems can be close to optimal, but the number of switches needs to be increased significantly. Particularly for the refrigerated semi-trailer and the air supply system, it is very difficult to obtain a large average switching time as the average switching time easily exceeds the maximum length of accurate prediction information. Still, by allowing more switches, a fuel reduction of up to 1.3 % can be achieved.

Validation on a high-fidelity vehicle model: Prediction of the disturbances is essential for DEMPC. The propulsion power needed for driving and the engine speed have been predicted by assuming that the vehicle follows a reference speed set by the cruise control or the downhill speed control, which is valid for high-way driving. This has allowed the vehicle speed to be predicted over a trajectory with a road slope predicted by an e-horizon sensor, e.g., ADASIS, leading to a prediction of the propulsion power and engine speed. The prediction algorithm has been validated with measured ADASIS information on a public road around Eindhoven, which demonstrated that sufficiently accurate prediction of the propulsion power and engine speed is feasible if the vehicle follows the most probable path.

The fuel reduction for the DEMPC approach to CVEM has been validated for a PAN European driving cycle. A fuel reduction of 0.58 % can be obtained compared to the best default control strategy and 0.98 % compared with the worst default control strategy. This is indeed lower than estimated with the low-fidelity vehicle model, which can partly be related to the 25 % less braking energy that is recovered in the high-fidelity vehicle model and the absolute fuel consumption of the default control strategy is 10 % higher.

The DEMPC approach uses first a dual decomposition that allows the optimization problem related to each subsystem to be solved separately, e.g., on a separate electronic control unit. To avoid a heavy-communication load, all sub-problems have been solved on the same platform and flexibility is obtained in the software, where subsystems can be added without redefining the optimal control problem. This type of implementation has been demonstrated by implementing the DEMPC approach on a dSpace Autobox. This has shown a maximum computation time is 3.2 ms per iteration, which demonstrates that real-time implementation is feasible.

6.2 Recommendations for Future Research

This thesis has presented a distributed optimization approach to CVEM for a hybrid heavy-duty vehicle with a refrigerated semi-trailer, an air supply system, an alternator, a DCDC converter, a low-voltage battery and a climate control system and is validated by simulation on a low-fidelity and high-fidelity vehicle model. Extensions for further research are summarized below.

Validation on the prototype vehicle: The online solution strategy proposed in this thesis is validated by simulation, the prediction algorithm is validated with real measurements and the solution strategy is successfully implemented on a dSpace Autobox. The next step is to validate the solution strategy on the prototype vehicle.

Online parameter estimation: Validation in the prototype vehicle requires estimating the disturbances that were known in the high-fidelity vehicle model, e.g., the ambient temperature. An interesting extension is to use online parameter estimation to update the parameters that are used to predict and optimize the decisions and states of each subsystem.

Eco-driving: An interesting extension to the optimal control problem amounts to taking into account the largest energy buffer in the vehicle, i.e., the vehicle mass. The energy in the vehicle mass consists of the sum of the kinetic energy and the potential energy of the vehicle. The potential energy is fixed by the elevation of the road, but the kinetic energy depends on the mass and velocity. An intuitive example is to increase the velocity when driving down hill to store some of the potential energy as kinetic energy. Finding the optimal reference velocity is not straightforward as the road slope is given as function of distance while the distance driven by the vehicle is depends on the vehicle speed. Moreover, constraints need to be taken into account, e.g., safety, comfort, traffic lights and gear selection. Still, the optimal control concepts presented in Chapter 3 and Chapter 4 demonstrated that by taking a distributed optimization approach, the optimization problems related to each subsystem are smaller and can be solved with different solution methods. This allows the vehicle mass to be considered as

another subsystem in the vehicle in which power can be stored as kinetic energy and the energy losses through air drag are minimized.

Continuous control of subsystems: A very strong trade-off between fuel consumption and switching frequency exists for subsystems that can only be turned on or off. These subsystems can be modified to be continuous controlled, e.g., with an electric motor that runs at variable speeds. This avoids a compromise between the number of switches and the fuel reduction for these components and fuel efficiency can be further improved.

Optimal sizing and topology design: The fuel consumption of a vehicle is strongly related to size of the components and the topology of the vehicle. The optimal size of the components often results in a trade-off, e.g., a larger battery allows more energy to be stored, but also adds more weight to the vehicle. At the same time, many different topologies exist, e.g., a (super) capacitor can be added to the high-voltage network to store temporary peak powers or the air supply system can be connected to the mechanical or low-voltage network instead of the high-voltage network. The flexibility and scalability of the optimal control concepts presented in Chapter 3 allows the topology to be changed easily so that many different topologies can be automatically generated and their optimal fuel consumption can be calculated. The results can be used to select the best topology for each application.

Optimal traffic management: In this thesis, the fuel consumption of a heavy-duty vehicle is reduced by optimally distributing the energy flows on vehicle level. The same ideas can be applied to a higher level, i.e., on the level of multiple vehicles that collaborate together to achieve on average a lower fuel consumption. Ultimately, this will lead to a joint control of all vehicles where braking at, e.g., road junctions is not necessary anymore.

Convergence properties of the computational schemes: All algorithms presented in this thesis converged within an acceptable computation time for energy management. The convergence, however, is not formally proven and no upper bounds on the convergence speed are given for the dual decomposition, the alternating direction method of multipliers and for the Lagrangian method.

An interesting problem is to formally prove the convergence of these methods for the general optimization problem and to find upper bounds on the convergence speed.

6.3 Implications

The contributions of this thesis can be a start for future research, possibly along the lines of the recommendations given above. The optimal control concepts in this thesis are presented in the context of smart control of all energy flows in the vehicle. In particular, smart control of the auxiliaries, e.g., the refrigerate semi-trailer received most attention. The fuel reduction potential for these auxiliaries can be limited compared to e.g., the fuel reduction potential of a hybrid system. Still, the main contribution of this thesis is not the fuel reduction for these auxiliaries, but the step that is taken towards a flexible and scalable framework that can handle the growing complexity of energy management systems that take into account more than just the power split between an internal combustion engine and electric machine. This will ultimately lead to close to optimal fuel consumption for the complete vehicle.



State Trajectories

A.1 Optimal state trajectories with continuous control

The optimal offline state trajectories over the full PAN European driving cycle are given in Figure A.1 which requires solving the CVEM problem with over 500.000 input constraints, 300.000 state constraints and 150.000 quadratic constraints. Here, $\tilde{x}_{hvb} = \frac{x_{hvb}}{E_{hvb}}$ is the high-voltage battery energy normalized with respect to the maximum battery capacity E_{hvb} , $\tilde{x}_{lvb} = \frac{x_{lvb}}{E_{lvb}}$ is the low-voltage battery energy normalized with respect to the maximum battery capacity E_{lvb} , T_{rst} is the air temperature in the refrigerated trailer, p_{as} is the air pressure in the air supply system and T_{ccs} is the wall temperature of the climate control system. This figure shows that all state constraints are met.

A.2 State trajectories for the low-fidelity vehicle model

The online state trajectories for the low-fidelity vehicle model for the full PAN European driving cycle are given in Figure A.2. This requires solving the reced-

ing horizon optimal control problem with distributed economic model predictive control (DEMPC) approach. Here, $\tilde{x}_{hvb} = \frac{x_{hvb}}{E_{hvb}}$ is the high-voltage battery energy normalized with respect to the maximum battery capacity E_{hvb} , $\tilde{x}_{lvb} = \frac{x_{lvb}}{E_{lvb}}$ is the low-voltage battery energy normalized with respect to the maximum battery capacity E_{lvb} , T_{rst} is the air temperature in the refrigerated trailer, p_{as} is the air pressure in the air supply system and T_{ccs} is the wall temperature of the climate control system. This figure shows that all state constraints are met.

A.3 State trajectories for the high-fidelity vehicle model

The online state trajectories for the high-fidelity vehicle model for the full PAN European driving cycle are given in Figure A.3. This requires solving the receding horizon optimal control problem with distributed economic model predictive control (DEMPC) approach. Here, $\tilde{x}_{hvb} = \frac{x_{hvb}}{E_{hvb}}$ is the high-voltage battery energy normalized with respect to the maximum battery capacity E_{hvb} , $\tilde{x}_{lvb} = \frac{x_{lvb}}{E_{lvb}}$ is the low-voltage battery energy normalized with respect to the maximum battery capacity E_{lvb} , T_{rst} is the air temperature in the refrigerated trailer, p_{as} is the air pressure in the air supply system and T_{ccs} is the wall temperature of the climate control system. This figure shows that all state constraints are met.

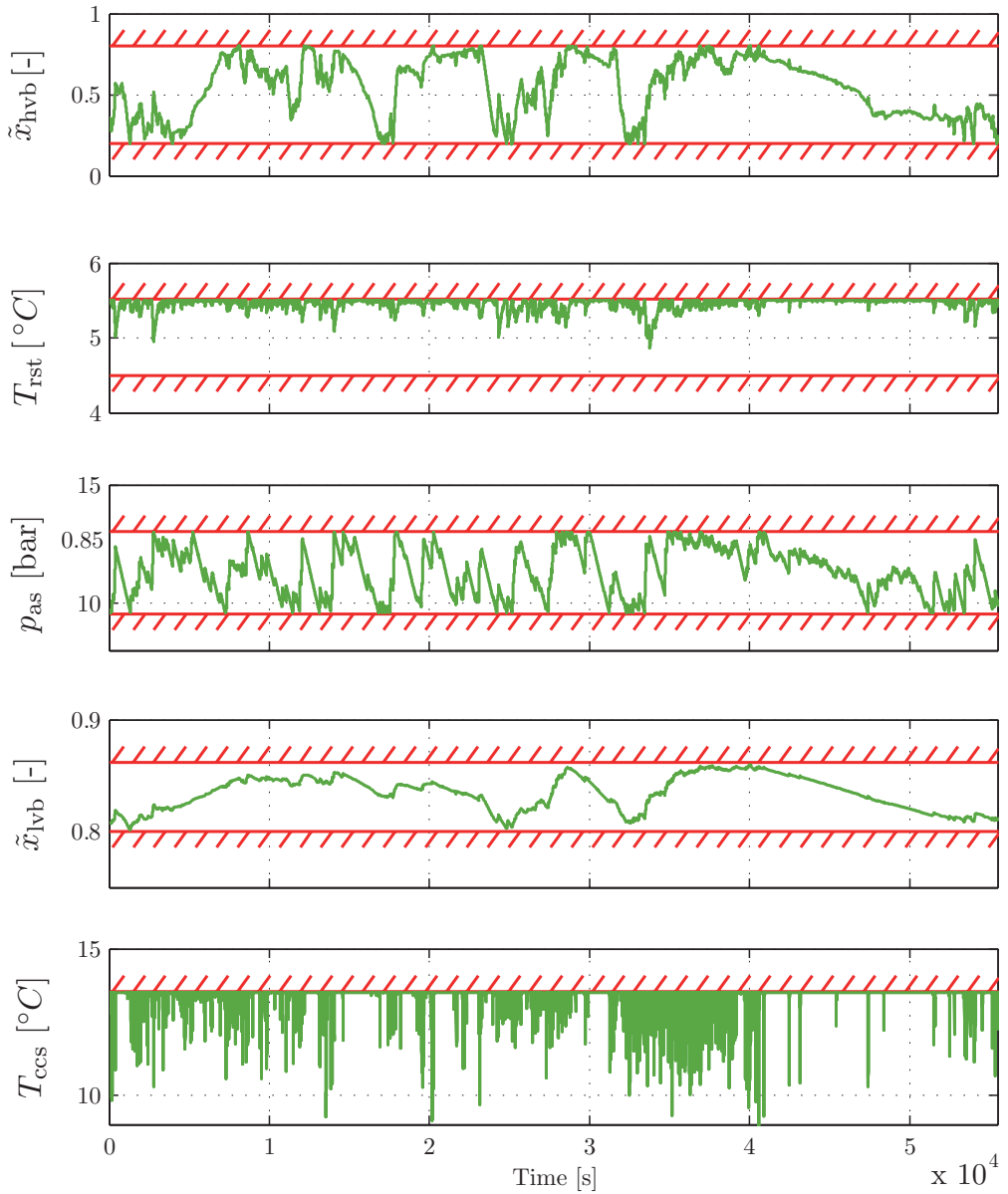


Figure A.1: Optimal state trajectories over the complete PAN European driving cycle.

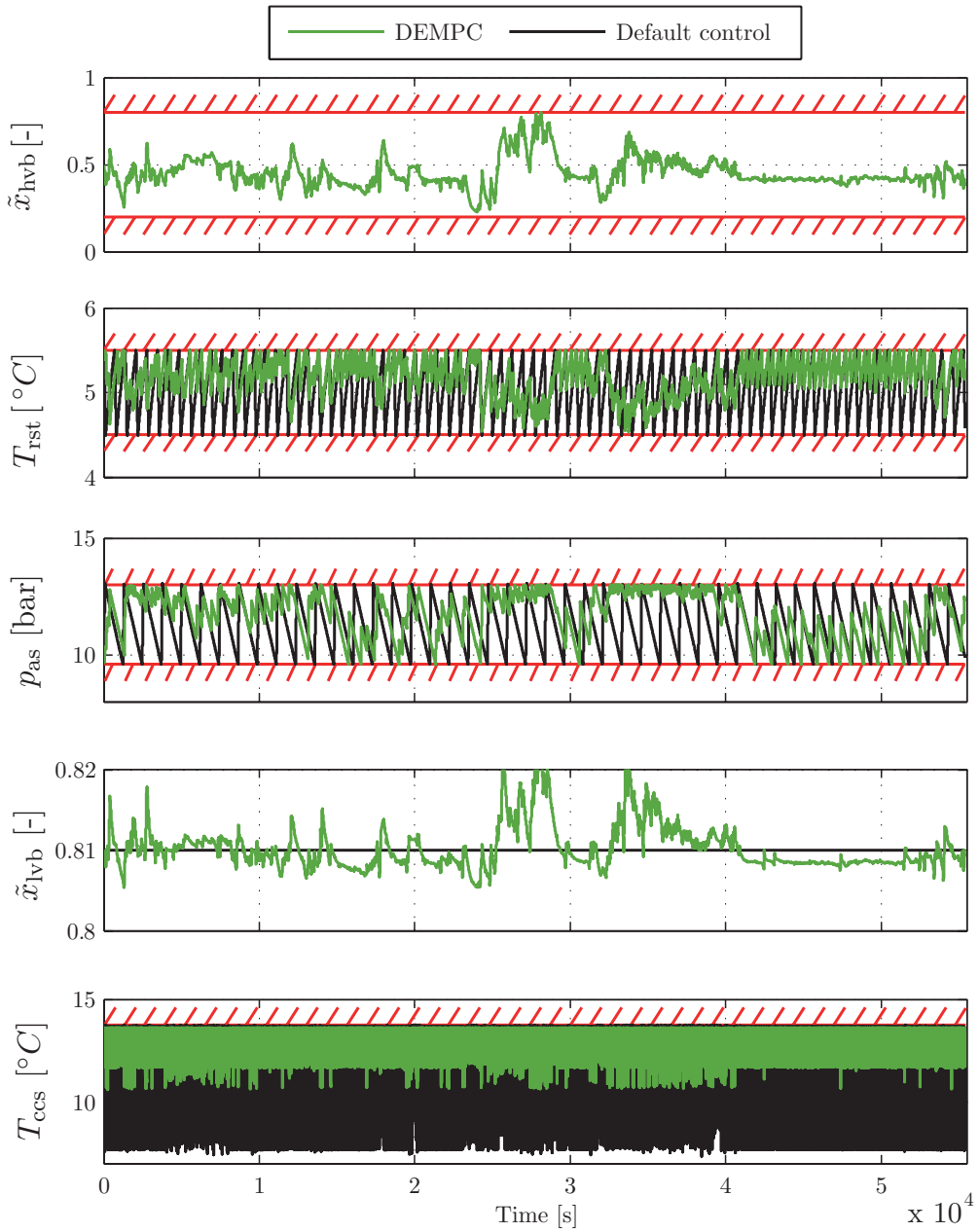


Figure A.2: State trajectories for the low-fidelity vehicle model over the complete PAN European driving cycle.

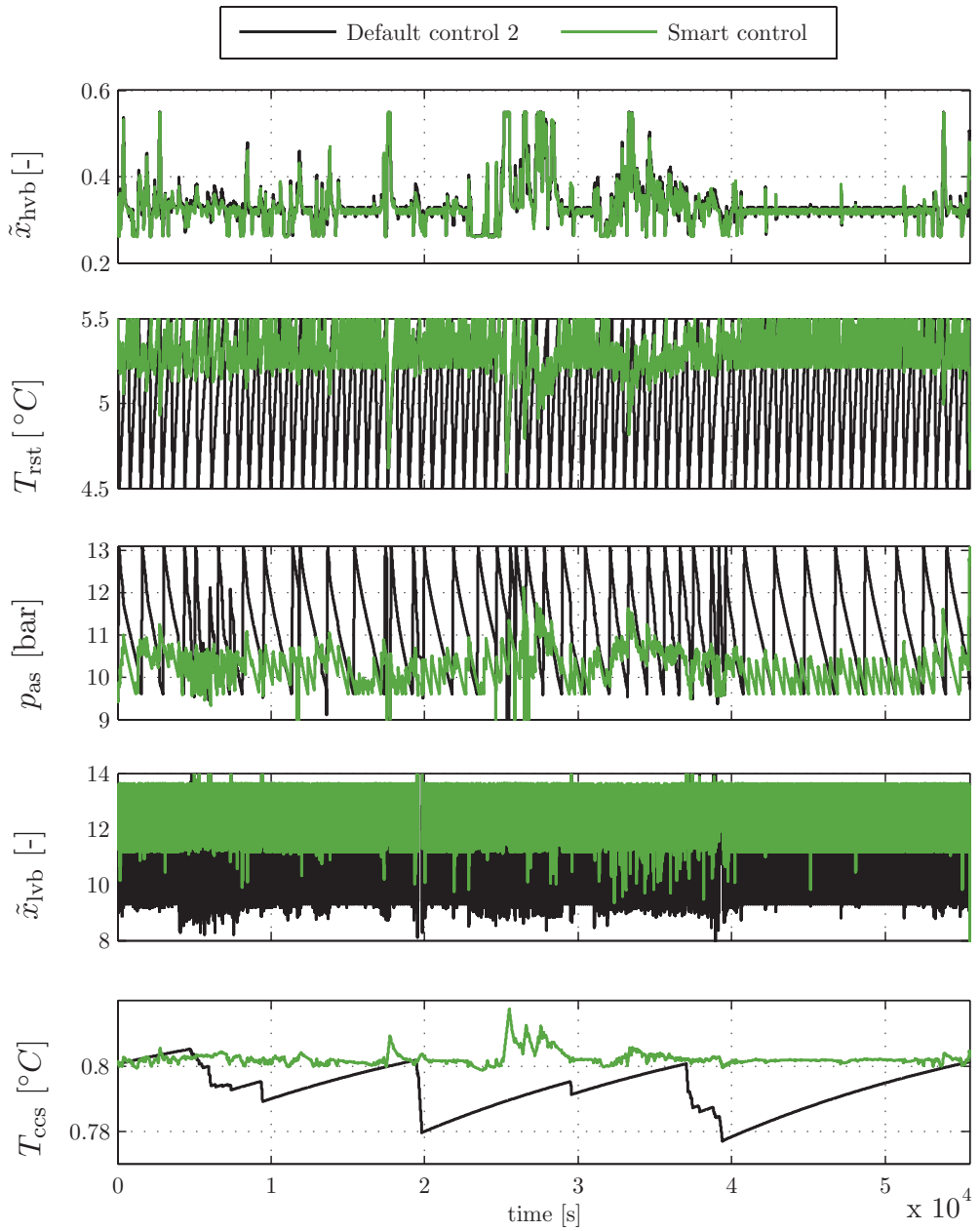


Figure A.3: State trajectories for the high-fidelity vehicle model over the complete PAN European driving cycle.

Bibliography

- [1] G. Ao, J. Qiang, H. Zhong, X. Mao, L. Yang, and B. Zhuo. Fuel economy and NO_x emission potential investigation and trade-off of a hybrid electric vehicle based on dynamic programming. In *Proc. of the Institution of Mechanical Engineers, Part D: Journal of Automobile Engineering*, 2008.
- [2] I. Arsie, M. Graziosi, C. Pianese, G. Rizzo, and M. Sorrentino. Optimization of supervisory control strategy for parallel hybrid vehicle with provisional load estimate. In *Proc. of AVEC04*. Citeseer, 2004.
- [3] M. Back, M. Simons, F. Kirschaum, and V. Krebs. Predictive control of drivetrains. *IFAC Proceedings Volumes*, 35(1):241–246, 2002.
- [4] B. M. Baumann, G. Washington, B. C. Glenn, and G. Rizzoni. Mechatronic design and control of hybrid electric vehicles. *IEEE/ASME Transactions On Mechatronics*, 5(1):58–72, 2000.
- [5] D. P. Bertsekas. *Dynamic programming and optimal control*, volume 1. Athena Scientific Belmont, MA, 1995.
- [6] B. Biegel, P. Andersen, J. Stoustrup, and J. Bendtsen. Congestion management in a smart grid via shadow prices. *IFAC Proceedings Volumes*, 45(21):518–523, 2012.
- [7] H. Borhan, A. Vahidi, A. M. Phillips, M. L. Kuang, I. V. Kolmanovsky, and S. Di Cairano. MPC-based energy management of a power-split hybrid electric vehicle. *IEEE Transactions on Control Systems Technology*, 20(3):593–603, 2012.

-
- [8] H. A. Borhan and A. Vahidi. Model predictive control of a power-split hybrid electric vehicle with combined battery and ultracapacitor energy storage. In *Proc. of the IEEE American Control Conference*, 2010.
 - [9] S. Boyd and L. Vandenberghe. *Convex Optimization*. Cambridge University Press, 2004.
 - [10] R. Cagienard, P. Grieder, E. C. Kerrigan, and M. Morari. Move blocking strategies in receding horizon control. *Journal of Process Control*, 17(6):563–570, 2007.
 - [11] H. Chen. *Game-theoretic solution concept for complete vehicle energy management*. PhD thesis, Technische Universiteit Eindhoven, 2016.
 - [12] H. Chen, J. Kessels, M. Donkers, and S. Weiland. Game-theoretic approach for complete vehicle energy management. In *Proc. of the IEEE Vehicle Power and Propulsion Conference*, 2014.
 - [13] H. Chen, J. Kessels, and S. Weiland. Adaptive ECMS: a causal set-theoretic method for equivalence factor estimation. 2015.
 - [14] H. Chen, J. Kessels, and S. Weiland. Online adaptive approach for a game-theoretic strategy for complete vehicle energy management. In *Proc. of the IEEE European Control Conference*, 2015.
 - [15] H. Chen, J. Kessels, and S. Weiland. Vehicle energy management for on/off controlled auxiliaries: fuel economy vs. switching frequency. In *Proc. IFAC Workshop on Engine and Powertrain Control, Simulation and Modeling*, 2015.
 - [16] J.-S. Chen and M. Salman. Learning energy management strategy for hybrid electric vehicles. In *Proc. of the IEEE Vehicle Power and Propulsion Conference*, 2005.
 - [17] S. Cikanek and K. Bailey. Regenerative braking system for a hybrid electric vehicles. In *Proc. of the IEEE American Control Conference*, 2002.
 - [18] R. Cipollone and A. Sciarretta. Analysis of the potential performance of a combined hybrid vehicle with optimal supervisory control. In *Proc. of the IEEE International Conference on Control Applications*, 2006.

-
- [19] E. Cortona, C. Onder, and L. Guzzella. Engine thermomanagement with electrical components for fuel consumption reduction. *International Journal of Engine Research*, 3(3):157–170, 2002.
- [20] E. Cortona and C. H. Onder. Engine thermal management with electric cooling pump. *SAE Technical Paper*, 2000.
- [21] G. Danzig and P. Wolfe. The decomposition algorithm for linear programming. *Econometrica*, 4:767–778, 1961.
- [22] B. De Jager, T. Van Keulen, and J. Kessels. *Optimal control of hybrid vehicles*. Springer, 2013.
- [23] S. Delprat, J. Lauber, T.-M. Guerra, and J. Rimaux. Control of a parallel hybrid powertrain: optimal control. *IEEE transactions on Vehicular Technology*, 53(3):872–881, 2004.
- [24] C. Dextreit and I. V. Kolmanovsky. Game theory controller for hybrid electric vehicles. *IEEE Transactions on Control Systems Technology*, 22(2):652–663, 2014.
- [25] S. Di Cairano, D. Bernardini, A. Bemporad, and I. V. Kolmanovsky. Stochastic MPC with learning for driver-predictive vehicle control and its application to HEV energy management. *IEEE Transactions on Control Systems Technology*, 22(3):1018–1031, 2014.
- [26] S. Ebbesen, P. Elbert, and L. Guzzella. Battery state-of-health perceptive energy management for hybrid electric vehicles. *IEEE Transactions on Vehicular technology*, 61(7):2893–2900, 2012.
- [27] S. Ebbesen, P. Elbert, and L. Guzzella. Battery state-of-health perceptive energy management for hybrid electric vehicles. *IEEE Transactions on Control Systems Technology*, 61(7):2893–2900, 2012.
- [28] L. Eckstein, B. Mohrmann, R. Hummel, S. Weiland, M. Donkers, H. Chen, and T. Romijn. Fuel consumption reduction measures for longhaul-trucks in the CONVENIENT project. In *Proc. of the 13th International Conference Commercial Vehicles*, 2015.

- [29] B. Egardt, N. Murgovski, M. Pourabdollah, and L. J. Mardh. Electromobility studies based on convex optimization: Design and control issues regarding vehicle electrification. *IEEE Control Systems*, 34(2):32–49, 2014.
- [30] M. Ehsani, Y. Gao, and A. Emadi. *Modern electric, hybrid electric, and fuel cell vehicles: fundamentals, theory, and design*. CRC press, 2009.
- [31] P. Elbert, T. Nüesch, A. Ritter, N. Murgovski, and L. Guzzella. Engine on/off control for the energy management of a serial hybrid electric bus via convex optimization. *IEEE Transactions on Vehicular Technology*, 2014.
- [32] M. Ellis, H. Durand, and P. D. Christofides. A tutorial review of economic model predictive control methods. *Journal of Process Control*, 24(8):1156–1178, 2014.
- [33] H. K. Fathy, D. Kang, and J. L. Stein. Online vehicle mass estimation using recursive least squares and supervisory data extraction. In *Proc. of the American Control Conference*, 2008.
- [34] H. Ferreau, C. Kirches, A. Potschka, H. Bock, and M. Diehl. qpOASES: A parametric active-set algorithm for quadratic programming. *Mathematical Programming Computation*, 6(4):327–363, 2014.
- [35] N. Fraser, H. Blaxill, G. Lumsden, and M. Bassett. Challenges for increased efficiency through gasoline engine downsizing. *SAE International Journal of Engines*, 2:991–1008, 2009.
- [36] C. E. Garcia, D. M. Prett, and M. Morari. Model predictive control: theory and practice, a survey. *Automatica*, 25(3):335–348, 1989.
- [37] N. Gatsis and G. B. Giannakis. Decomposition algorithms for market clearing with large-scale demand response. *IEEE Transactions on Smart Grid*, 4(4):1976–1987, 2013.
- [38] H. P. Geering. *Optimal control with engineering applications*, volume 113. Springer, 2007.
- [39] B. Gu and G. Rizzoni. An adaptive algorithm for hybrid electric vehicle energy management based on driving pattern recognition. In *Proc. of the ASME Int. Mechanical Engineering Congress and Exposition*, 2006.

-
- [40] L. Guzzella and A. Sciarretta. *Vehicle propulsion systems*. Springer, 2007.
- [41] T. Hendricks and M. O’Keefe. Heavy vehicle auxiliary load electrification for the essential power system program: Benefits, tradeoffs, and remaining challenges. *SAE Technical Paper*, 2002.
- [42] T. Hofman, M. Steinbuch, R. Van Druten, and A. Serrarens. Rule-based energy management strategies for hybrid vehicles. *International Journal of Electric and Hybrid Vehicles*, 1(1):71–94, 2007.
- [43] K. Holmberg, P. Andersson, N.-O. Nylund, K. Mäkelä, and A. Erdemir. Global energy consumption due to friction in trucks and buses. *Tribology International*, 78:94–114, 2014.
- [44] I. Husain. *Electric and hybrid vehicles: design fundamentals*. CRC press, 2011.
- [45] IBM Corp: IBM ILOG CPLEX V12.1. *User’s Manual for CPLEX (2009)*.
- [46] Intergovernmental Panel on Climate Change. *Climate change 2014: mitigation of climate change*, volume 3. Cambridge University Press, 2015.
- [47] N. Jalil, N. A. Kheir, and M. Salman. A rule-based energy management strategy for a series hybrid vehicle. In *Proc. of the IEEE American Control Conference*, 1997.
- [48] S. James, C. James, and J. Evans. Modelling of food transportation systems, a review. *International Journal of Refrigeration*, 29(6):947–957, 2006.
- [49] L. Johannesson, M. Asbogard, and B. Egardt. Assessing the potential of predictive control for hybrid vehicle powertrains using stochastic dynamic programming. *IEEE Transactions on Intelligent Transportation Systems*, 8(1):71–83, 2007.
- [50] V. H. Johnson, K. B. Wipke, and D. J. Rausen. HEV control strategy for real-time optimization of fuel economy and emissions. *SAE Transactions*, 109(3):1677–1690, 2000.

-
- [51] J. Kessels, M. Koot, and P. Van den Bosch. Optimal adaptive solution to the powersplit problem in vehicles with integrated starter/generator. In *Proc. of the IEEE Vehicle Power and Propulsion Conference*, 2006.
- [52] J. Kessels, J. Martens, P. Van den Bosch, and W. Hendrix. Smart vehicle powernet enabling complete vehicle energy management. In *Proc. of the IEEE Vehicle Power and Propulsion Conference*, 2012.
- [53] J. Kessels, P. Van den Bosch, M. Koot, and B. de Jager. Energy management for vehicle power net with flexible electric load demand. In *Proc. of the IEEE Conference on Control Applications*, 2005.
- [54] J. Kessels, F. Willems, W. Schoot, and P. Van den Bosch. Integrated energy & emission management for hybrid electric truck with SCR aftertreatment. In *Proc. of the IEEE Vehicle Power and Propulsion Conference*, 2010.
- [55] Z. Khalik, T. Romijn, M. Donkers, and S. weiland. Effects of battery charge acceptance and battery aging in complete vehicle energy management. In *Proc. of the IFAC World Congress*, 2017.
- [56] N. Kim, A. Rousseau, and D. Lee. A jump condition of PMP-based control for PHEVs. *Journal of Power Sources*, 196(23):10380–10386, 2011.
- [57] T. S. Kim, C. Manzie, and R. Sharma. Model predictive control of velocity and torque split in a parallel hybrid vehicle. In *Proc. of the IEEE International Conference on Systems, Man and Cybernetics*, 2009.
- [58] F. Kirschbaum, M. Back, and M. Hart. Determination of the fuel-optimal trajectory for a vehicle along a known route. *IFAC Proceedings Volumes*, 35(1):235–239, 2002.
- [59] A. Kleimaier and D. Schroder. An approach for the online optimized control of a hybrid powertrain. In *Proc. of the IEEE 7th International Workshop on Advanced Motion Control*, 2002.
- [60] I. Kolmanovsky, I. Siverguina, and B. Lygoe. Optimization of powertrain operating policy for feasibility assessment and calibration: Stochastic dynamic programming approach. In *Proc. of the IEEE American Control Conference*, 2002.

- [61] A. Kozma, J. V. Frasch, and M. Diehl. A distributed method for convex quadratic programming problems arising in optimal control of distributed systems. In *Proc. of the IEEE 52nd Annual Conference on Decision and Control*, 2013.
- [62] R. Langari and J.-S. Won. Intelligent energy management agent for a parallel hybrid vehicle-part i: system architecture and design of the driving situation identification process. *IEEE Transactions on Vehicular Technology*, 54(3):925–934, 2005.
- [63] G. K. Larsen, N. D. van Foreest, and J. M. Scherpen. Distributed control of the power supply-demand balance. *IEEE Transactions on Smart Grid*, 4(2):828–836, 2013.
- [64] S. Larsson. Commercial vehicles, fuel efficiency and CO₂ challenges & possible solutions. In the International Energy Agency (IEA) Freight Truck Fuel Economy Workshop, May 2011. Retrieved from <https://www.iea.org/workshops/iea-freighttruck-fuel-economy-workshop-200511.html>.
- [65] J. Lescot, A. Sciarretta, Y. Chamaillard, and A. Charlet. On the integration of optimal energy management and thermal management of hybrid electric vehicles. In *Proc. of the IEEE Vehicle Power and Propulsion Conference*, 2010.
- [66] C.-C. Lin, H. Peng, and J. Grizzle. A stochastic control strategy for hybrid electric vehicles. In *Proc. of the IEEE American Control Conference*, 2004.
- [67] C.-C. Lin, H. Peng, J. W. Grizzle, and J.-M. Kang. Power management strategy for a parallel hybrid electric truck. *IEEE Transactions on Control Systems Technology*, 11(6):839–849, 2003.
- [68] P. Lingman and B. Schmidtbauer. Road slope and vehicle mass estimation using kalman filtering. *Vehicle System Dynamics*, 37:12–23, 2002.
- [69] J. Liu and H. Peng. Control optimization for a power-split hybrid vehicle. In *Proc. of the IEEE American Control Conference*, 2006.

- [70] J. M. Maestre and R. R. Negenborn. *Distributed model predictive control made easy*. Springer, 2014.
- [71] J. Mattingley and S. Boyd. CVXGEN: a code generator for embedded convex optimization. *Optimization and Engineering*, 13(1):1–27, 2012.
- [72] F. Merz, A. Sciarretta, J. Dabadie, and L. Serrao. On the optimal thermal management of hybrid-electric vehicles with heat recovery system. *Oil & Gas Science and Technology*, 2012.
- [73] C. Mi, M. A. Masrur, and D. W. Gao. *Hybrid electric vehicles: principles and applications with practical perspectives*. John Wiley & Sons, 2011.
- [74] J. M. Miller. *Propulsion systems for hybrid vehicles*, volume 45. Iet, 2004.
- [75] Z. Mohamed-Kassim and A. Filippone. Fuel savings on a heavy vehicle via aerodynamic drag reduction. *Transportation Research Part D: Transport and Environment*, 15(5):275–284, 2010.
- [76] B. Mohrmann, R. Hummel, J. Gissing, and J. Kessels. Holistic energy system design. Technical report, CONVENIENT project deliverable report D A3.2.1, 2014.
- [77] S. J. Moura, H. K. Fathy, D. S. Callaway, and J. L. Stein. A stochastic optimal control approach for power management in plug-in hybrid electric vehicles. *IEEE Transactions on Control Systems Technology*, 19(3):545–555, 2011.
- [78] N. Murgovski, L. Johannesson, J. Sjöberg, and B. Egardt. Component sizing of a plug-in hybrid electric powertrain via convex optimization. *Mechanics*, 22(1):106–120, 2012.
- [79] C. Musardo, G. Rizzoni, Y. Guezennec, and B. Staccia. A-ECMS: An adaptive algorithm for hybrid electric vehicle energy management. *European Journal of Control*, 11(4):509–524, 2005.
- [80] W. Nessim and F. Zhang. Powertrain warm-up improvement using thermal management systems. *International Journal of Technology Enhancements and Emerging Engineering Research*, 1(4):151–155, 2012.

- [81] K. D. Nguyen, E. Bideaux, M. T. Pham, and P. Le Brusq. Game theoretic approach for electrified auxiliary management in high voltage network of HEV/PHEV. In *Proc. of the IEEE International Electric Vehicle Conference*, 2014.
- [82] M. Nilsson and L. Johannesson. Convex optimization for auxiliary energy management in conventional vehicles. In *Proc. of the IEEE Vehicle Power and Propulsion Conference*, 2014.
- [83] M. Nilsson, L. Johannesson, and M. Askerdal. ADMM applied to energy management of ancillary systems in trucks. In *Proc. of the IEEE American Control Conference*, 2015.
- [84] E. Nuijten, M. Koot, J. Kessels, B. de Jager, M. Heemels, W. Hendrix, and P. van den Bosch. Advanced energy management strategies for vehicle power nets. In *Proc. EAEC 9th International Congress: European Automotive Industry Driving Global Changes*, 2003.
- [85] Oliver Wyman Analysis. European truck customer, 2010.
- [86] S. Onori and L. Serrao. On Adaptive-ECMS strategies for hybrid electric vehicles. In *Proc. of the International Scientific Conference on Hybrid and Electric Vehicles*, 2011.
- [87] T. M. Padovani, M. Debert, G. Colin, and Y. Chamaillard. Optimal energy management strategy including battery health through thermal management for hybrid vehicles. In *Proc. of the IFAC Symposium Advances in Automotive Control*, 2013.
- [88] G. Paganelli, G. Ercole, A. Brahma, Y. Guezennec, and G. Rizzoni. General supervisory control policy for the energy optimization of charge-sustaining hybrid electric vehicles. *JSAE review*, 22(4):511–518, 2001.
- [89] G. Paganelli, T. Guerra, S. Delprat, J. Santin, M. Delhom, and E. Combes. Simulation and assessment of power control strategies for a parallel hybrid car. *Institution of Mechanical Engineers, Part D: Journal of Automobile Engineering*, 214(7):705–717, 2000.

- [90] L. V. Pérez, G. R. Bossio, D. Moitre, and G. O. García. Optimization of power management in a hybrid electric vehicle using dynamic programming. *Mathematics and Computers in Simulation*, 73(1):244–254, 2006.
- [91] T. Pham. *Integrated Energy and Battery Life Management for Hybrid Vehicles*. PhD thesis, Eindhoven University of Technology, 2015.
- [92] T. Pham, J. Kessels, P. van den Bosch, R. Huisman, and R. Nevels. On-line energy and battery thermal management for hybrid electric heavy-duty truck. In *Proc. of the IEEE American Control Conference*, 2013.
- [93] T. Pham, P. van den Bosch, J. Kessels, and R. Huisman. Cost-effective energy management for hybrid electric heavy-duty truck including battery aging. In *Proc. of the ASME Dynamic Systems and Control Conference*, 2013.
- [94] T. Pham, P. van den Bosch, J. Kessels, and R. Huisman. Integrated online energy and battery life management for hybrid long haulage truck. In *Proc. of the IEEE Vehicle Power and Propulsion Conference*, 2014.
- [95] S. Pretsch and M. Winter. Electrification of a commercial vehicle’s auxiliaries: A chance of reducing fuel consumption and CO₂ emissions. In *Proc. of the 12th International Symposium of Heavy Vehicle Transportation Technology*, 2012.
- [96] A. Rantzer. Dynamic dual decomposition for distributed control. In *Proc. of the IEEE American Control Conference*, 2009.
- [97] J. Redfield, B. Surampudi, R. Gustavo, A. Montemayor, H. McKee, T. Edwards, and M. Lasecki. Accessory electrification in class 8 tractors. *SAE Technical Paper*, 2006.
- [98] C. Röss, D. Balzer, A. Bracht, S. Durekovic, and J. Löwenau. ADASIS protocol for advanced in-vehicle applications. In *Proc. of the 15th World Congress on Intelligent Transport Systems*, 2008.
- [99] T. Romijn, M. Donkers, J. Kessels, and S. Weiland. A distributed optimization approach for complete vehicle energy management. *Submitted to Transactions on Control Systems Technology*.

- [100] T. Romijn, M. Donkers, J. Kessels, and S. Weiland. Real-time distributed model predictive control for complete vehicle energy management. *MDPI Energies: Special issue on Energy Management Control*.
- [101] T. Romijn, M. Donkers, J. Kessels, and S. Weiland. A dual decomposition approach to complete energy management for a heavy-duty vehicle. In *Proc. of the IEEE 53rd Annual Conference on Decision and Control*, 2014.
- [102] T. Romijn, M. Donkers, J. Kessels, and S. Weiland. Complete vehicle energy management with large horizon optimization. In *Proc. of the IEEE 54th Annual Conference on Decision and Control*, 2015.
- [103] T. Romijn, M. Donkers, J. Kessels, and S. Weiland. Receding horizon control for distributed energy management of a hybrid truck with auxiliaries. In *Proc. of the IFAC Workshop on Engine and Powertrain Control, Simulation and Modeling*, 2015.
- [104] S. Schepmann and A. Vahidi. Heavy vehicle fuel economy improvement using ultracapacitor power assist and preview-based MPC energy management. In *Proc. of the IEEE American Control Conference*, 2011.
- [105] N. J. Schouten, M. A. Salman, and N. A. Kheir. Fuzzy logic control for parallel hybrid vehicles. *IEEE Transactions on Control Systems Technology*, 10(3):460–468, 2002.
- [106] A. Sciarretta, M. Back, and L. Guzzella. Optimal control of parallel hybrid electric vehicles. *IEEE Transactions on Control Systems Technology*, 12(3):352–363, 2004.
- [107] L. Serrao, S. Onori, and G. Rizzoni. ECMS as a realization of Pontryagin’s minimum principle for HEV control. In *Proc. of the IEEE American Control Conference*, 2009.
- [108] L. Serrao, S. Onori, A. Sciarretta, Y. Guezennec, and G. Rizzoni. Optimal energy management of hybrid electric vehicles including battery aging. In *Proc. of the IEEE American Control Conference*, 2011.

- [109] L. Serrao, S. Onori, A. Sciarretta, Y. Guezennec, and G. Rizzoni. Optimal energy management of hybrid electric vehicles including battery aging. In *Proc. of the IEEE American Control Conference*, 2011.
- [110] L. Serrao and G. Rizzoni. Optimal control of power split for a hybrid electric refuse vehicle. In *Proc. of the IEEE American Control Conference*, 2008.
- [111] G. Stathopoulos, T. Keviczky, and Y. Wang. A hierarchical time-splitting approach for solving finite-time optimal control problems. In *Proc. of the IEEE European Control Conference*.
- [112] G. Steinmaurer and L. Del Re. Optimal energy management for mild hybrid operation of vehicles with an integrated starter generator. *SAE Technical Paper*, 2005.
- [113] O. Sundstrom and L. Guzzella. A generic dynamic programming Matlab function. In *Proc. of the Conference on Control Applications*, 2009.
- [114] O. Sundström, L. Guzzella, and P. Soltic. Optimal hybridization in two parallel hybrid electric vehicles using dynamic programming. *IFAC Proceedings Volumes*, 41(2):4642–4647, 2008.
- [115] E. D. Tate and S. P. Boyd. Finding ultimate limits of performance for hybrid electric vehicles. *SAE Technical Paper*, 2000.
- [116] A. Vahidi and W. Greenwell. A decentralized model predictive control approach to power management of a fuel cell-ultracapacitor hybrid. In *Proc. of the IEEE American Control Conference*, 2007.
- [117] A. Vahidi, A. Stefanopoulou, and H. Peng. Experiments for online estimation of heavy vehicle’s mass and time-varying road grade. In *Proc. of the ASME Int. Mechanical Engineering Congress and Exposition*, 2003.
- [118] N. van der Sanden. Model identification of DAF’s EURO-6 air-conditioning system applied in an optimal control study. Master’s thesis, Eindhoven University of Technology, 2014.
- [119] T. van Keulen. *Fuel Optimal Control of Hybrid Vehicles*. PhD thesis, Eindhoven University of Technology, 2011.

- [120] T. Van Keulen, J. Gillot, B. De Jager, and M. Steinbuch. Solution for state constrained optimal control problems applied to power split control for hybrid vehicles. *Automatica*, 50(1):187–192, 2014.
- [121] D. van Leeuwen. A model-based simulation tool for optimal component sizing for heavy-duty hybrid trucks. Master’s thesis, Eindhoven University of Technology, 2011.
- [122] H. Wallentowitz and R. Ludes. System control application for hybrid vehicles. In *Proc. of the third IEEE Conference on Control Applications*, 1994.
- [123] R. Wang and S. M. Lukic. Review of driving conditions prediction and driving style recognition based control algorithms for hybrid electric vehicles. In *Proc. of the IEEE Vehicle Power and Propulsion Conference*, pages 1–7. IEEE, 2011.
- [124] F. Willems, M. Donkers, and F. Kupper. *Optimal Control of Diesel Engines with Waste Heat Recovery System*. Springer, 2014.
- [125] F. Willems, F. Kupper, and R. Cloudt. Integrated powertrain control for optimal CO₂- NO_x tradeoff in an Euro-VI diesel engine with waste heat recovery system. In *Proc. of the IEEE American Control Conference*, 2012.
- [126] V. Winstead and I. V. Kolmanovskiy. Estimation of road grade and vehicle mass via model predictive control. In *Proc. of the IEEE Conference on Control Applications*, 2005.
- [127] T. M. Wolf. New bearing technology enables significant CO₂ savings. *ATZ worldwide*, 111(9):68–71, 2009.
- [128] L. Xiao, M. Johansson, and S. P. Boyd. Simultaneous routing and resource allocation via dual decomposition. *IEEE Transactions on Communications*, 52(7):1136–1144, 2004.
- [129] X. Zeng and J. Wang. A parallel hybrid electric vehicle energy management strategy using stochastic model predictive control with road grade preview. *IEEE Transactions on Control Systems Technology*, 23(6):2416–2423, 2015.
- [130] X. Zhang and C. Mi. *Vehicle power management: modeling, control and optimization*. Springer Science & Business Media, 2011.

Acknowledgements

The work presented in this thesis is a result of a four year journey which would not have been the same without the support of the people around me.

First of all, I would like to express my gratitude towards my supervisor Dr. Tijs Donkers for all his support and the countless discussions. I would not have been able to write this thesis without your advice and continuous encouragement. Your endless source of optimism and enthusiasm has been very inspiring.

Next, I would like to thank my promotor Prof. Siep Wieland for his support and interesting discussions. I remember our first meeting after I applied for this PhD position. This meeting strongly motivated me to work on this fascinating topic of energy management, but also to broaden my knowledge on a wider range of topics in the control systems field. Thank you for all your suggestions that significantly improved the readability of this thesis.

Besides Tijs and Siep, I was privileged to have Dr. John Kessels as my second supervisor. I enjoyed our discussions, which were mainly on engineering topics. This provided a nice alternative to the mainly theoretical discussions with Tijs and Siep. Thank you for all the help in getting around at DAF Trucks N.V. and putting me into contact with the people at that company. I owe my gratitude to them as well for sharing their knowledge on the subject.

I am also very grateful to the members of my dissertation committee. Prof. Bo Egardt, Prof. Lars Grüne, Prof. Jacqueline Scherpen and Prof. Maarten Steinbuch, thank you for your efforts to read my thesis and for providing me relevant feedback to further improve this thesis.

It was very pleasant to work together with the people in the CONVENIENT project. In particular, I would like to thank Björn Mohrmann and Raphael Hummel from the Institute für Kraftfahrzeugen Aachen for their support with the high-fidelity vehicle model and the work on the energy management system

operator. A special thanks goes out to Will for the technical support but also for the interesting conversations, the introduction to different genres of Jazz and for the occasional tennis match during the lunch break. I also owe my gratitude to my fellow PhD candidate Handian. I enjoyed working together with you on the same topic.

My time as a PhD candidate would not have been the same without my colleagues. I would like to thank all the group members of the Control Systems group for creating a very pleasant working environment. In particular, I really enjoyed playing futsal with the ‘Team of Rob’. Thanks Koen, Handian, Thinh, Veaceslav, Michel, Quang, Rian, Tuan, Hernan, Pepijn, Mohammed, Mohsin, Mircea, Daming, Henrik, Giuseppe, Harm, Ionanis, Alejandro, Giulio, etc. for keeping up the team spirit. I also share good memories from the travels together to various conferences. Thanks Alina, Bahadir, Senna, Harm, Sofie, Pepijn, Veaceslav, etc. for all these memorable moments. A special thanks goes out to Henrik. It was always fun to travel together and I really enjoyed the many casual discussions we had in the office.

Next, I would like to thank my friends for frequently taking my mind off the work by playing squash, going out for cycling, going to the gym, enjoying epic game nights and many more awesome activities. A special gratitude goes out to Luke for designing the cover of this thesis.

This thesis would not have been feasible without the support of my family. I owe my gratitude to my parents for all their support and all the opportunities they offered to me. I also want to express my gratitude towards Joop van Dongen. It is always a pleasure to work in the garden every Saturday and I enjoy the coffee breaks filled with interesting conversations on a broad range of topics. You have been very inspiring to me, which strongly motivated me to continue with a PhD after my MSc studies.

Finally, I would like to thank my lovely girlfriend Alina for her support and encouragement during my PhD. This PhD would not have been the same without you being part of it.

*Constantijn Romijn
Eindhoven, August 2017*

Curriculum Vitae

Constantijn Romijn was born on June 15, 1988 in Kockengen, Netherlands. He received his Bachelor degree from HAN University of Applied Sciences in 2010 majoring in automotive technology. After that, he followed the Master program in Automotive Engineering Science at the Department of Mechanical Engineering at Eindhoven University of Technology. His Master project was on regenerative brake torque control for hybrid and electric vehicles. In 2013, he obtained his Master degree and was appointed as a PhD candidate in the Control Systems group at the Department of Electrical Engineering at Eindhoven University of Technology in the same year. His PhD research involves the development of energy management strategies for complete vehicle energy management by applying distributed control to energy management incorporating the mechanical, electrical and thermal domain. The research is carried out as part of the European Union project "Complete Vehicle Energy-saving Technologies for Heavy-Trucks" (CONVENIENT). The results of this research are presented in this thesis. During his PhD, Constantijn received the Best Poster Award (first place) of the 2015 IEEE West European Student & Young Professional Congress.

